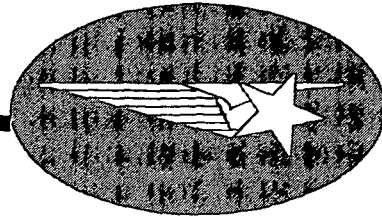FINAL REPORT

LASER HOLOGRAPHIC
NONDESTRUCTIVE TESTING
OF

CASE FILE
COPY

LOCKHEED MISSILES & SPACE COMPANY, INC.
Manufacturing Research Investigation

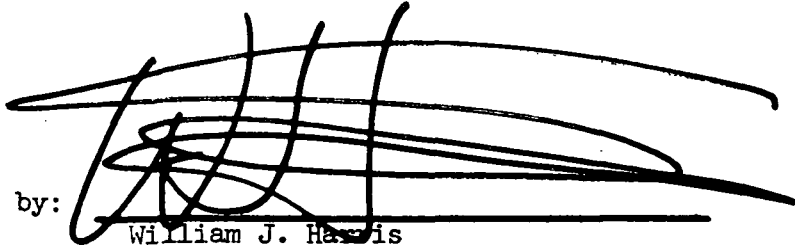FINAL REPORT

LASER HOLOGRAPHIC

NONDESTRUCTIVE TESTING

OF

THE NASA X-248 ROCKET MOTOR

NASA Contract: NASI 11419

December 1972

Prepared by: _____
William J. Harris
Manufacturing Research Engineer, Sr.

LOCKHEED MISSILES & SPACE COMPANY

ABSTRACT

In coordination with the National Aeronautics and Space Administration
of Langley Research Center at Hampton, Virginia, a program to apply
holography for nondestructive testing of the X-249 rocket motor was
undertaken. The objective was to establish the capability of holography
in detecting known unbonding between liner and propellant. Holography
was performed employing stressing techniques: acoustical, thermal,
radiative and static loading. Radiative stressing was successful in
locating a large area of liner/propellant unbond. The results were
correlated with destructive testing. Theoretical analysis provided
an understanding of motor case holography in conjunction with radiative
stressing.

LOCKHEED MISSILES & SPACE COMPANY

Page Intentionally Left Blank

CONTENTS

LOCKHEED MISSILES & SPACE COMPANY

CONTENTS

LOCKHEED MISSILES & SPACE COMPANY

Section 1

INTRODUCTION

The work reported herein on laser holographic inspection of the X-248 rocket motor case was done at the request of the National Aeronautics and Space Administration, Langley Research Center, Hampton, Virginia. The effort was the response to NASI Order No. 11419 issued on 23 March 1972.

The purpose of the program was to evaluate laser holographic nondestructive testing for detection of separation in the bondlines of the casing/liner/propellant interfaces of the X-248 motor case. Two motor cases having known areas of separation were provided for the program. A radiographic report showing actual positions of separations was furnished. After holographic analysis, the results were correlated with destructive examination. A large area of separation, about 180 in.^{2}, between liner and propellant was detected. Perfect correlation was not realized. An uncertainty exists concerning the size of the separation when holography was performed.

The current technique for inspecting rocket motor cases at Lockheed Missiles and Space Company, and in the aerospace industry in general, is radiography. Radiography can measure slight density variations of under 1% in materials but unless there is a physical separation or void in materials, the technique is inadequate for bonded structures. Also, on cylindrical geometries such as motor cases, many exposures are required since little more than a tangent view is practical in a single x-ray.

Depending on size and geometry, ultrasonic scanning is sometimes used to reveal bondline separation. But, this method, because of adaptability and operating costs, is rarely employed on complex designs or on large structures.

LOCKHEED MISSILES & SPACE COMPANY

Infrared scanning has been applied to the problem with marginal success. However, the technique suffers many of the disadvantages of ultrasonics and does not offer comparable resolution of ultrasonics.

For inspecting bonded structures, such as honeycomb panels and metal-to-metal sandwiches, laser holography offers great sensitivity plus the ability to cover large surface areas at one time. A variety of structures and components ranging from bonded panels to complex rocket nozzles have successfully been inspected with laser holography. Materials inspected includes metals, plastics, foams and composites. In addition, testing procedures, once developed, are easily mastered by a competent operator.

Clearly then, if laser holography can be developed for inspecting rocket motor cases, it offers a rapid method for testing a large surface area. In addition, laser holography may be able to detect separation of bondlines as well as disbonded areas that are in physical contact providing an important advantage over conventional x-ray.

Section 2

EQUIPMENT AND PROCEDURE

2.1 HOLOGRAPHY

This investigation was accomplished with a Model 1309D laser holography system, manufactured by the GC Optronics Company of Ann Arbor, Michigan. It consists of a 50 milliwatt helium-neon gas laser; optics to control laser beam direction, intensity and divergence; a photographic plate holder; and a vibration isolation air suspended table. The system is shown in Fig. 1. Also shown is motor S/N 424 in position mounted for holographic testing. The motor was resting on the 8 in. high steel base, fabricated for this program. A mounting plate can also be seen bolted to the forward mounting flange. This plate was used for moving the motor from the shipping container to the holographic table.

To accomplish this project, the holography system was relocated from Building No. 150 of the Lockheed Missiles and Space Company in Sunnyvale, California, to the utility room, Building No. 6344, adjacent to Building 635, Test Stand No. 3 at the Lockheed Test Base in Santa Cruz, California.

Laser holography is an optical system capable of seeing strain on the surfaces of materials which have been stressed externally by heat or mechanical loading. The ability to observe surface strains on materials provides a means to correlate surface behavior with subsurface anomalies which, in this study, was bondline separation.

The procedure for observing strains consists of superimposing a virtual image onto the workpiece and studying the resultant interference between the two. A schematic of the holographic optical system can be seen in Fig. 2.

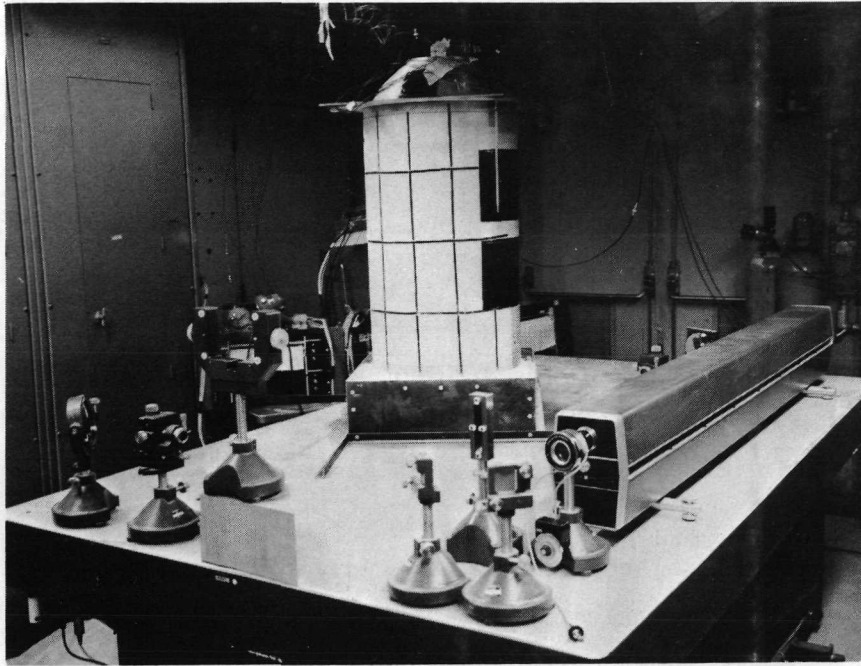**LOCKHEED MISSILES & SPACE COMPANY**

Fig. 1 Motor Case S/N 424 Mounted on Table of Holographic
System Located in Utility Room of Test Stand No.3
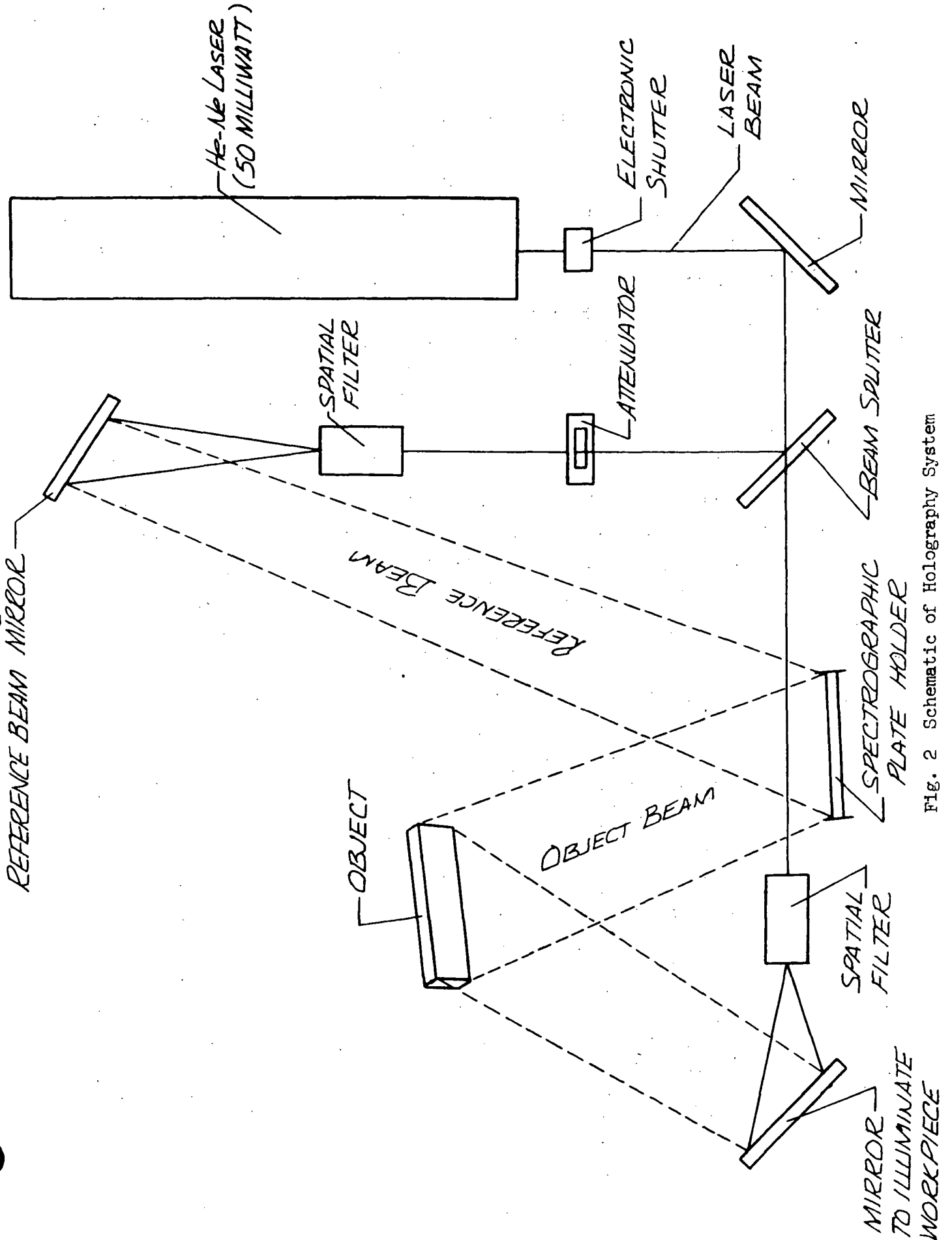at Lockheed Santa Cruz Test Facility

Fig. 2 Schematic of Holography System

In operation, the laser beam is divided by the beam splitter, which transmits
50% of the beam intensity (object beam) and reflects the remaining 50% (reference
beam). The transmitted beam is subsequently focused and diverged by the spatial
filter before being reflected to the workpiece. The beam which is reflected by
the beam splitter passes through an attenuator to adjust intensity before enter-
ing the spatial filter and being reflected to the photographic plate holder.
The photographic plate records both the light from every illuminated point on
the object as well as the interference of this light with the reference beam.
This is a holograph or a diffraction pattern that records the history of ampli-
tude and phase created from the interference of the two beams.

The hologram is placed in the plate holder and is observed under illumination by
the reference beam. The beam interacts with the diffraction patters (or hologram)
and regenerates a new wave field identical to the original; in other words, it
produces a virtual image. Microscopic displacements down to 12 micro-in. between
the vertical image and the real image (workpiece) can be detected as interference
fringes.

There are three types of holograms: time-average, double exposure and real-time.
The time-average hologram is produced by exposing the photographic plate while
the workpiece vibrates in a cyclic motion. With this technique the plate exposure
time must be long compared to the cyclic period of the workpiece. The hologram
records the time average of all positions of the object during vibration. Upon
reconstruction of the hologram, an interference pattern is observed which is
weighted toward the deformation extremes of the workpiece showing node and anti-
node locations and amplitudes of vibrations across the total surface. A double
exposure hologram records the workpiece surface condition before and after a
change has taken place. Both views of the workpiece are recorded in the same
hologram. When the double-exposed hologram is viewed the interference resulting
from the two exposures are seen. The real-time hologram is the simplest of the
three. This hologram is made with the workpiece at rest and observed as the

workpiece is changed. A variation on this technique consists of making the hologram with the workpiece in the altered state and observing the hologram when the workpiece as returned to a static condition. All three holographic techniques were applied in this study.

The 4 by 5 in. photograph plates commercially available for laser holography are Kodak 649F and Gevaert 10E70. The former provides resolution of over 2000 lines/mm, whereas the latter resolves 100 lines/mm. The Kodak plates require 10 times the exposure time of the Gevaert plates. Kodak plates are exposed for seconds compared to fractions of a second for AGFA plates. Both are developed with different solutions; Kodak 649F requires Kodak D-19 developer for 8 minutes and the Gevaert 10E70 develops in Kodak HRP for 5 minutes. The temperature of developer solutions should be held at 68° ± 2.

2.2   PHOTOGRAPHY

The interference fringe patterns, superimposed on an image of the workpiece, were photographed with an MP-3 Polaroid camera having a 5-in. focal lens. Black and white Polaroid film, Type 52, gave optimum contrast. Consequently, it was used exclusively. When an enlargement was desired, 4 by 5 in. Kodak Royal Pan film was exposed, developed, and subsequently printed onto an 8 by 10 in. positive.

2.3   RADIATIVE STRESSING

A 3-kilowatt quartz lamp manually held at distances of 6-in. to 24-in. away from rocket motors was used to induce thermal strain. The lamp operates on 210 volts, single phase power and it was fabricated by LMSC personnel.

2.4   THERMAL STRESSING

A heat gun directed on the motor cases was employed to apply hot air by manual scanning. The hot-air gun, Model No. 12300, was purchased from the Master Heat Gun Company of Racine, Wisconsin.

2.5 ACOUSTICAL STRESSING

Audio stressing was performed as indicated in the following schematic:
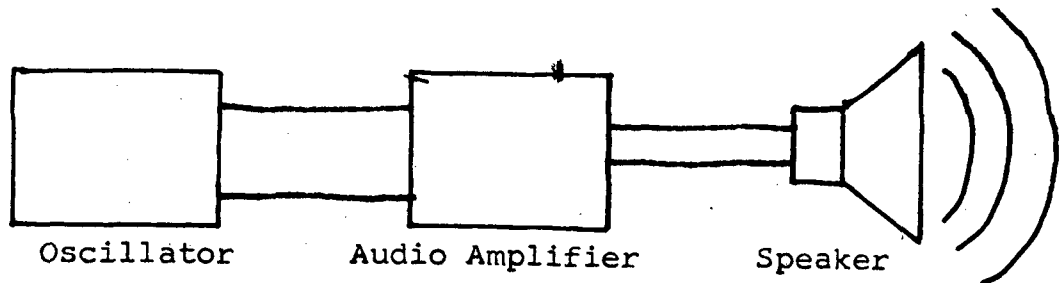
The 110V-60 cycle wide range oscillator was a Hewlett Packard Model 200 CD. Frequencies available range from a few cycles per second to one-half a megahertz.
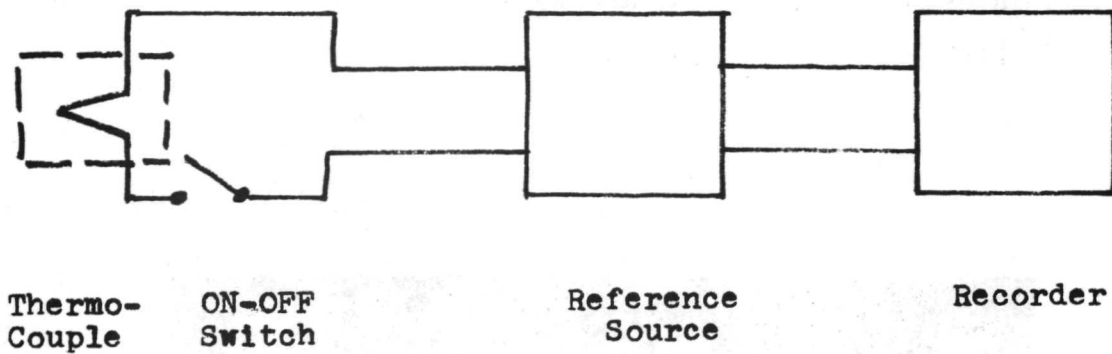
Oscillator signals were amplified by a McIntosh 30-watt audio amplifier, Model MC-30.

The speaker was a 40 watt, 12 in. diameter unit made by the Oaktron Company of Monroe, Wisconsin.

2.6 TEMPERATURE RECORDING

For thermal stressing during holography temperature measurements were recorded for two important purposes. One was to determine what motor case temperatures produced optimum fringe information in holographic testing. The other objective was to limit short term temperature rises to 125°F for no more than 10 minutes as required by the contract. In addition, when exposing the motors to environmental temperatures approaching the specified contractual limits of 40°F minimum and 100°F maximum, temperature recording was also performed.

A functional shcematic of the temperature recording system utilized is shown:

LOCKHEED MISSILES & SPACE COMPANY

| Thermo-Couple | ON-OFF Switch | | Reference Source | | Recorder |

The thermocouples attached to the motor cases were of the microminiature self-adhering grid type. The chromel-alumel thermocouples were manufactured by the BLH Electronics Company of Waltham, Massachusetts. A photograph of one of these is shown in Fig. 3.
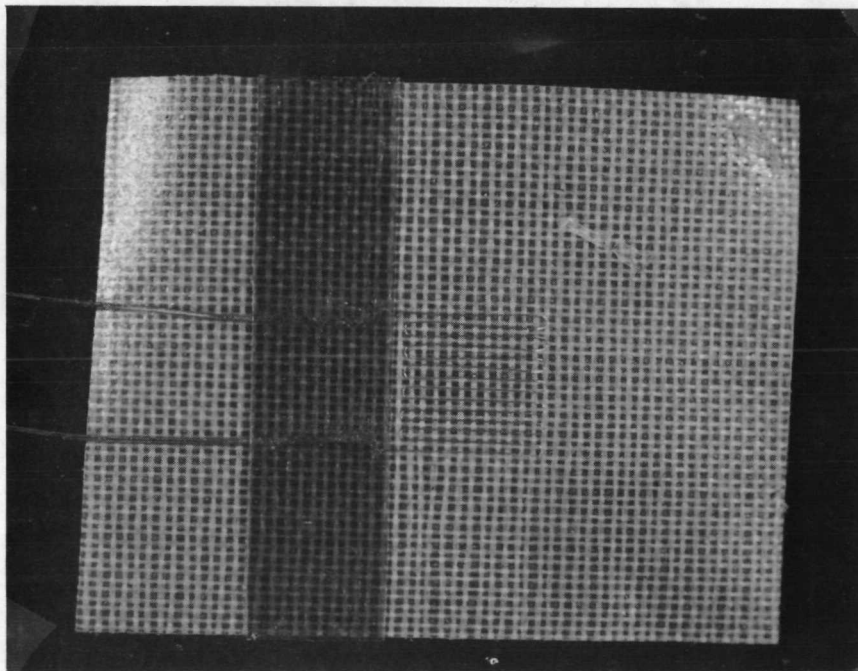

Fig. 3 Grid Type Thermocouple Used for Temperature Measurement on Motor Case   (3X)

LOCKHEED MISSILES & SPACE COMPANY

The locations of the six grid type thermocouples on a motor case can be seen in Fig. 4. This represents a typical arrangement for testing. They are approximately 90° apart with a 9 in. spacing.
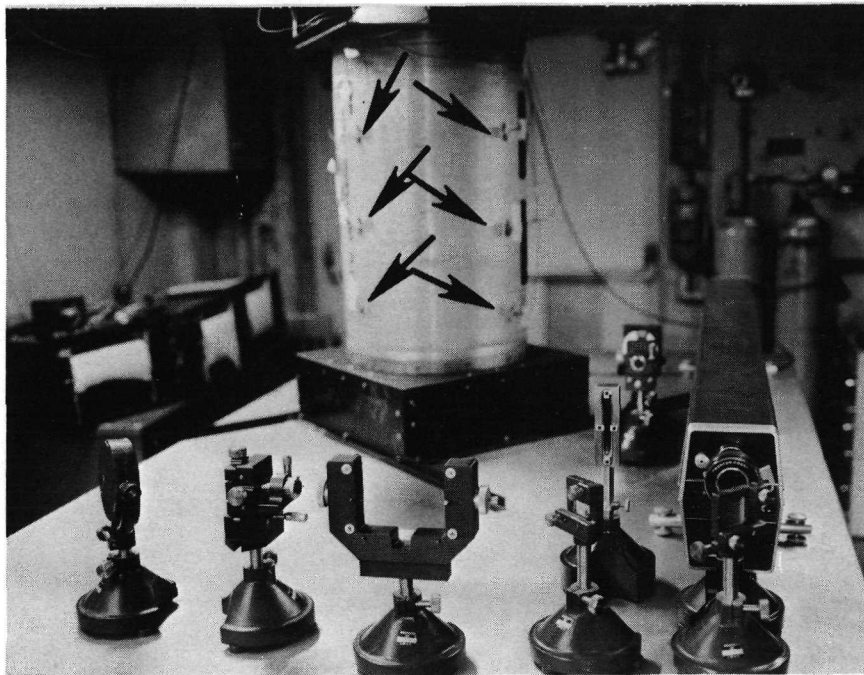

Fig. 4   Motor Case S/N 424 Shown Mounted on the Holographic
         Air Suspended Table for Testing. Arrows Point to
         the Position of (6) Chromel-Alumel thermocouples
         for Temperature Monitoring

A 150°F. thermocouple Reference Junction, manufactured by the Pace Engineering Company of North Hollywood, California, was employed as a fiducial base.

For recording temperatures, three Dual Pen Varian Recorders, Model No. G4000, were utilized. One of these is depicted in Fig. 5.

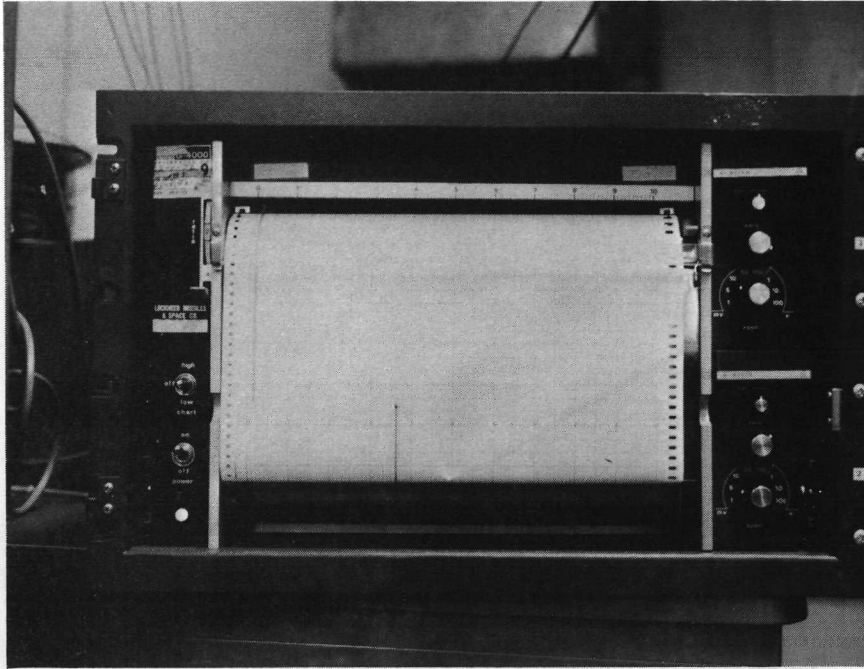**LOCKHEED MISSILES & SPACE COMPANY**

Fig. 5   Dual Pen Recorder Used for Temperature Recording
in Thermal Stressing of Motor Cases

Since the temperature band to be measured was below 150°F, the voltage printed
out on the 12 in. wide paper obeyed the following relationship:

$$V_r = V_{150} - V_T$$

where V_{150} is the voltage generated by a chromel-alumel thermocouple at the
temperature of 150-F., which is simulated by the reference source, and V_T equals
the voltage created at the thermocouple.

The on-off switch, shown in the functional schematic, is necessary to zero V_{150}
so only V_T is recorded which gives the temperature readings in accordance with
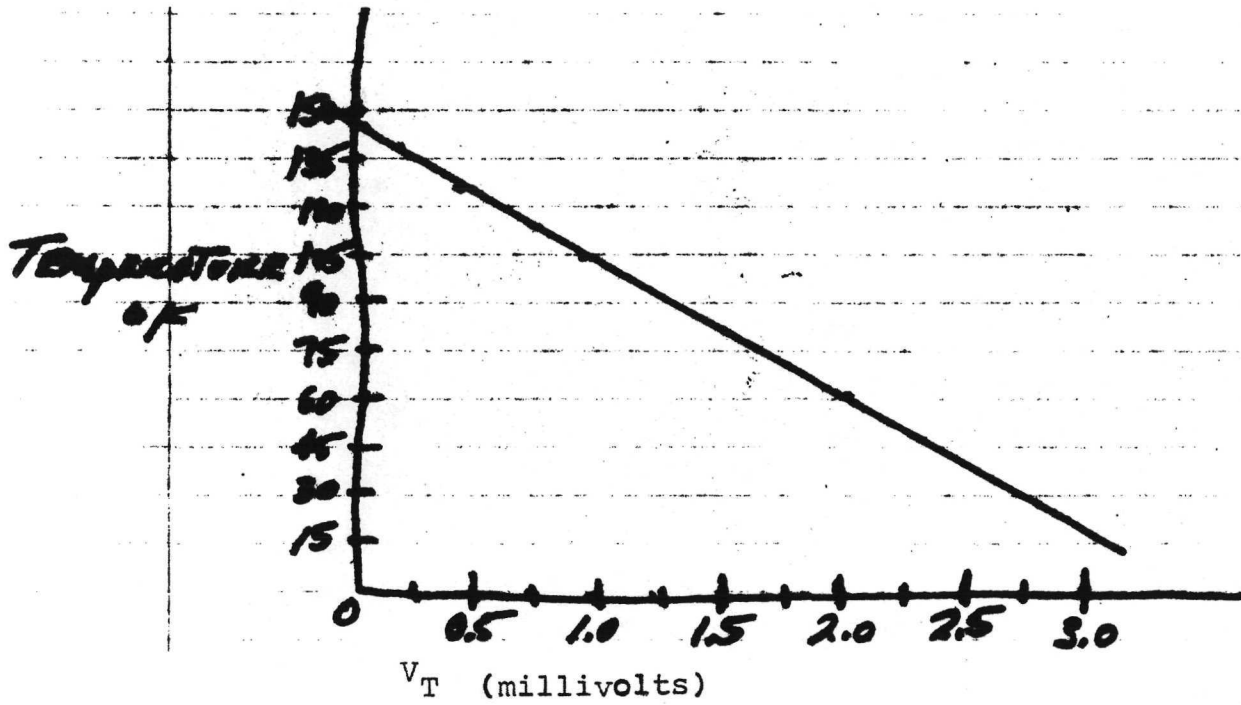the graph shown on Fig. 6.

LOCKHEED MISSILES & SPACE COMPANY

Fig. 6 Conversion Chart for Temperature Measurements
with Alumel-Chromel Thermocouples

LOCKHEED MISSILES & SPACE COMPANY

Section 3

RESULTS AND DISCUSSION

3.1   CONSTRUCTION OF MOTOR CASE

3.1.1   Motor Case NPP-424

The motor NPP-424 was fabricated from ECG glass rovings and Shell 828 epoxy. The cylindrical case had six windings producing a total thickness of .055 in. The diameter of the cylindrical section was 18.1 in. and its length was 30.5 in. Internally, from the aft end, was a 17 in. high rubber-type liner which tapered in thickness from about .375 in. to .125 in.

Radiography was performed on this motor case as well as NPP-426 by NASA personnel. The x-ray results from the NASA report are included in the Appendix.

3.1.2   Motor Case NPP-426

Motor NPP-426 was identical in construction to NPP-424 except for the casing which had seven windings and wall thickness of .078 in.

3.2   HOLOGRAPHIC ANALYSES OF MOTOR CASE NPP-424

3.2.1   Acoustical Stressing

A real-time holograph was made of the motor case S/N 424 mounted on the air-suspended table. The vertical centerline, as viewed through the hologram plate holder, was on the 270° position. The loud speaker was directed at the horizontal center of the motor case at the 270° position.

After developing the hologram, the sonic frequency range was scanned from 100 CPS to 18,000 CPS to determine the resonant frequency of the motor case. The power

---

[1]ERNIE R.B. AND HITT C.R.
"Comprehensive Report on NASA Motor Defects Investigation" NASA CR 66813.

output, at this time, as well as throughout this study, was estimated at 20-W. Initially, a resonant frequency could not be found despite careful scanning of the spectrum. This is determined by observing the casing through the developed and replaced real-time hologram and examining the inherent static fringe field for movement.

A time-average hologram was subsequently made at 1200 CPS but no related fringes were observed. A similar result occurred at 1000 CPS. However, sonic spectrum was again scanned with this latter hologram and a faint movement of fringes was detected at 1770 CPS. Another hologram was made at this frequency and it revealed three dark zones in the second quadrant at about the 290° position. However, these were not fringe lines but dark circular areas about 2 inches in diameter. This suggests a surface displacement caused by the acoustical stressing of something less than 25 microinches.

Using this latter hologram, the sonic spectrum was again searched and a resonance seemed to occur at 795 CPS, but no fringe information was evident in the hologram made at this frequency.

Finally three time-average holograms were generated at 1650 CPS, 1750 CPS and 1850 CPS. These frequencies were chosen to span the 1770 CPS frequency which previously had created dark zones in a hologram. Dark areas were observed in the holograms made at the upper and lower frequencies. The 1650 CPS hologram had dark spots in the repaired area of the motor at 300°. The hologram made at 1850 CPS had dark horizontal band in the area where the motor casing liner terminates, 17 in. above the cylinder base.

The illumination levels were too low for photography. A photograph of the speaker location on the air suspended table can be seen in Fig. 7.

3.2.2 Thermal Stressing

The hot air gun was applied over the surface of the motor casing from a distance of 1 ft. The entire casing was scanned for periods up to three minutes. However, the
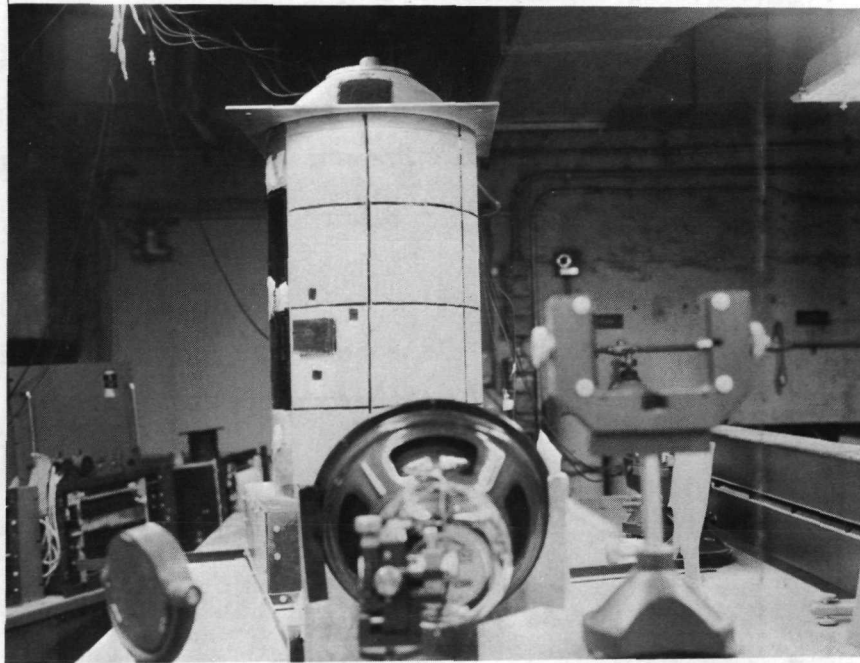
LOCKHEED MISSILES & SPACE COMPANY

Fig. 7   40-W Speaker Mounted on Air-Suspended Holographic
Table Prior to Acoustical Stressing Tests

casing temperature rises, as recorded by the attached thermocouples did not exceed 1 to 2°F. When viewing a real-time hologram, the number of fringe lines did not increase. Obviously then, without a meaningful interference field, fringe anomalies could not be observed. Consequently, this method of straining the motor casing was not pursued.

3.2.3   Chronological Results of Radiative Stressing

Temperature measurements were developed to ascertain magnitudes for heating times with the 3 kilowatt quartz lamp. These data were essential for personnel safety as well as for relative indications of radiative stressing during holographic testing. The temperature specified as safe was 125°F on the casing surface.

The temperature increases at a function of time were developed by scanning the casing hemi-cylinder, facing the hologram plate holder, from a distance of 8 in. The resultant data are reported in Fig. 8. A thermocouple was also detached from the casing for comparison.
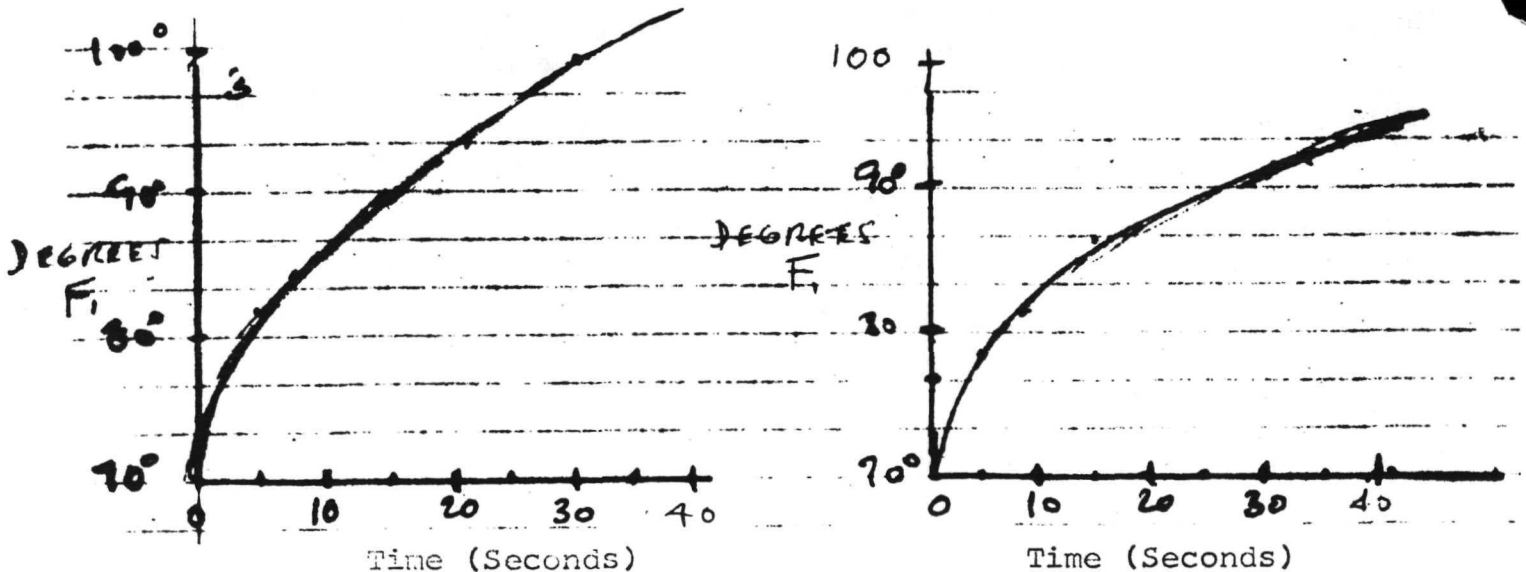
Temperature Rise of Thermocouple Detached from motor casing.

Average Temperature Rise of Thermocouples on motor casing.

Figure 8

3-4

The initial radiative tests undertaken involved the motor orientation shown in Fig. 9. The centerline of the motor is at approximately 100° angle.

A number of holographs were produced to determine optimum fringe contrast for the illumination present. Both Kodak 649F and AGFA-Gevaert 10E75 photographic plates were employed. The latter proved more desirable because of much shorter exposure periods which ranged from 1 to 3 seconds.

The view through one of the holograms is shown in Fig. 10.

It was important to optimize hologram parameters for viewing and photographic reasons.

It was also necessary to generate a fresh hologram each morning since the air-suspended table was lowered at the end of the previous day of testing. The table was operated with bottled nitrogen which leaked 600 pounds of pressure over a 24 hour period making it generally impractical to leave the table raised overnight. The pressure in a full bottle of nitrogen is 2400 psi and, as would be expected, the table movement destroyed the fringe field of a hologram made on the previous day of testing.

Stressing periods of 30 to 40 seconds which raised casing temperatures to a maximum of 90°F obliterated interference fringes. Obviously, excessive displacement occurred as an immediate response to radiative stressing; but, upon cooling, fringes became visible.

During this phase, illumination levels were unsatisfactory; consequently, numerous optical adjustments were instituted. In addition, the alignment mirrors of the He-Ne laser were manipulated to maximize power output at about .097 watts.

Light leakage of the facility was also found to fog holograms, so this problem was corrected. In addition, the temperature of the Kodak HRP development solution also tended, on warm days, to fog holograms.
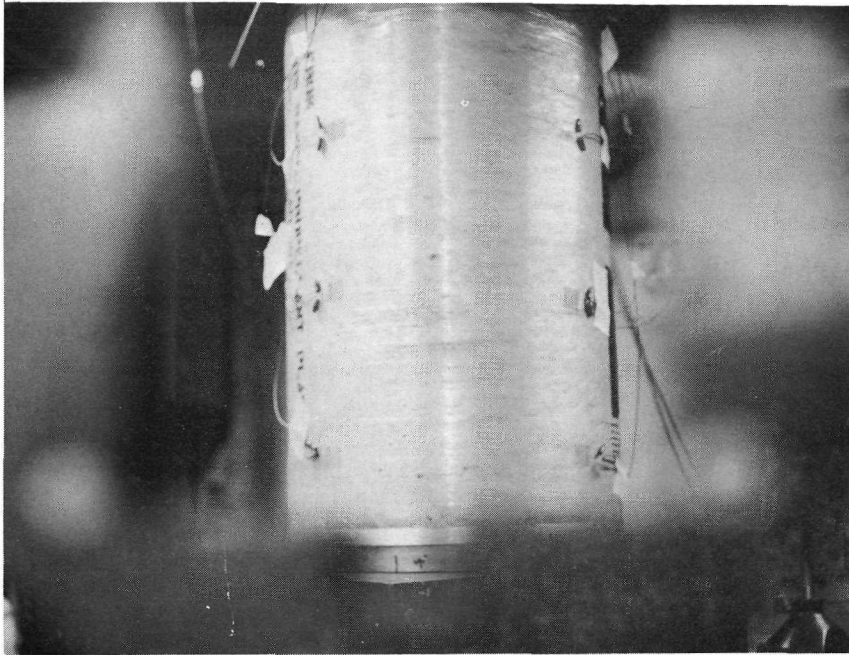
Fig. 9 Motor Case S/N 424 as seen through Hologram Plate Holder Prior to Initiation of Radiative Stressing. Aft end is down
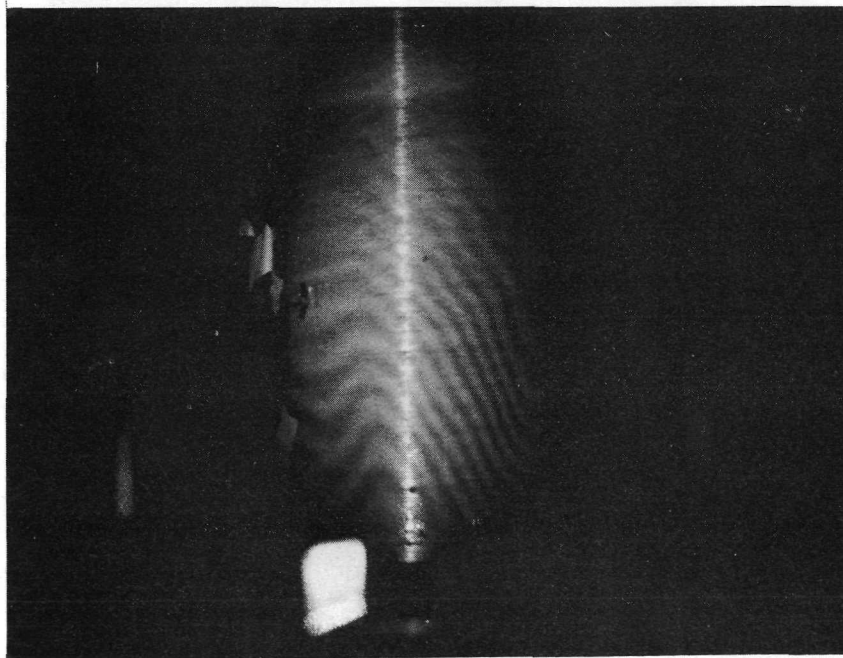

Figure 10 View Through Real-Time Hologram No. 15. Interference Fringes and Spectral Line are Apparent. Square Shaped Area of Light is a Reflection from the Plate Holder.

One of the views, through real-time hologram, seen at this period is shown in Fig. 11.
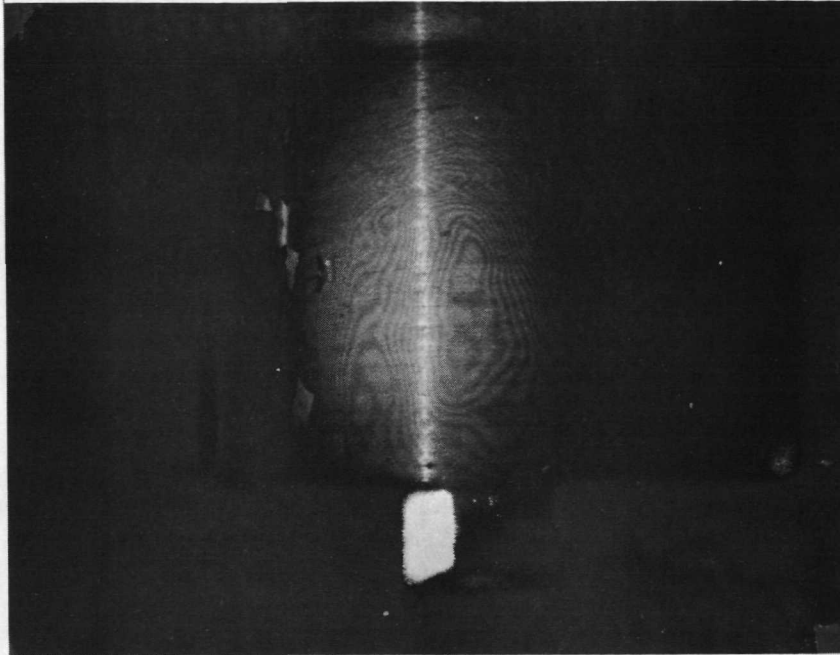

Fig. 11   View Through Hologram No. 22 about 2 min. After Stressing the Casing for 20 sec.

Camera Settings: f27 - 30 seconds

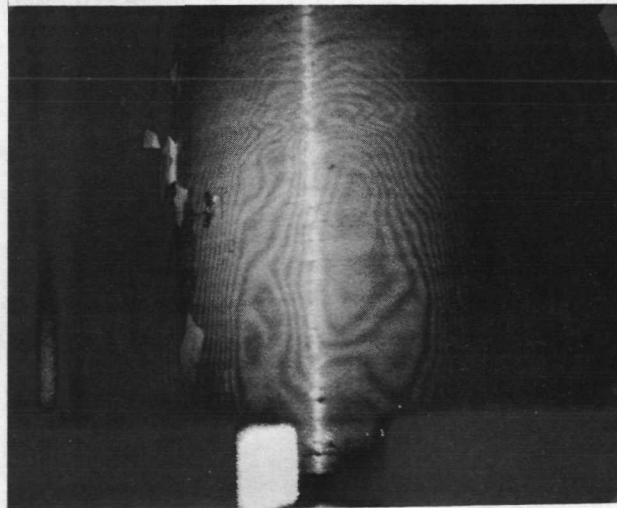Another view through hologram No. 22 about 3 minutes after stressing is shown in Fig. 12.

Fig. 12   Another View Through Hologram No. 22 about 3 min. After Stressing the Casing for 20 sec.

Camera Settings: f27 - 60 seconds

LOCKHEED MISSILES & SPACE COMPANY

About 5 minutes later the motor appeared as shown in Fig. 13. The fringe distortions, rings, bent and spread lines, are numerous. The condition suggested the application of fringe control for defining the size of the area represented by such anomaly.
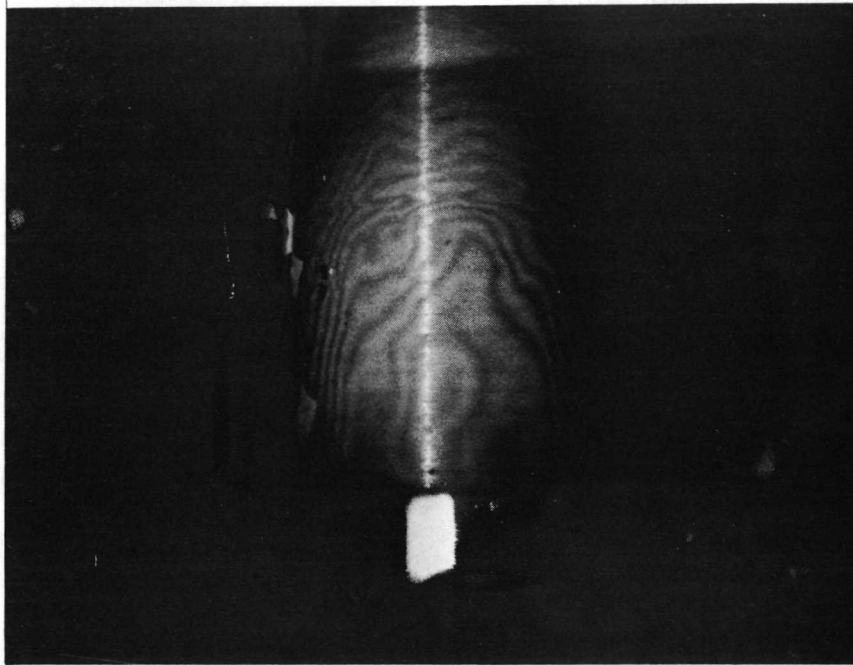

Fig. 13   After 5 min. from Stressing, the Fringe Field
Through Holograms No. 22 Appeared as Shown.
Camera Settings: f27 - 60 sec

To establish the significance of overnight temperature change, the table was left suspended. In observing the motor through hologram No. 22 the following day, the fringe density was found to increase sharply. The density was higher than indicated in Fig. 11. An effort was made to photograph the scene but little success was achieved. The best photograph is shown in Fig. 14.
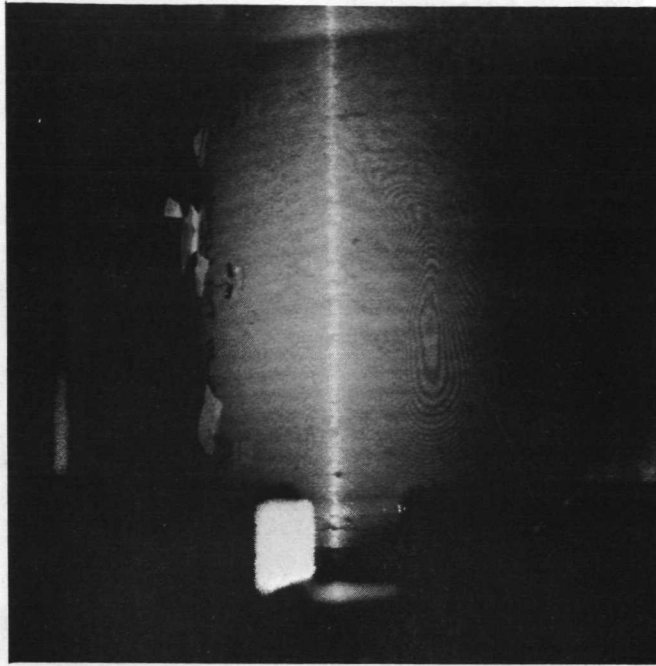
Fig. 14   Photograph Through Hologram No. 22 the Morning
          After Producing the Hologram. High Fringe Density
          Resulted from Ambient Temperature decrease (use
          hand lens for viewing).

                 Camera Settings: f27 - 120 sec

A view through a hologram also made a day later is shown in Fig. 15.

A number of double exposures were attempted. The purpose was to improve photo-
graphy. However, these were unsuccessful. The time necessary for the second
exposure when the casing was stressed was too long. This was approximately 1 sec
using the AGFA plates. The motion of the casing after stressing and during expo-
sure was uniform preventing any observable interference between photographic images.

It was also observed that slight variations in ambient temperature generated high
line densities in real time holograms. A picture through a hologram made an hour
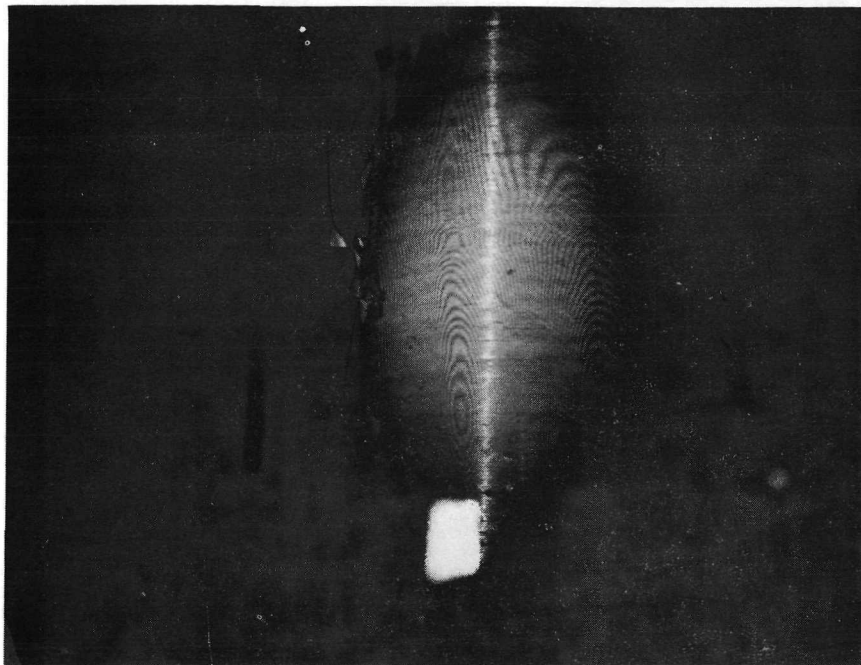earlier before the temperature had risen a few degrees is shown in Fig. 16

Fig. 15   The Fringe Field Resulting from Change in Ambient
Temperature.   Hologram No. 23 was made a Day Before
the Polaroid was taken.
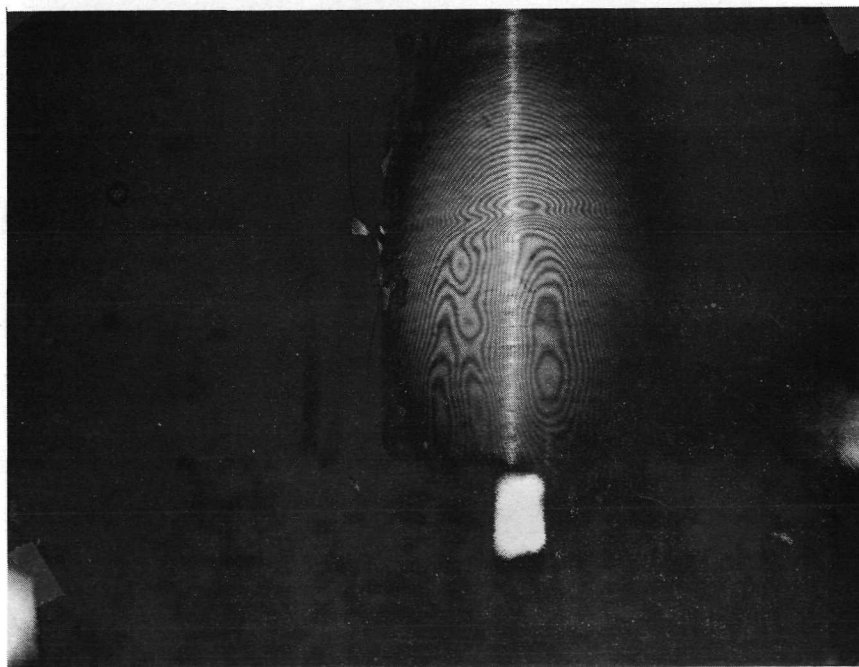
Camera Settings: f27 - 20 sec

Fig. 16   Interference Field Generated After the Ambient Temperature
Rose a Few Degrees in 1 Hour.   Hologram No. 29

Camera Settings: f27 - 10 sec

Another effort to improve photography and to freeze the dynamic fringe behavior associated with real-time testing was undertaken. The technique involved a reverse hologram. This hologram is exposed at the time of radiative stressing and viewed after developing which, of course, is also at a time when the subject has cooled back to ambient temperature. Upon viewing the hologram the fringes remain fixed, occasionally altered by ambient temperature variations. However, early attempts were unsatisfactory for the identical reason double exposures were not successful. The motor movement during exposure of the photographic plate precluded fringe information. This difficulty was resolved by finding the optimum times to stress the casing and expose the plate. A number of trial and error tests solved the problem. Fig. 17 shows a view through a reverse hologram made 4 min. after stressing for a 30 sec period.
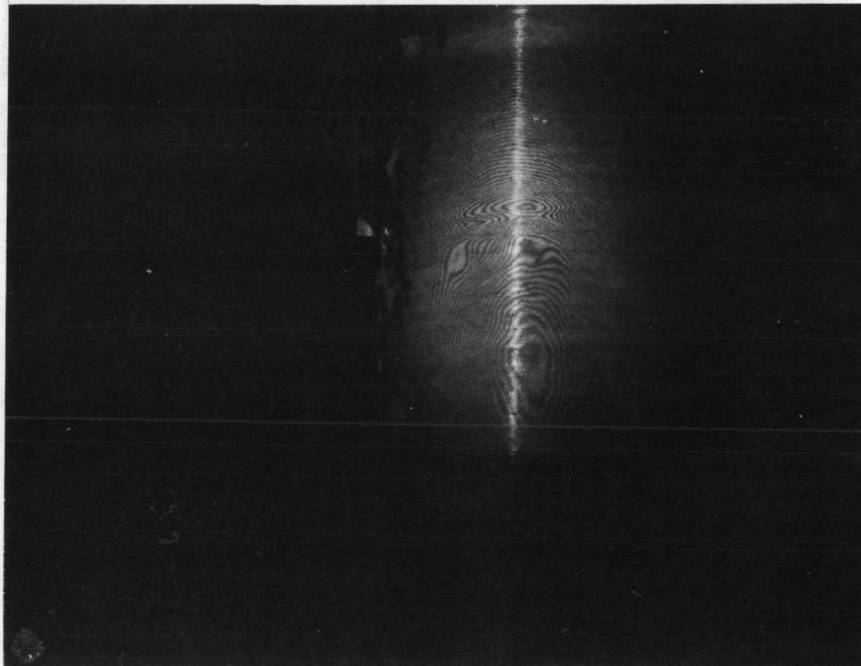

Fig. 17 View Through Hologram No. 33 Made in Reverse. Casing Was Heated for 30 sec and the Hologram Was Made 4 min. later

Camera Settings: f27 - 10 sec

The interference pattern of Fig. 17 shows an anomaly that suggested an area of bondline separation. To verify the location of an anomaly, on the casing was placed 1/4" wide black tape. A photograph of the taped motor can be seen in Fig. 18.
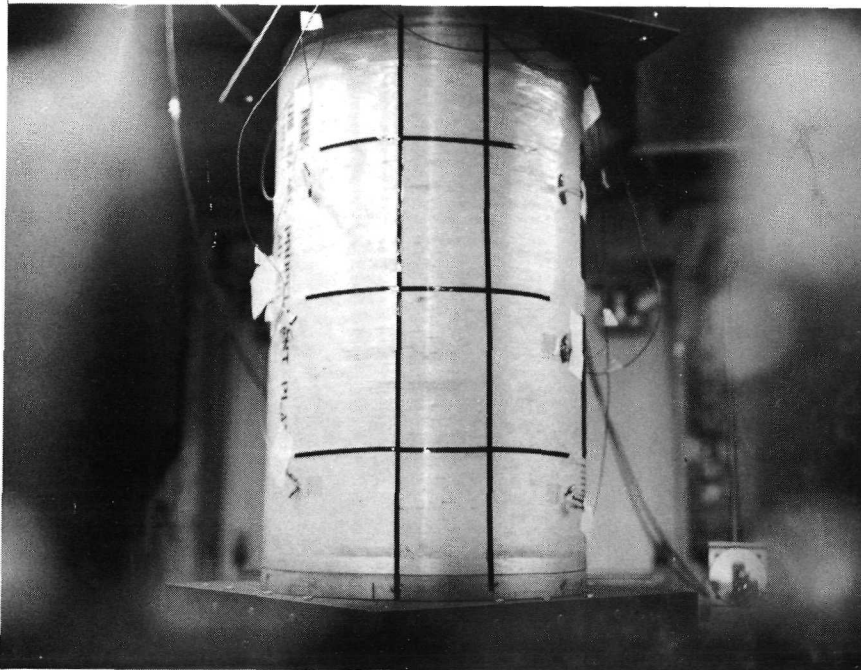

Fig. 18 Location of 1/4 in. wide Tape for Defining Position of Fringe Anomalies. Vertical Line on Left is at 120° and the other at 90°

A temperature recording was also made over a weekend to obtain an estimate on excursions that the motor case experiences over a 24 hour period. A HYGRO-Thermograph was used. The unit also records humidity which can be seen in the graph of Fig. 19.
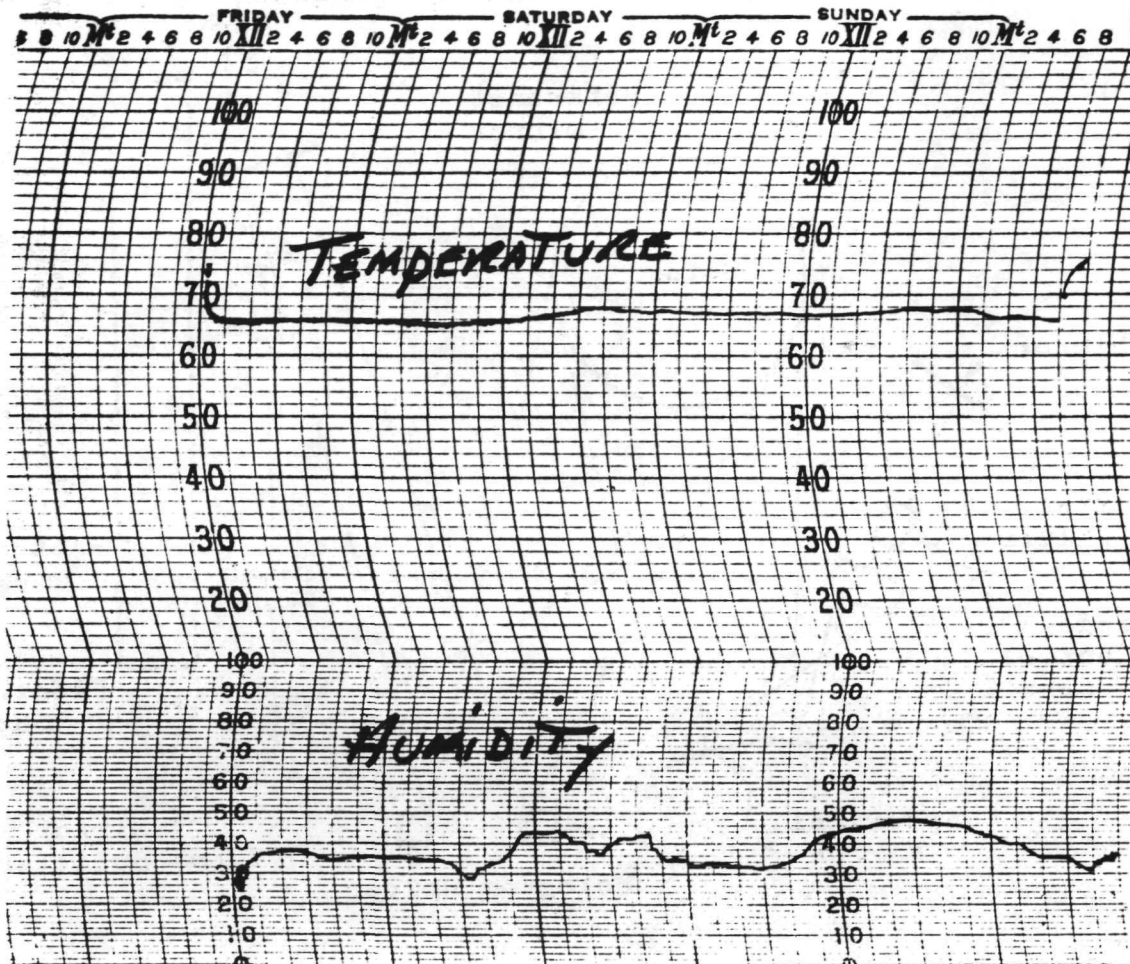
Fig. 19   Traces of Temperature and Humidity in Room
Where Holography Was Performed

The temperature ranged from 65°F to 69°F. The temperature tends to be higher in the afternoons than the mornings which is consistent with the results of reverse holograms.

The optics were manipulated and adjusted to perform fringe control. After numerous trial and error tests to maximize object-beam intensity and area of illumination, the scheme in Fig. 20 was arrived at.
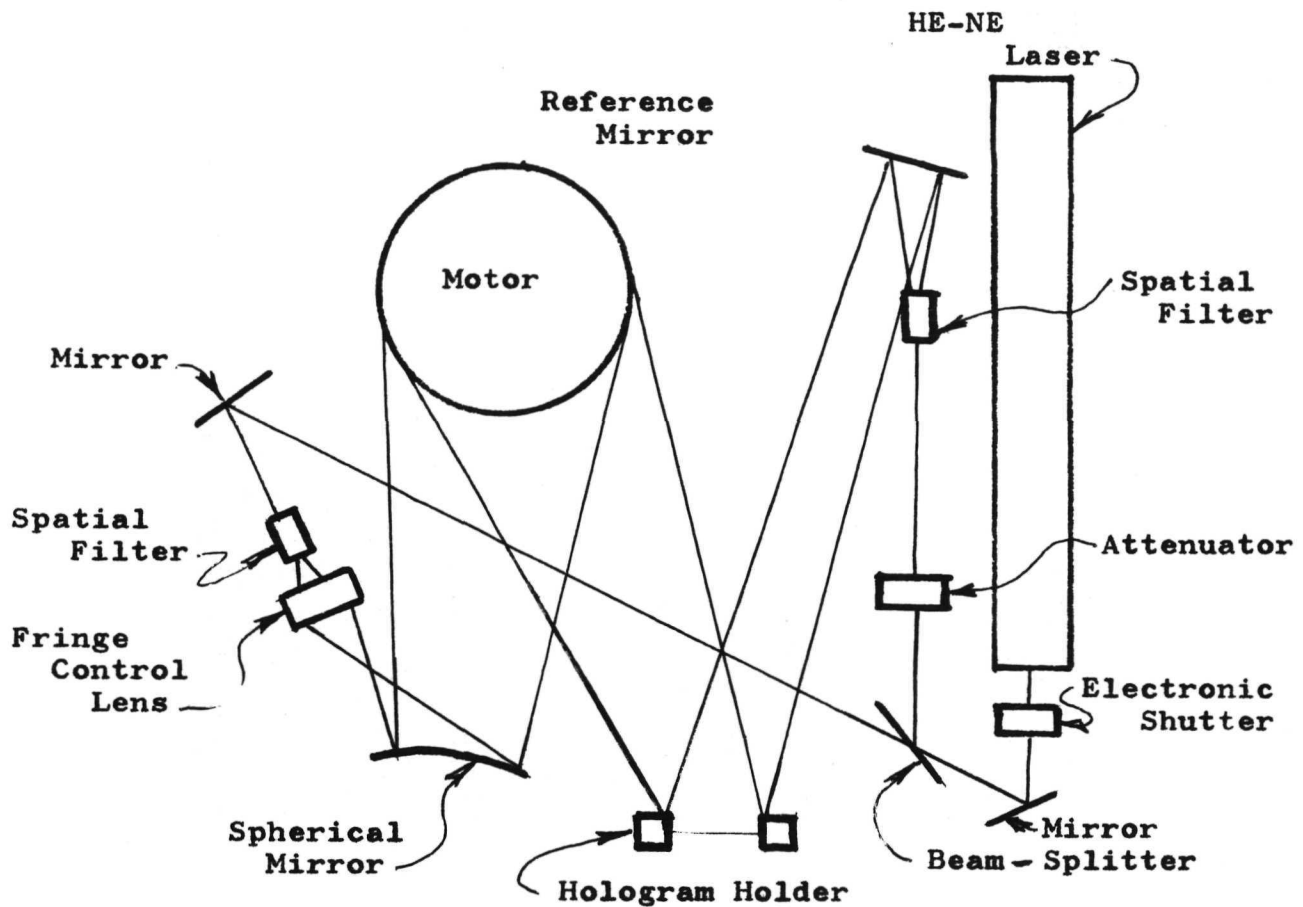
Fig. 20   Arrangement of Optical Components of Holography
System to Perform Fringe Control

In applying fringe control optics, two detracting complications arose. First, the
rather long object beam length sharply reduced the intensity of the light reflected
from the motor.   Second, the diverging lens of the fringe control system reduced
the useful cone of light coming from the spatial filter which illuminated less than
one-half of the casing surface.   Much effort was undertaken to remedy these problems,
but with little success.   When working with large areas in holography, it is impor-
tant to maximize the field of fringes to be able to distinguish anomalies that
indicate subsurface conditions from normal line distortions caused by geometry.   In
general, the greater the fringe field, in relation to the workpiece, the more fringe
information available for analysis.   The fringe control system functioned satis-
factory in real-time and reverse holograms for the area illuminated.   However, the

3-14

fringe fields were too small for analysis. An example of the illuminated area size resulting from the insertion of fringe control can be seen in Fig. 21.
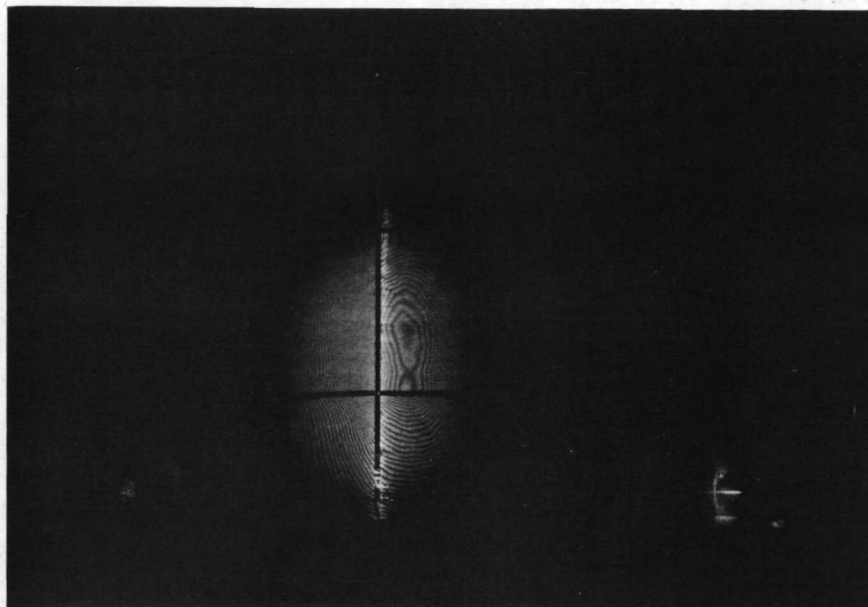

Fig. 21   Photograph of Area Illuminated When Fringe Control
System is Inserted in the Object Beam of Holographi
Optics.

The use of fringe control was abandoned. At this time an effort was made to improve the illumination for photography by repositioning pinholes of the spatial filters and experimenting with reference beam/object beam intensity ratios. Also, the placement of the plate holder and polaroid camera were improved. A number of holograms, real-time, reverse and double exposure were made. However, the illumination available for photography did not increase but was generally unchanged. Also, a problem was encountered with coherency of the object and reference beams due to the mounting of the plate holder above the plane of the two beams. Filing corners on the aluminum mounting block solved the coherency problem which, of course, turned out to be caused by vibration of the plate holder and not a coherency problem as first presumed.

There was only one certain answer to the low illumination levels and that was to coat the casing with a reflective coating. To accomplish this, penetrant developer was sprayed over the surface from an aerosol can. The developer used was Type SKD-NF manufactured by the Magnaflux Corporation. A Polaroid of the coated motor can be seen in Fig. 22.
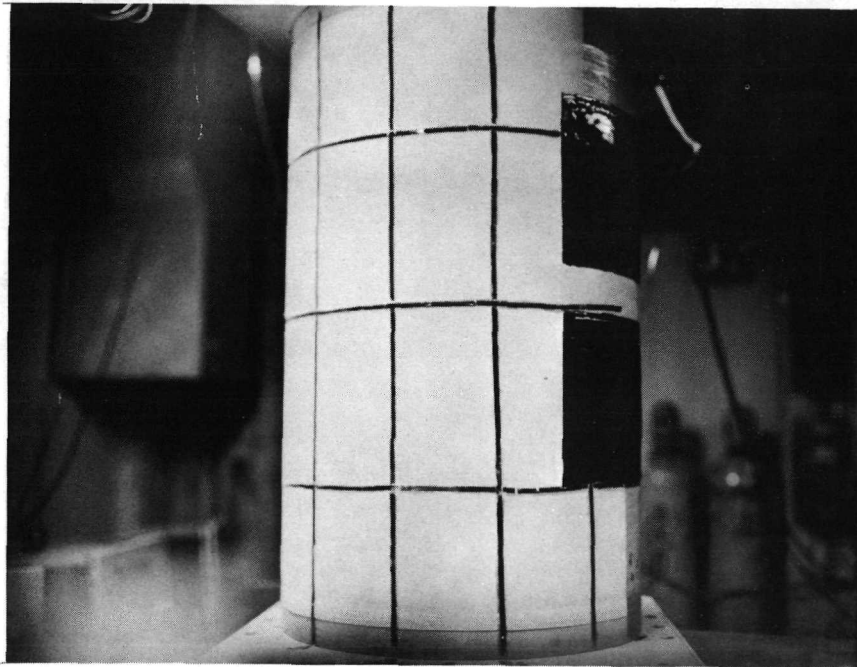

Fig. 22 Picture Through Plate Holder of Casing S/N 424 as it Appeared After Spraying with Penetrant Developer. Black Vertical Lines Repres ent the 150°, 120°, 90° and 60° Positions

A photograph through one of the first real-time holograms made after coating the motor can be seen in Fig. 23. The illumination level has increased by a factor of three.

LOCKHEED MISSILES & SPACE COMPANY
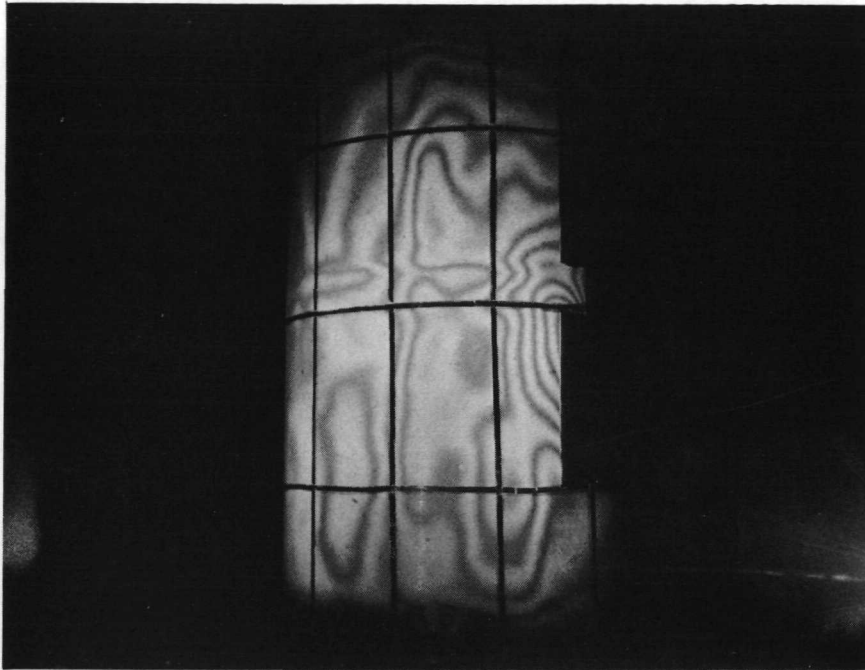
Fig. 23   Increase in Illumination Level Resulted from
           Application of Reflective Coating. View
           Through Real-Time Hologram No. 96 Before
           Stressing

                Camera Settings: f16 - 5 sec

The interference field in Fig. 23 was caused by emulsion shrinkage when the
hologram underwent development. Room temperature fluctuations may also have
affected the interference field.

The casing was stressed for varying periods. One of the Polaroids made is shown
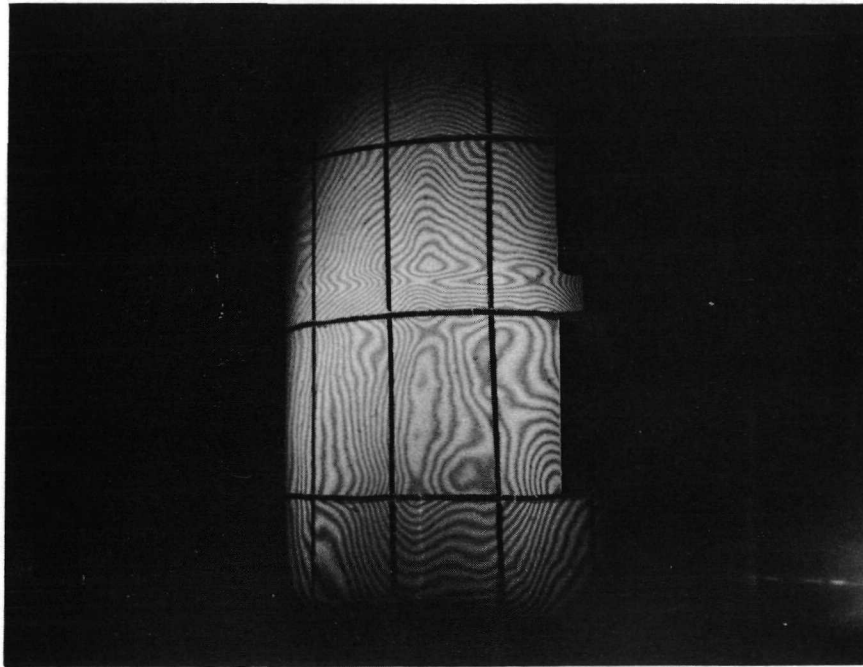in Fig. 24.

Fig. 24   Stressing for 5 sec Produced this Interference Field.
The Photograph Was Taken 30 sec Later Using Hologram
No. 96

Camera Settings: f16 - 2 sec

The casing was stressed for increasingly longer periods. The interference
pattern effected by 10 sec with the quartz lamp is shown in the subsequent
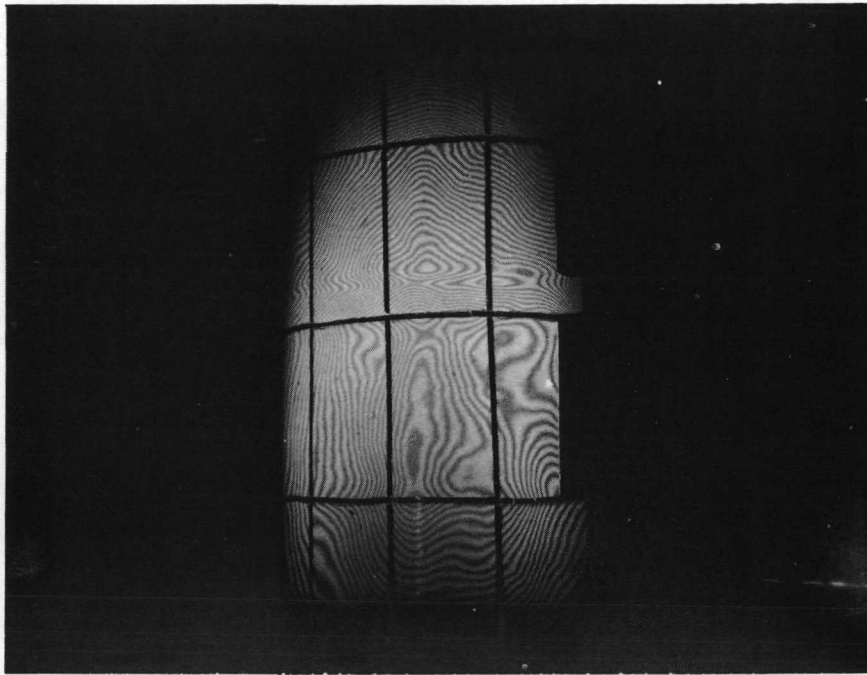figure.

Fig. 25   Stressing for 10 sec Created This Fringe Field.
The Polaroid was Taken About 15 sec Afterwards

Camera Settings: f16 - 2 sec

For a 15 sec heating period, the fringe field appeared as revealed by Fig. 26

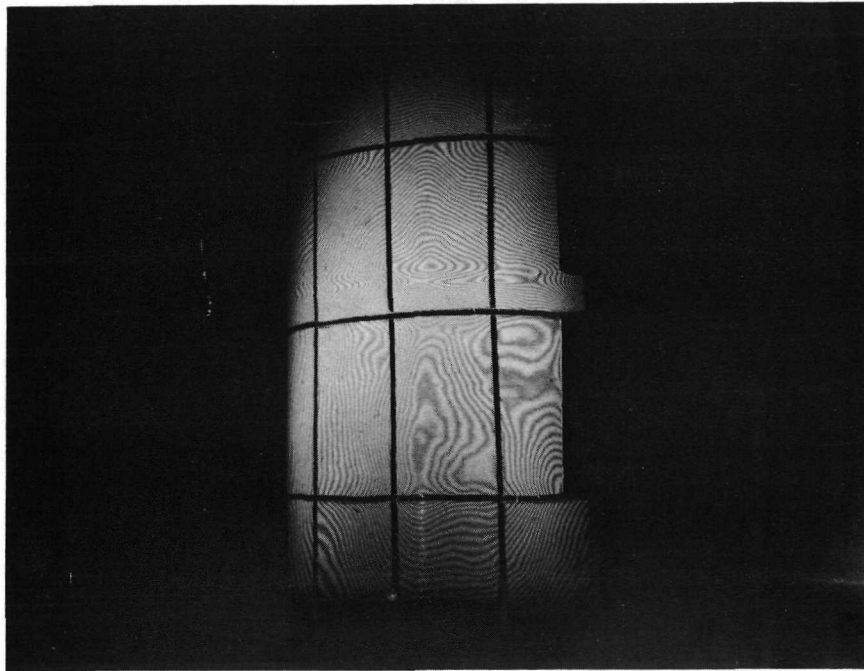LOCKHEED MISSILES & SPACE COMPANY

Fig. 26   Interference Field As Seen Through Hologram No. 96
Some 15 sec After Heating the Motor Surface

Camera Settings: f16 - 2 sec

The line density continued to go up but the fringe pattern remained constant. The
view after 20 sec of stressing can be observed in Fig. 27

LOCKHEED MISSILES & SPACE COMPANY

Fig. 27   The Line Density Increase After 20 sec of Stressing.
(Employ hand lens for viewing). The View Represents
the Scene 10 sec Later.

Camera Settings: f16 - 1-1/2 sec

In the previous photograph, it is apparent that 20 sec of stressing almost causes
sufficient displacement to destroy first order interference. As the casing cools,
as expected, the quantity of fringes decreases. Fig. 28 shows fringes 15 sec
after the Polaroid of Fig. 27 was exposed.

Fig. 28   Polaroid Exposed 15 sec After Taking Fig. 27.
The Time from Stressing the Casing is 25 sec
Camera Settings: f16 - 1-1/2 sec

A reverse hologram was attempted. It was made about 15 sec after heating the motor for 20 sec.   The hologram was satisfactory and a Polaroid was taken as shown in Fig. 29.
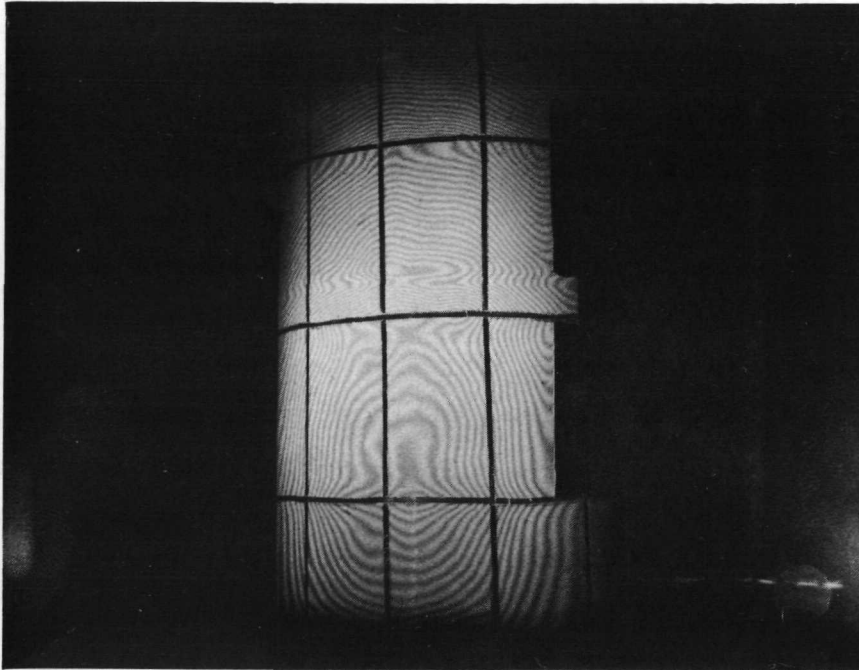
Fig. 29   Scene Through Reverse Hologram No. 98 Which Was
           Made After Heating the Casing for 20 sec. The
           Picture was Taken 25 min. later

Camera Settings: f27 - 15 sec

The advantage of utilizing reverse holograms for photography can be appreciated
by contrasting Figs. 28 and 29. Obviously, the casing in a static condition
permits long Polaroid exposure times.

The interference fields between Figs. 26 and 29 show some differences. The
reason being that a real-time view represents the instantaneous displacement
whereas a reverse hologram reflects a summation of casing displacements.

Another reverse hologram was similar to No. 98 but the stressing time was 30 sec. The resultant fringe pattern, although greater in line density, had identical forms.

An analyses of real-time stressing behavior suggested that the displacement was caused by differential expansion across sections exhibiting variations in epoxy content. Since epoxy has a coefficient of expansion 5 times greater than fiber-glass, areas deficient in epoxy displace less than adjacent areas. Previous testing with glass/epoxy matrices has substantiated this condition. The thermal response of the casing was minimized by use of the reverse hologram. It was also predicted that cyclic heating combined with reverse holograms would further reduce any thermal response of the casing. In addition, holograms made at ambient tempera-tures greater than the viewing temperatures should also reduce casing cross-sectional response. Work was first begun on this latter approach.

One of the initial holograms made using a time delay of about 18 hours and a temperature differential of 7°F produced the interference field pictured in Fig. 30.

Another view through a hologram which occurred for a temperature decrease of 5°F and a two day delay can be seen in Fig. 31.

The motor was subsequently rotated to the position where separation between liner and propellant was reported in the NASA investigation. The location of the separa-tion began at 277-1/2 degrees and continued radially to 327-1/2 degrees as can be seen in the x-ray results on NPP-424 included in the appendix. In the axially direction it was located in the lower half of the cylindrical section. The posi-tion of the motor after rotation, as it appeared through the hologram plate holder, can be seen in Fig. 32.

The three black areas are tape squares placed over holes drilled previously for repair tests. In the center of the squares is the igniter. The repair procedure involved pumping epoxy by regulated air pressure through a flexible tubing into a lower hole which is not visible. Resin flows upward and outward expelling air
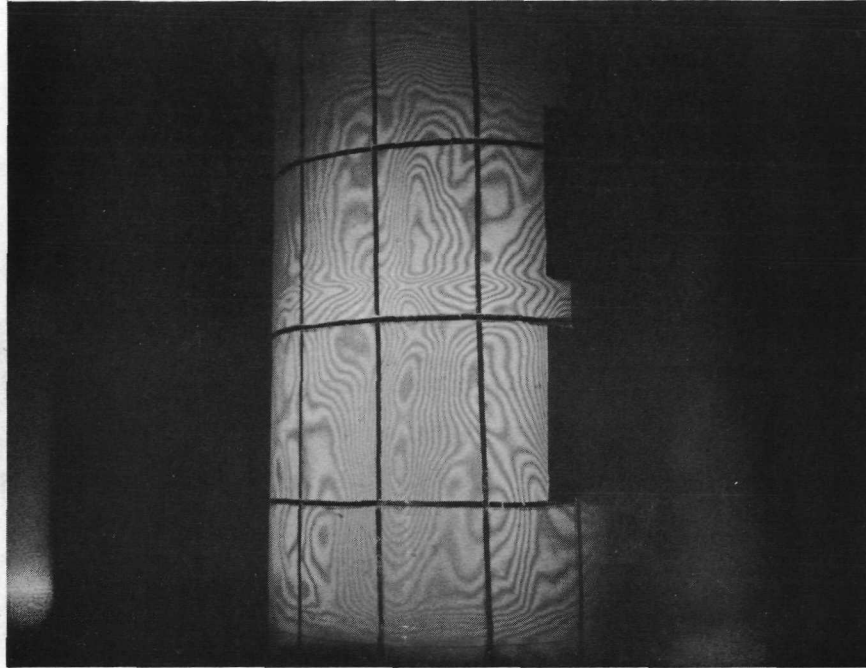
Fig. 30   A View Through Hologram No. 103. It Was Exposed When
          the Ambient Temperature was at 80°F. The Following Day
          the Temperature was 73°F. When the Polaroid Was Taken.
          Vertical Lines From Left to Right: 120°, 90°, 60° and 30°
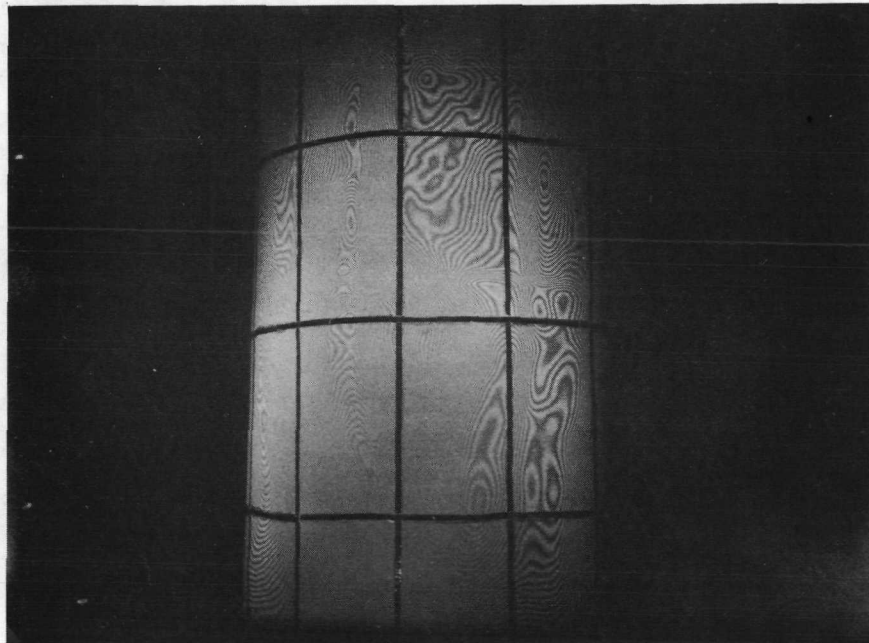
Camera Settings: f16 - 10 sec

Fig. 31   Hologram No. 112 Revealed Complex Fringe Field Two
          Days Later. Ambient Temperature had Dropped 5°F.
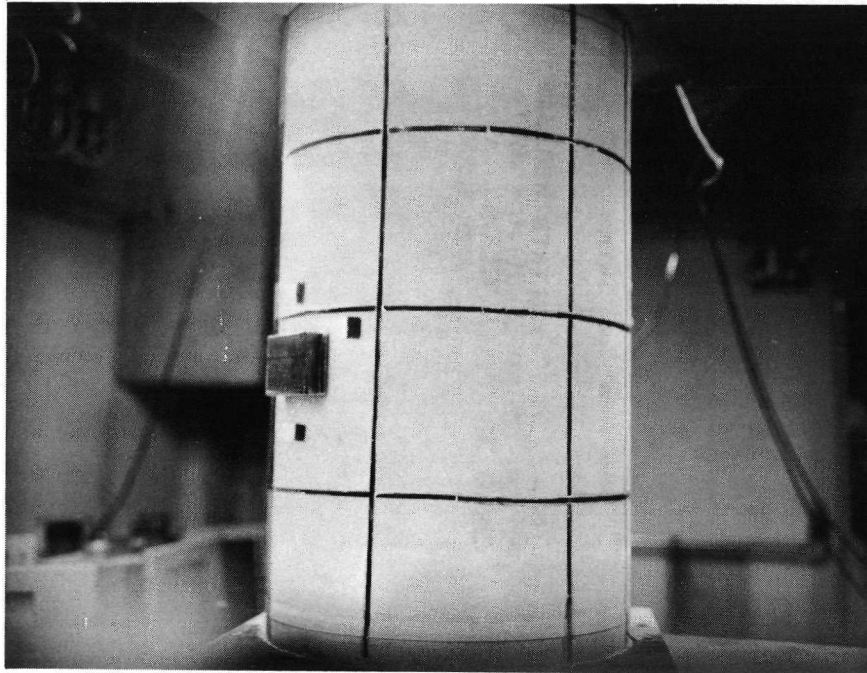
Camera Settings: f22 - 4 sec

Fig. 32 Motor Case Rotated for Holographic Analysis of Area
Reported Separated. Vertical Lines Left to Right:
270° and 210°

from the drilled holes. The repair attempted on this motor was unsuccessful.
Ostensibly, epoxy could not be forced through the fill hole. However, after
conditioning the motor to a temperature of 40°F it was possible to blow air into
all the holes. Therefore, the separation, as reported in the NASA radiography
document existed for the holography program. But the accuracy of the documented
area of separation did not seem consistent with the hole position seen at the
right in Fig. 32. This hole was located at the 304° radial position and the
separation reportedly began at 307-1/2°.

LOCKHEED MISSILES & SPACE COMPANY

A reverse hologram was one of the first efforts on the area of known separation. It involved a 2°F temperature drop over a 16 hour period. A photograph through the hologram can be seen in Fig. 33.
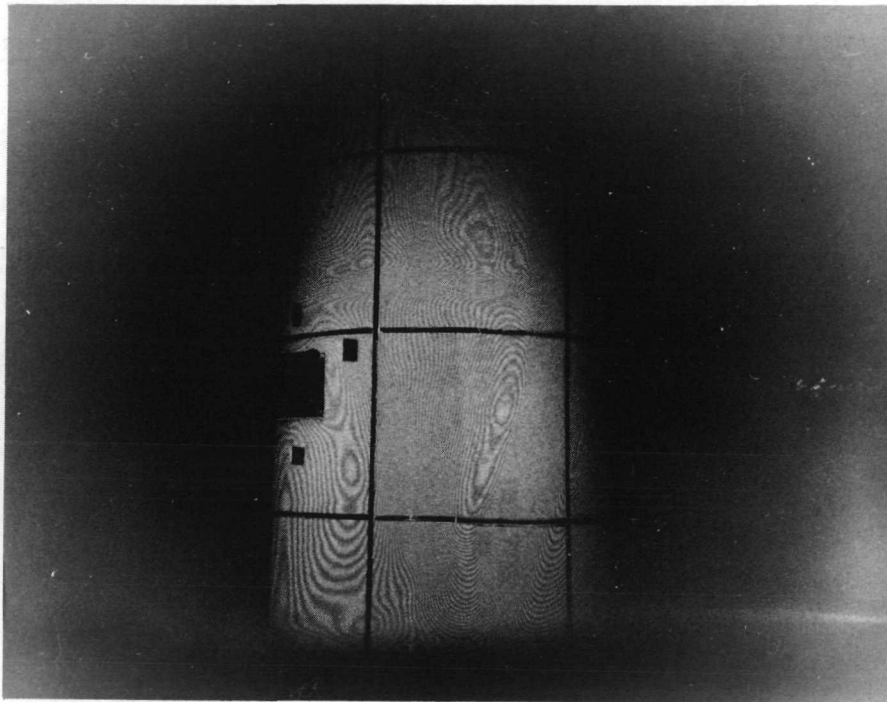

Fig. 33 View in Hologram No. 120 a Day After Exposure.
Ambient Temperature Decreased 2°F.

Camera Settings: f22 - 3 sec

Other reverse holograms showed formations similar to Fig. 33.

Cyclic heating tests were performed by stressing the hemi-cylinder facing the hologram plate holder.   Radiative heating was confined to scanning the length of the cylinder over a 120° to 150° area.

3-27

The procedure consisted of periodic heating and finally making a reverse hologram. Holograms were sometimes made between cycles as well as a real-time hologram before the first cycle.

The following sequence was used for cyclic heat test No. IT.

CYCLIC HEAT TEST NO. IT

	Operation	Elapsed Time
1.	Exposed Real-Time Hologram No. 123	--
2.	20 Seconds of Heat	0
3.	" " "	5 minutes
4.	" " "	12 minutes
5.	" " "	18 minutes
6.	Exposed Reverse Hologram No. 124	29 minutes

A photograph was taken through the real-time hologram No. 123 about 2 min. after the first heat cycle. The interference pattern appeared as shown in Fig. 34.
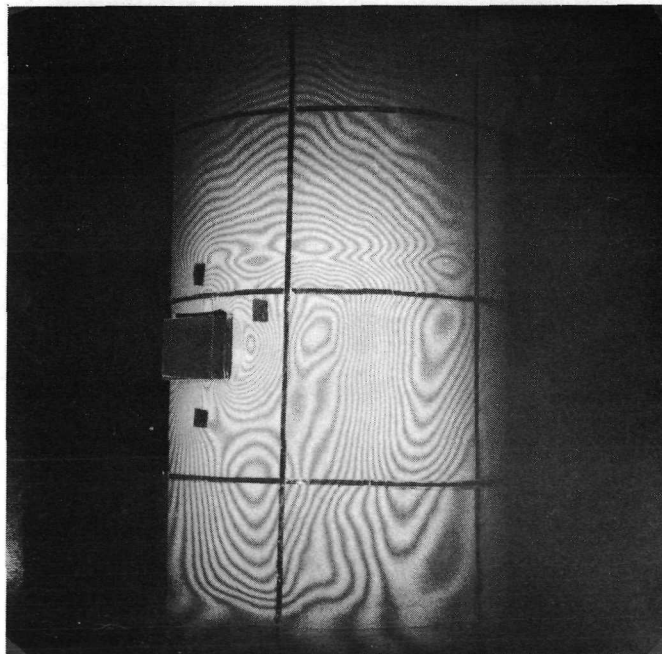

Fig. 34 Fringe Field as it Appeared Through Real-Time Hologram No. 123 2 min. After First Heat Cycle

Camera Settings: f16 - 3 sec

LOCKHEED MISSILES & SPACE COMPANY

The line density continued to increase after each heat cycle as would be expected.
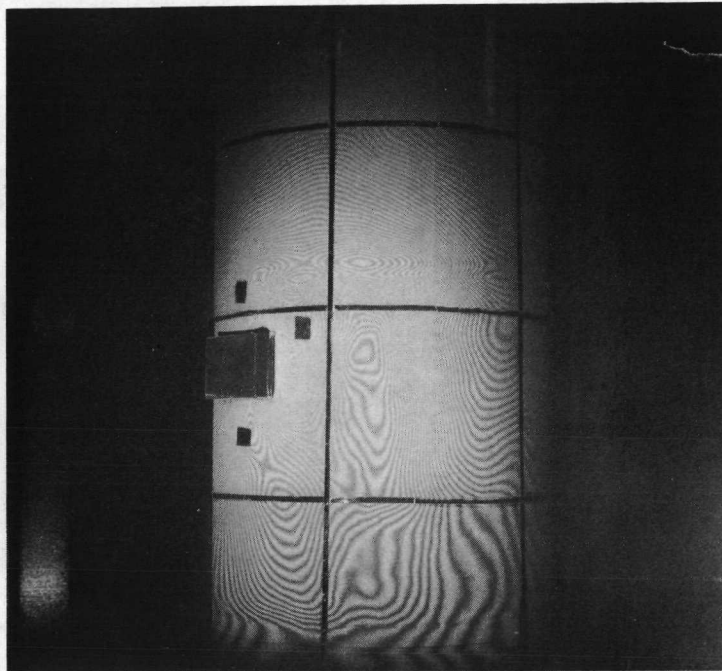The view 2 min. past the second heat cycle looked like Fig. 35.

Fig. 35   After the Second Heat Cycle the Fringe Field Through
Real-Time Hologram No. 123 Shown Above Occurred

Camera Settings: f16 - 3 sec

Polaroids were taken two minutes after the final 2 heat cycles also. They are
included as Figs. 36 and 37.

LOCKHEED MISSILES & SPACE COMPANY
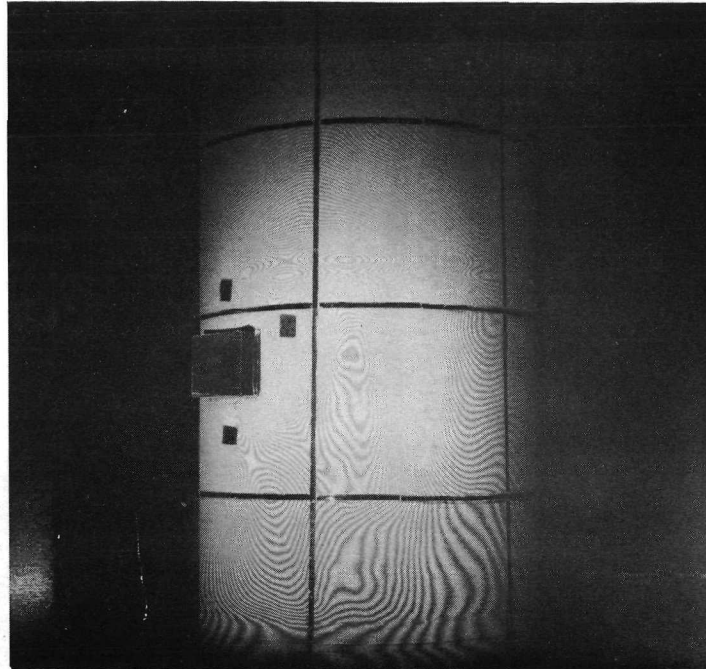
Fig. 36   Hologram No. 123 Revealed this Fringe Field 2 min.
           After the Third Heat Cycle

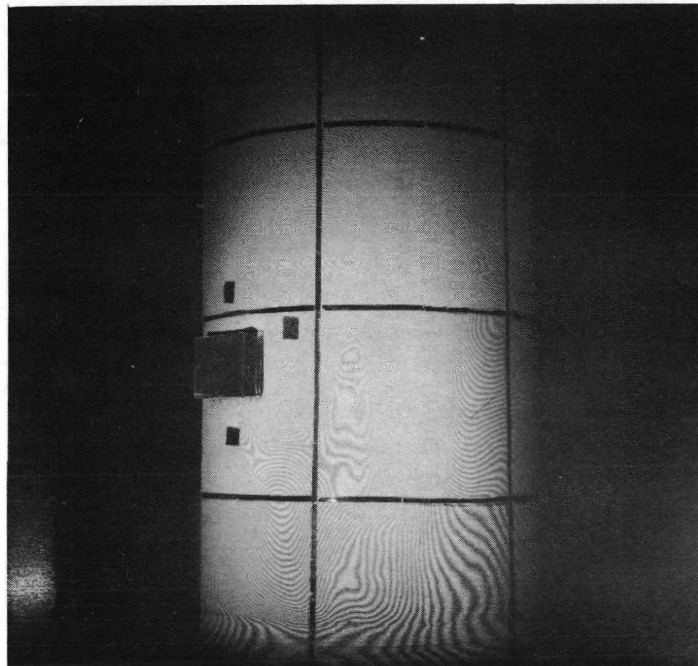Camera Settings: f16 - 3 sec

Fig. 37   The Final Heat Cycle Generated a Complex Fringe
           Field 2 min. After Heat Application in Hologram No. 123

Camera Settings: F16 - 3 sec

The interference field through the reverse hologram No. 124 had a much different interference pattern 9 minutes after exposure and development. The Polaroid taken at that time is shown in Fig. 38.
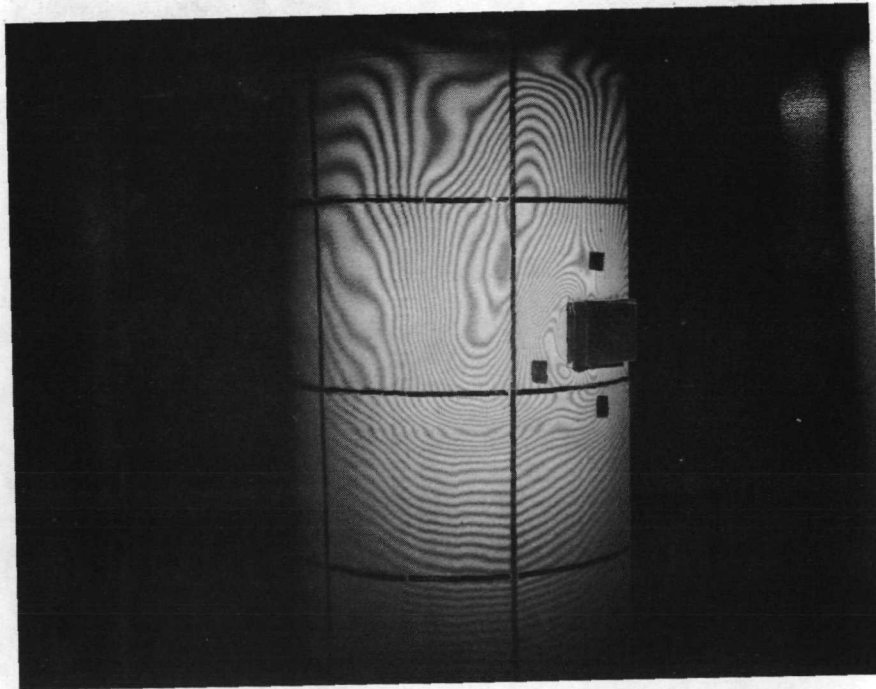

Fig. 38   View in Reverse Hologram No. 124 as it Appeared 20 min. from Cyclic Heating

Camera Settings: f16 - 3 sec

Hologram No. 124 showed a similar fringe field the next day in which the line density increased significantly. The change can be seen in Fig. 39.

LOCKHEED MISSILES & SPACE COMPANY
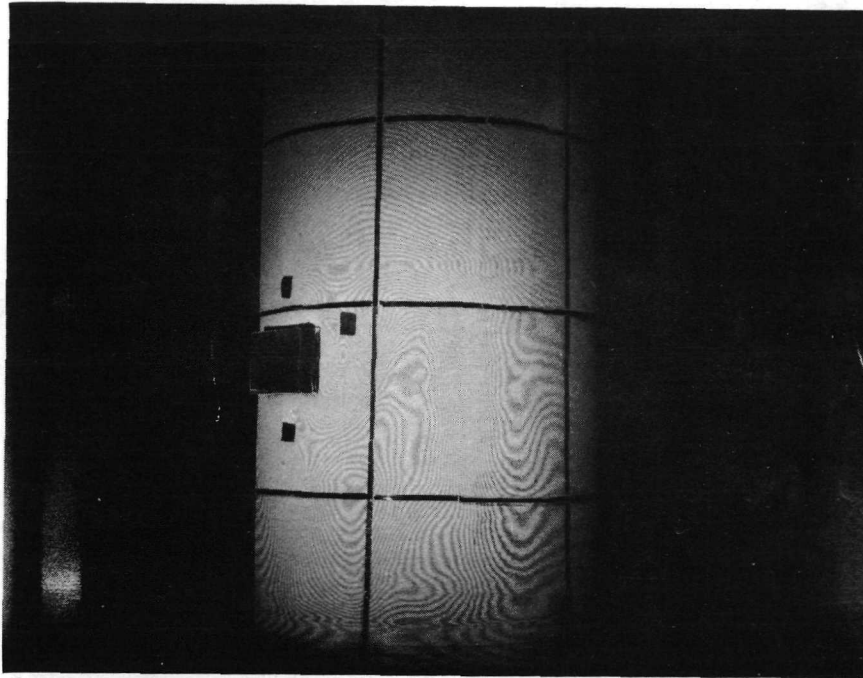
Fig. 39 Fringe Lines Increased in Hologram No. 124 a Day
Later. Correlation with Previous Figure Shows
Pattern Remained Constant

Camera Settings: f22 - 6 sec

Another cyclic heating test, No. 2T, was performed in accordance with the following procedure.

CYCLIC HEAT TEST NO. 2T

Operation				Elapsed Time
1. 40 seconds of heat				0
2. "	"	"	"	5 minutes
3. "	"	"	"	10 minutes
4. "	"	"	"	15 minutes
5. Exposed Reverse Hologram No. 126				20 minutes

3-32

The developed hologram No. 126 was absent of fringes. The motor casing displacement
apparently destroyed first order fringes in the period between making the hologram
and viewing it 29 min. later.

To acquire data on extent of casing movement, a study employing a real-time hologram
was undertaken. A stressing period of 40 sec. was applied over the entire cylin-
drical surface. The first satisfactory hologram was No. 127. A picture through it
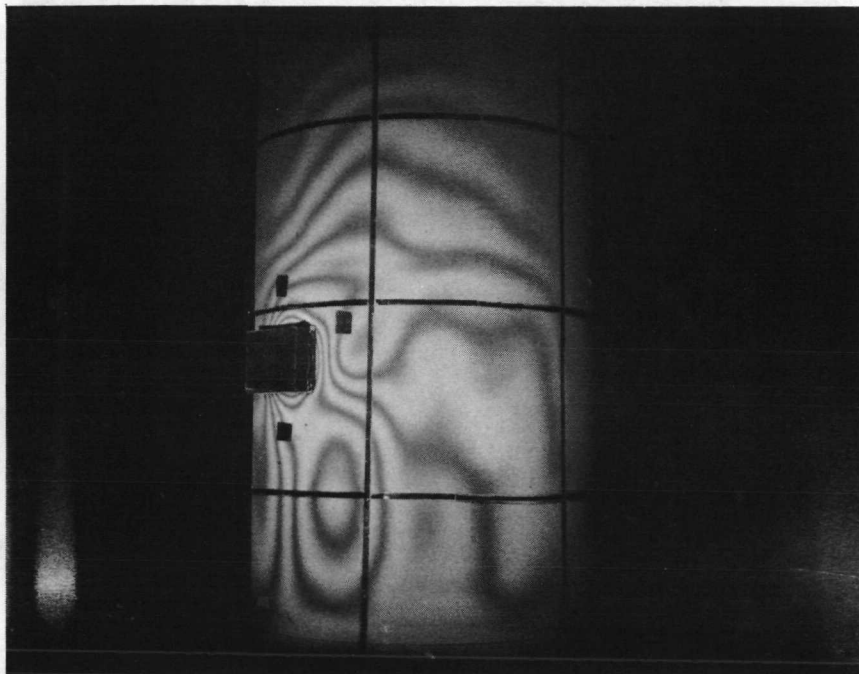before case stressing is included as Fig. 40.

Fig. 40   Real-Time Hologram No. 127 Showing Interference
Pattern Prior to Stressing

Camera Settings: F16 - 3 sec

LOCKHEED MISSILES & SPACE COMPANY

After photographing the picture in Fig. 40, the casing was heated for 40 sec. A series of Polaroids were taken at varying times from stressing. The figs. 41, 42, 43, 44, 45, 46, 47, 48, 59, 50, and 51 illustrate the resultant strain patterns.

Fig. 41   Photograph Through Real-Time Hologram No. 127 2 min. After a 40 sec Radiative Stressing of the Cylindrical Casing

Camera Setting: f16 - 3 sec

Fig. 42   Photograph Through Real-Time Hologram No. 127 3 min.
After a 40 sec Radiative Stressing of the Cylindrical
Casing

Camera Settings: f16 - 3 sec

Fig. 43   Photograph Through Real-Time Hologram No. 127 5 min.
after a 40 sec Radiative Stressing of the Cylindrical
Casing

Camera Settings: f16 - 3 sec

Fig. 44   Photograph Through Real-Time Hologram No. 127 7 min.
After a 40 sec Radiative Stressing of the Cylindrical
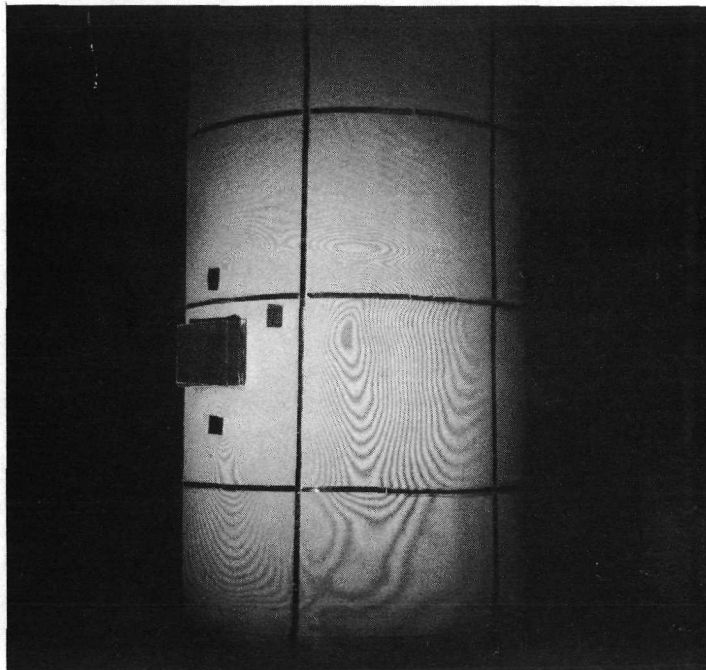Casing

Camera Settings: f16 - 3 sec

Fig. 45   Photograph Through Real-Time Hologram No. 127 9 min.
After a 40 sec Radiative Stressing of the Cylindrical
Casing

Camera Settings: f16 - 3 sec

Fig. 46   Photograph Through Real-Time Hologram No. 127 11 min.
After a 40 sec Radiative Stressing of the Cylindrical
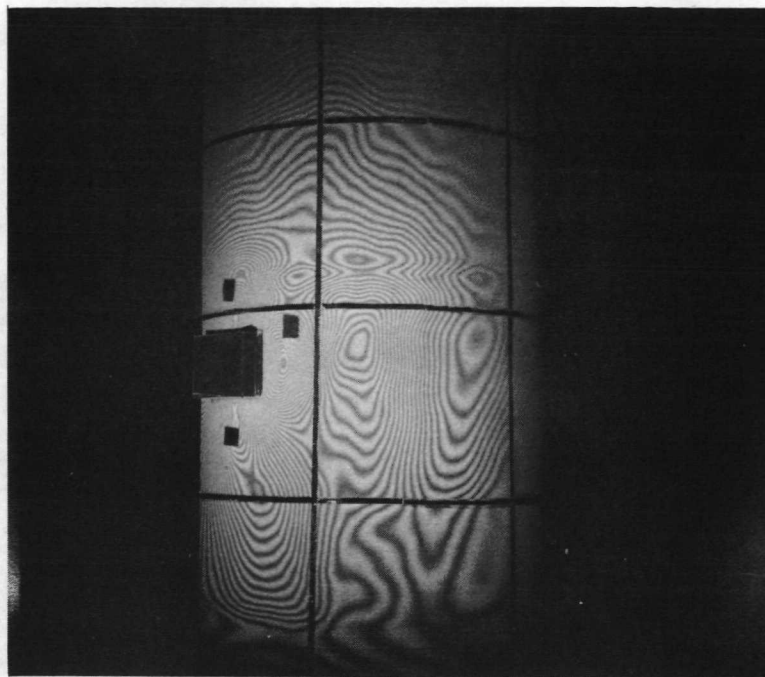Casing

Camera Settings: f16 - 3 sec

Fig. 47   Photograph Through Real-Time Hologram No. 127 15 min.
After a 40 sec Radiative Stressing of the Cylindrical
Casing

Camera Settings: f16 - 3 sec

Fig. 48   Photograph Thrugh Real-Time Hologram No. 127 19 min.
After a 40 sec Radiative Stressing of the Cylindrical
Casing

Camera Settings: f16 - 3 sec
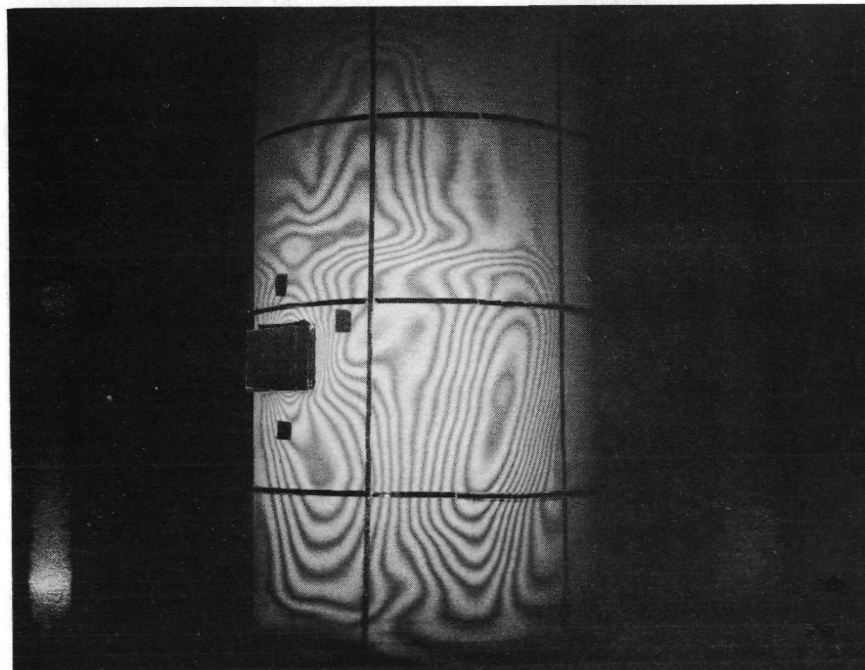
Fig. 49   Pnotograph Through Real-Time Hologram No. 127 23 min.
After a 40 sec Radiative Stressing of the Cylindrical
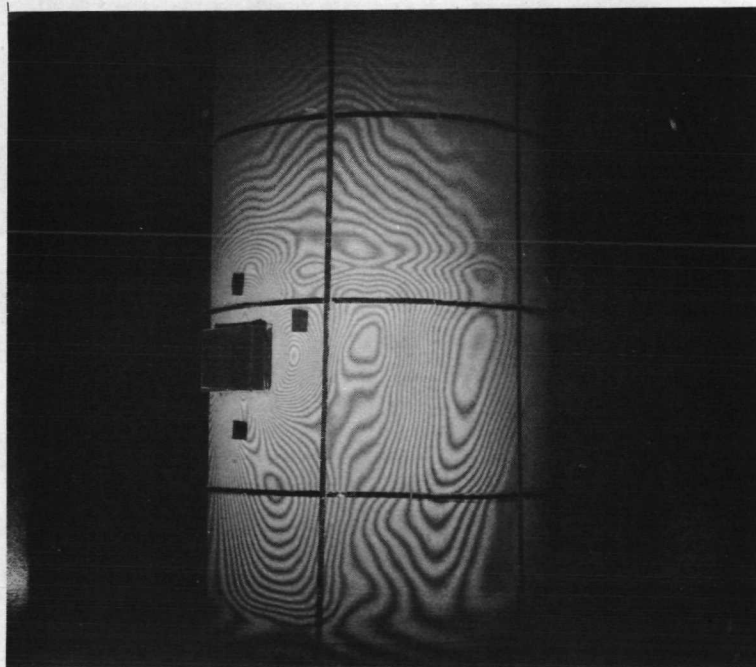Casing
Camera Settings: f16 - 3 sec
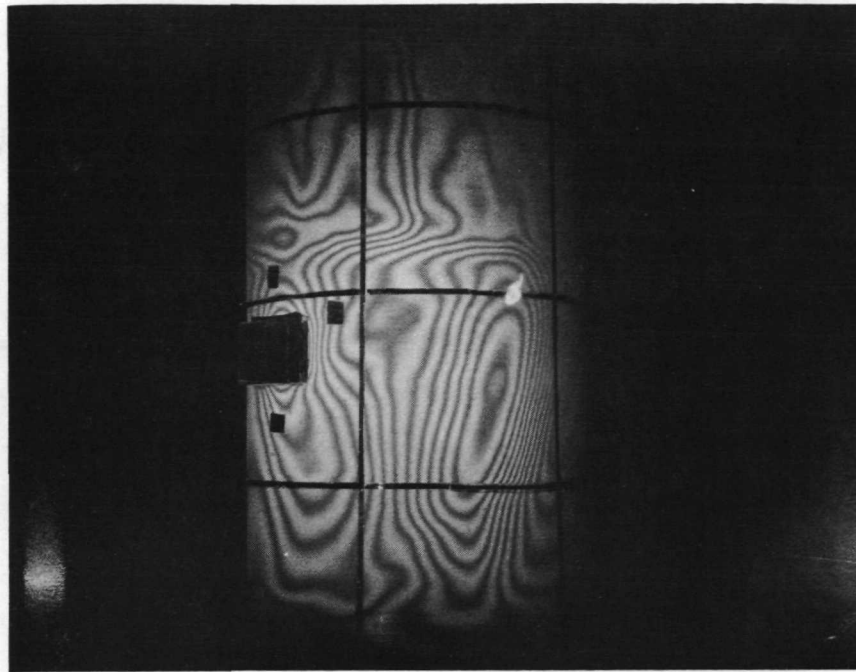
Fig. 50   Photograph Through Real-Time Hologram No. 127 30 min.
           After a 40 sec Radiative Stressing of the Cylindrical
           Casing

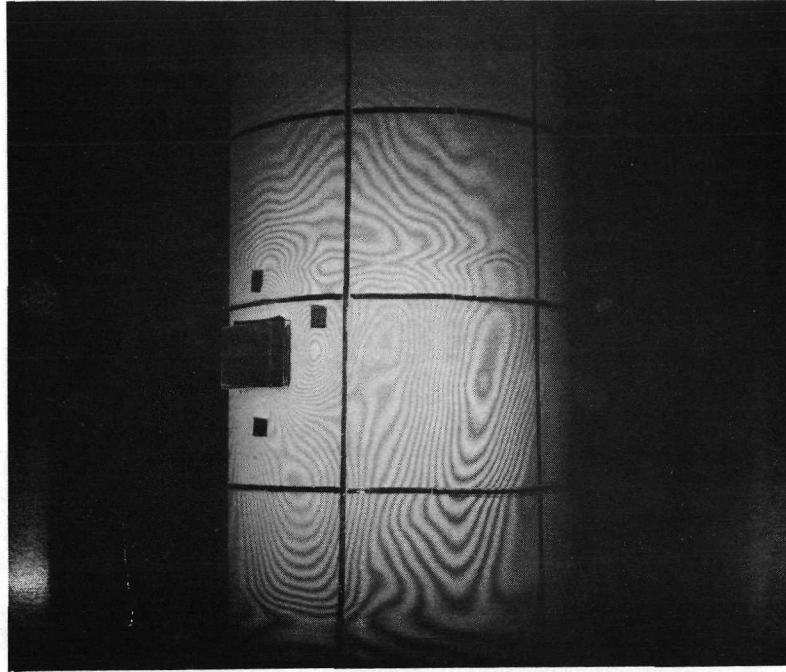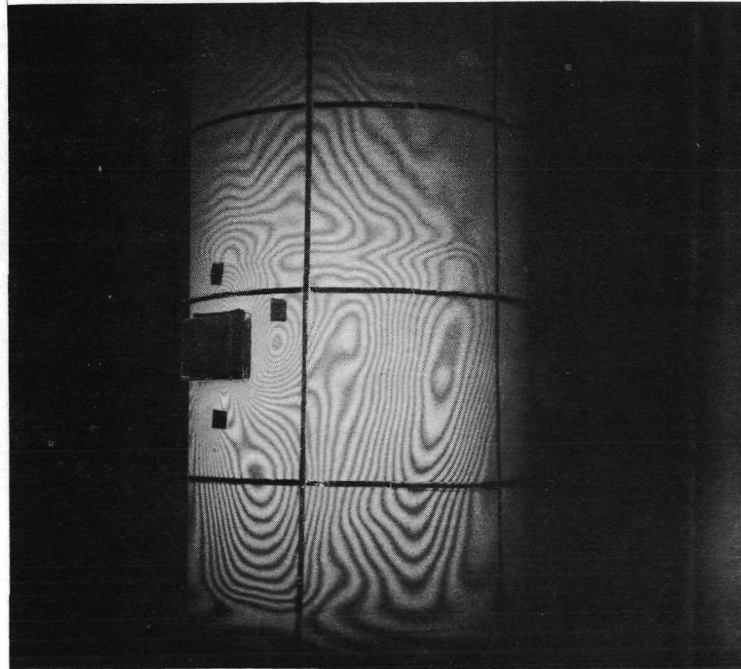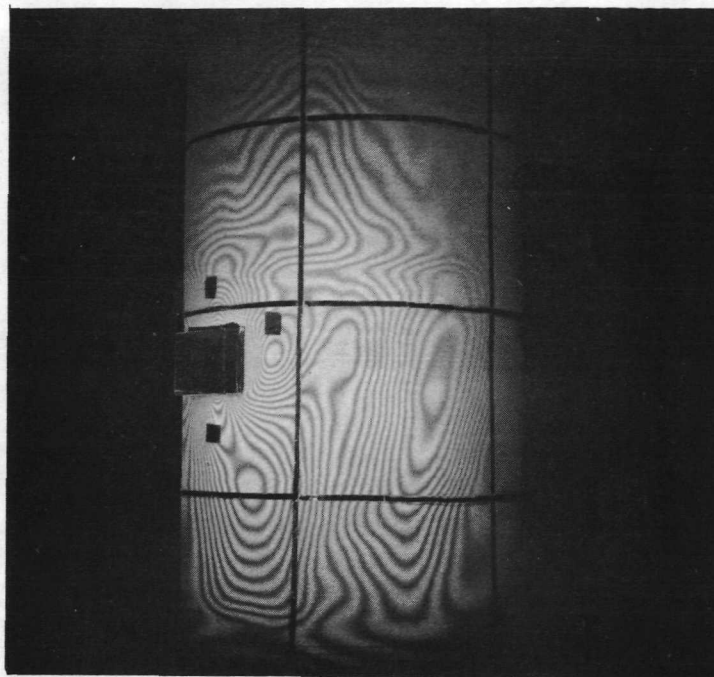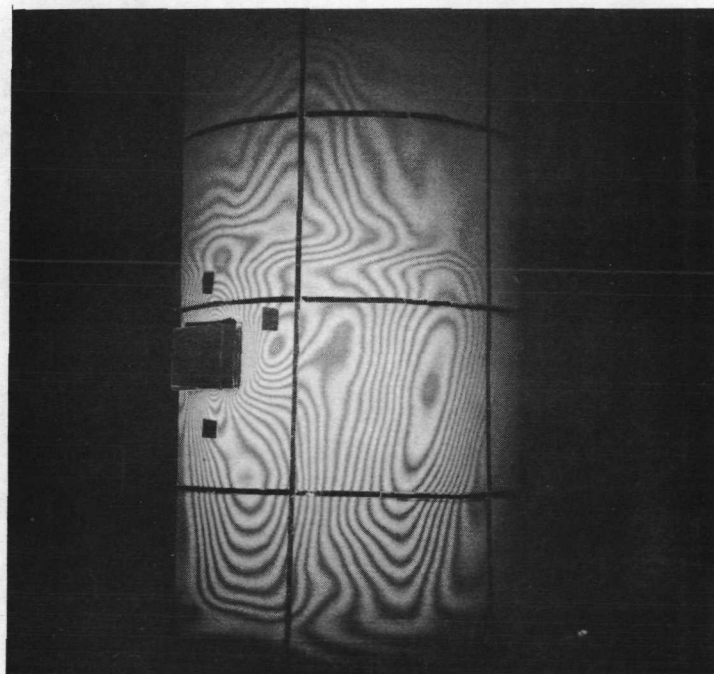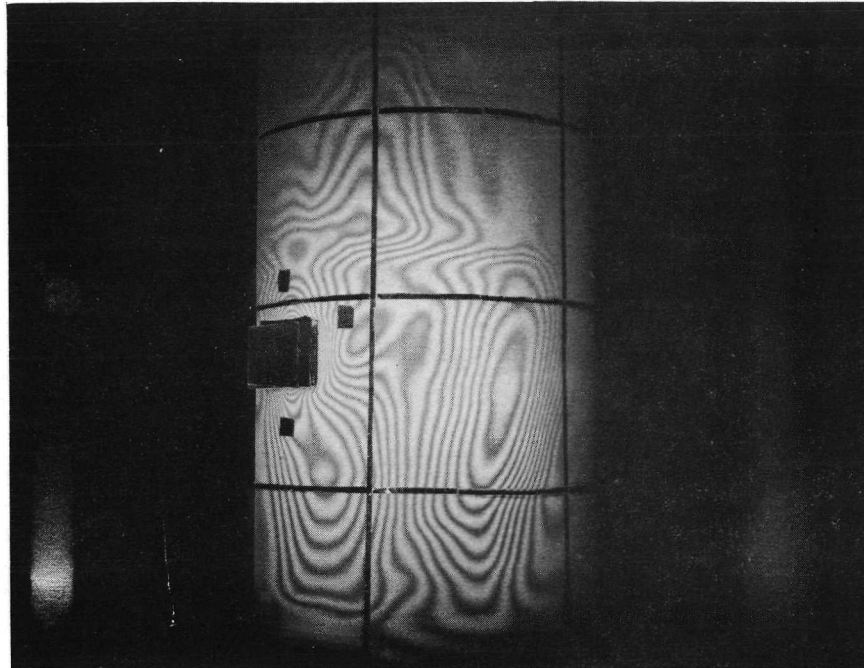Camera Settings: f16 - 3 sec
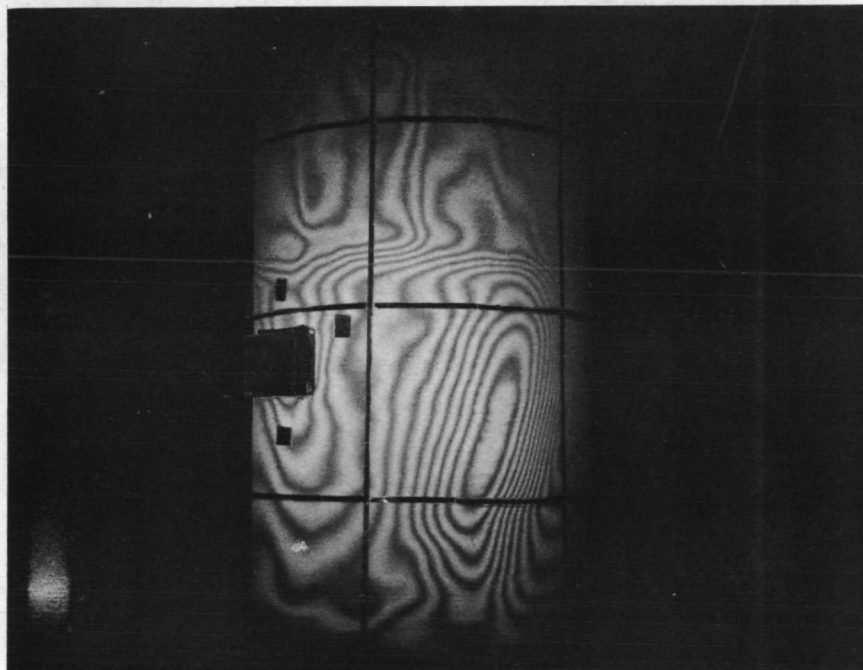
Fig. 51   Photograph Through Real-Time Hologram No. 127 43 min.
           After a 40 sec Radiative Stressing of the Cylindrical
           Casing

Camera Settings: f16 - 3 sec

Since the sequence of photographs figures 41 through 51 represent instantaneous recordings of surface displacements, some measure of localized movement can be estimated by checking the variations in the number of lines. It is therefore clear that much movement occurred in the minute between figures 41 and 42. And the movement from figure 42 to figure 48 seemed slight. Based on these figures and considering that a reverse hologram tends to represent a displacement summation, a delay of 3 min. was used to produce a reverse hologram. This was done. The view through hologram No. 128 can be seen in figure 52.
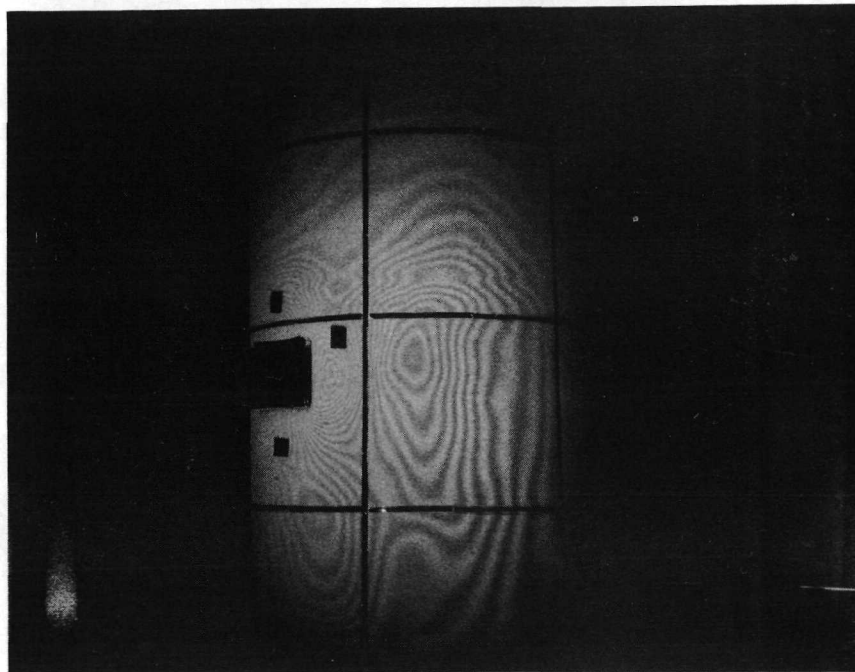
Fig. 52   Fringe Field Seen Through Reverse Hologram No. 128
           Entire Casing was Heated for 40 sec and Hologram Made
           3 min. Later. 20 min. After, the Photo was Snapped.

Camera Settings: f27 - 8 sec

LOCKHEED MISSILES & SPACE COMPANY

A third cyclic heating test, 3T, was performed utilizing the temperature recording system. The procedure and recorded average peak temperatures are listed below.

CYCLIC HEAT TEST NO. 3T

	Operation	Elapsed Time (minutes)	Average Peak Temperature °F
1.	Recorder Turned On	-	65.1
2.	20 Seconds of Heat	0	71.5
3.	" " " "	6	72.2
4.	" " " "	12	72.5
5.	" " " "	18	71.0
6.	Exposed Reverse Hologram No. 131	41	67.9
7.	Photograph Taken	65	66.5

Hologram No. 131 was developed and observed 24 min. after exposure. It appeared as shown in Fig. 53

Fig. 53   Interference Field of Hologram No. 131 Which Occurred After Cyclic Heating Test 3T

Camera Settings: f16 - 3.53 sec

3-41

LOCKHEED MISSILES & SPACE COMPANY

The following test was implemented to expose a series of holograms for a single heat cycle. In this test half of the casing was stressed. The procedure and average peak temperature are specified.

CYCLIC HEAT TEST NO. 4T

Operation	Elapsed Time (minutes)	Average Peak Temperature °F
1. Recorder Turned On	-	65.6
2. 30 Seconds of Heat	0	71.5
3. Exposed Reverse Hologram No. 132	8	66.4
4. " " " No. 133	11	66.2
5. " " " No. 134	15	66.1
6. Photograph of Figure 54 taken	39	65.9
7. Photograph of Figure 55 taken	49	65.7

The fringe patterns which resulted are shown in the following figures.

Fig. 54 Photograph Through Hologram No. 132
Camera Settings: f16 - 3.53 sec

3-42

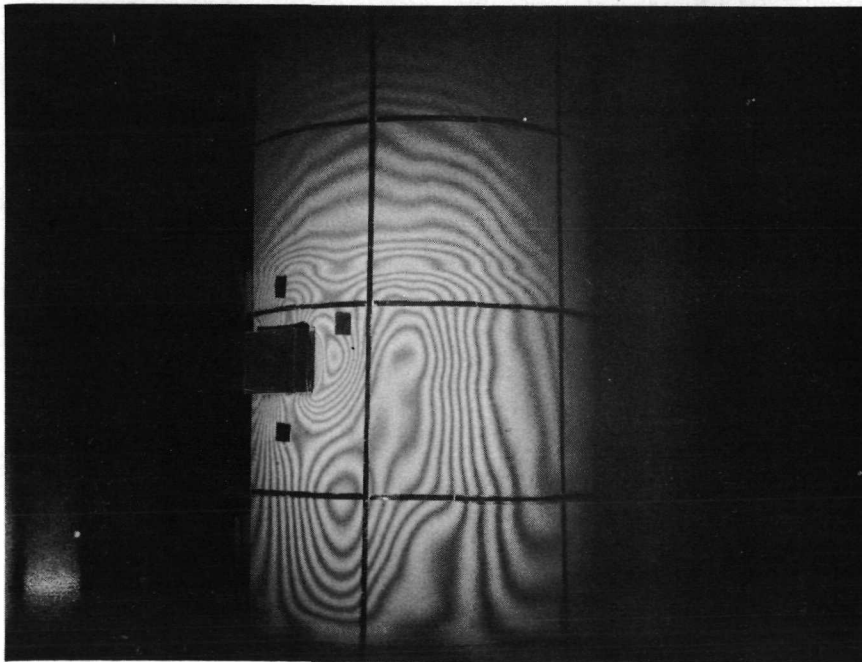LOCKHEED MISSILES & SPACE COMPANY

Fig. 55 Photograph Through Hologram No. 138
Camera Settings: f16 - 3.53 sec
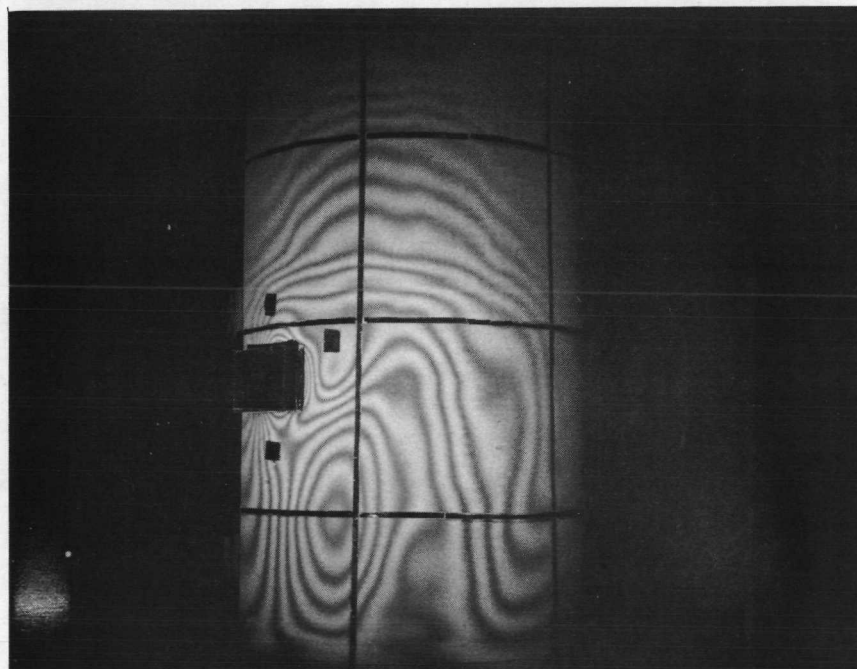
Fig. 56 Photograph Through Hologram No. 134
Camera Settings: f16 - 2.53 sec

Another heat test, 5T, was instituted to increase the line density over what was observed in Fig. 54. However, the motor contraction obliterated first order fringe formation. Consequently, no fringe lines were discernible in hologram No. 135. The procedure employed is listed below:

CYCLIC HEAT TEST NO. 5T

	Operation	Elapsed Time (Minutes)	Average Peak Temperatures °F
1.	Recorder Turned On	-	65.6
2.	30 Seconds of Heat	0	72.1
3.	" " " "	3	73.8
4.	Reverse Hologram, No. 135 Exposed	13	66.7
5.	No Fringe-Lines in Hologram	35	66.2

A final heat test, 6T, was attempted to determine optimum thermal stressing parameters that create maximum observable line densities. The approach was patterned after Test 4T where a single heat cycle was applied to the casing.

CYCLIC HEAT TEST NO. 6T

	Operation	Elapsed Time (Minutes)	Average Peak Temperatures °F
1.	Recorder Turned On	-	59.6
2.	30 Seconds of Heat	0	72.1
3.	Exposed Reverse Hologram No. 139	5	62.9
4.	" " " No. 140	8	62.8
5.	" " " No. 141	10	62.3
6.	Photograph of Figure 57 taken	51	61.9
7.	" " " 58 taken	69	61.9
8.	" " " 59 taken	84	61.9
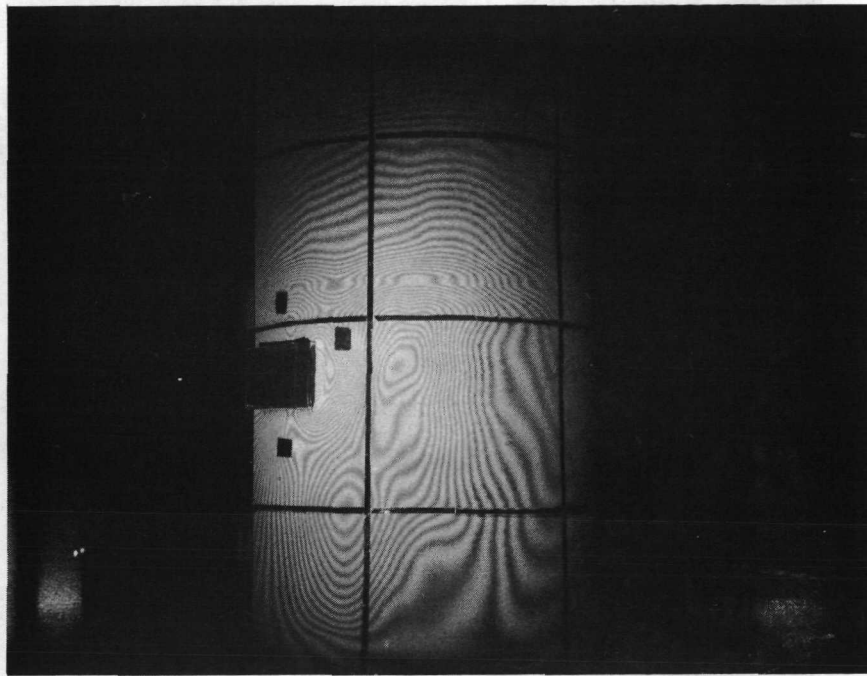
Fig. 57   Fringe Field Photographed Through Hologram No. 139
Camera Settings: f19 - 4.0 sec
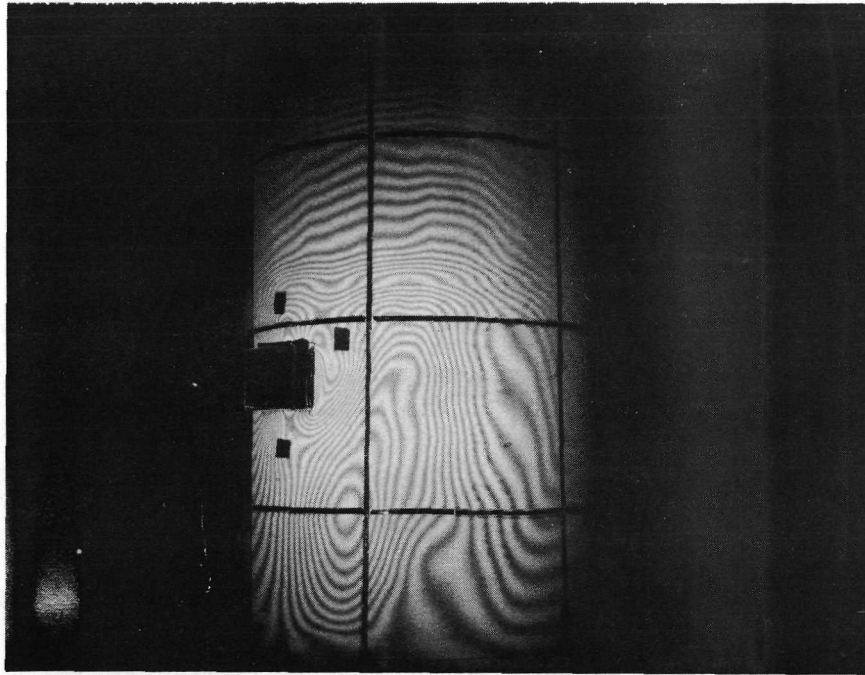
Fig. 58 **Fringe** Field Photographed Through Hologram No. 140
Camera Settings f19 - 4.0 sec
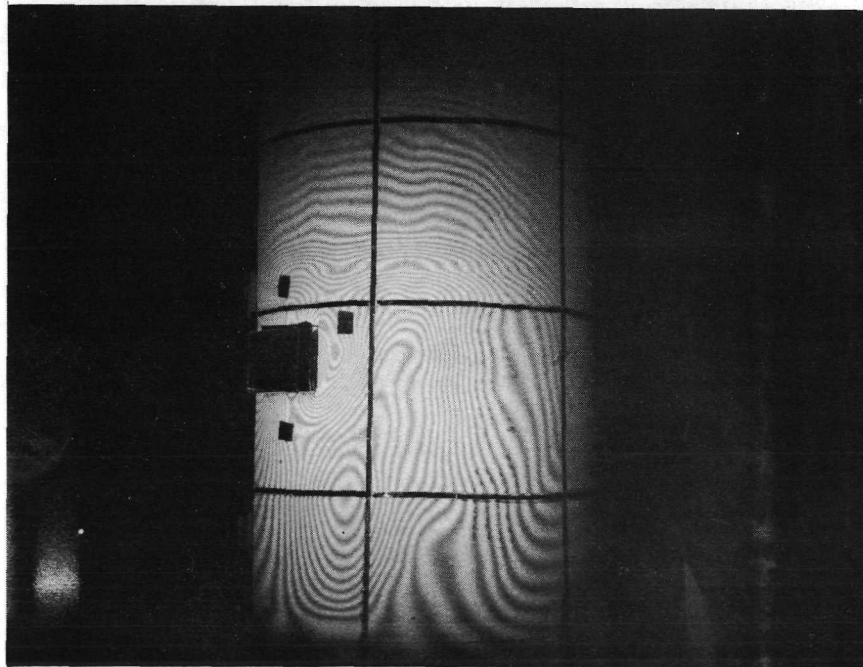
Fig. 59 Fringe Field Photographed Through Hologram No. 141
Camera Settings: f19 - 4.0 sec

To apply heat test, No. 6T, over the total inspectable area of the cylinder, 270°, it was rotated about 120°. The 90° not inspectable has large repair patches that can be seen in Fig. 22. The new position was photographed through the plate holder and it is shown in Fig. 60. The vertical lines from left to right were the 210, 180, 150 and 120 degree lines.
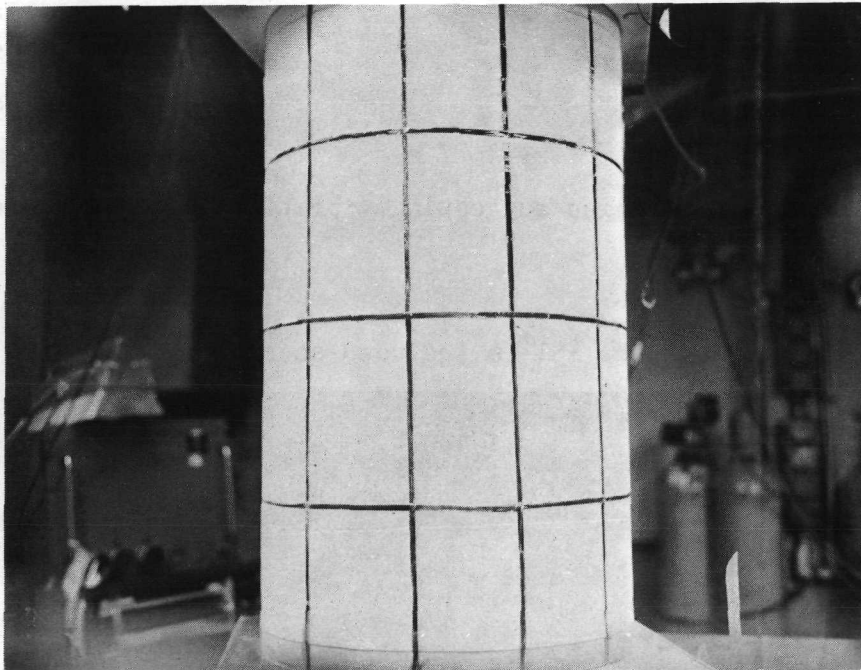
Fig. 60   Position of Motor Case After Rotation
Photograph was Taken Through Plate Holder

LOCKHEED MISSILES & SPACE COMPANY

After rotation of the motor, the following procedure was used on the motor case subsequent to a satisfactory test hologram:

CYCLIC HEAT TEST NO. 7T

Operation	Elapsed Time (Minutes)
1. 30 Seconds of Heat	0
2. Exposed Reverse Hologram No. 151	5
3. " " " No. 152	9
4. " " " No. 152	12
5. Photograph of Figure 61 taken	44
6. " " " 62 "	59

Hologram No. 152 showed no fringes suggesting vibration in the holographic setup.

The photograph taken through No. 151 is included as Fig. 61.
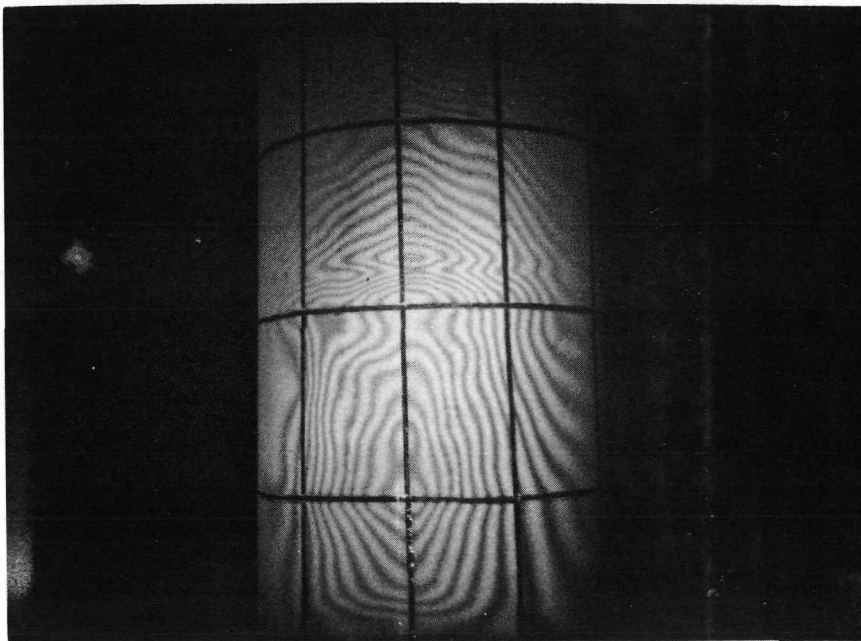
Fig. 61   Polaroid Through Hologram No. 151
Camera Settings: F17.5 - 4.4 sec
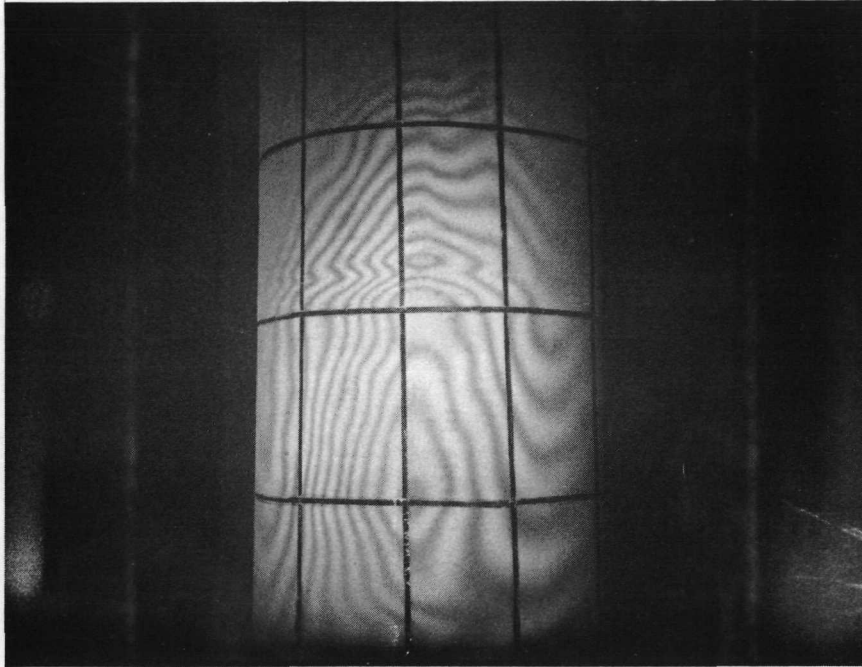
Fig. 62 Polaroid Through Hologram No. 153
Camera Settings: f17 - 44 sec

To achieve a line density greater than that indicated in Figs. 60 and 61,
another test designed to reduce the elapsed time between stressing and holo-
gram exposure was completed. A satisfactory hologram was experienced by expos-
ing it 3.5 min. from the 30 sec stress. The pattern of Fig. 63 was observed
some 20 mins. later.
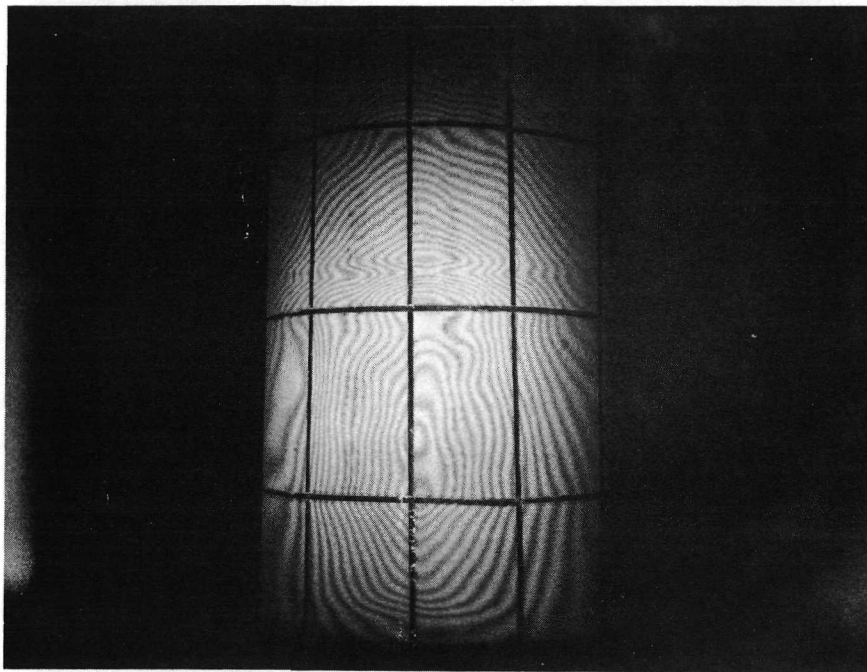
Fig. 63   Polaroid Through Hologram No. 156 Made 3.5 min
After Heating the Casing for 30 sec

Camera Settings: f22 - 5.0 sec

The motor was again rotated about 90°. The new position as shown in Fig. 64
had vertical-line locations at 150, 120, 90, 60 and 30 degrees. The center
vertical line represents the 90° angle.

LOCKHEED MISSILES & SPACE COMPANY
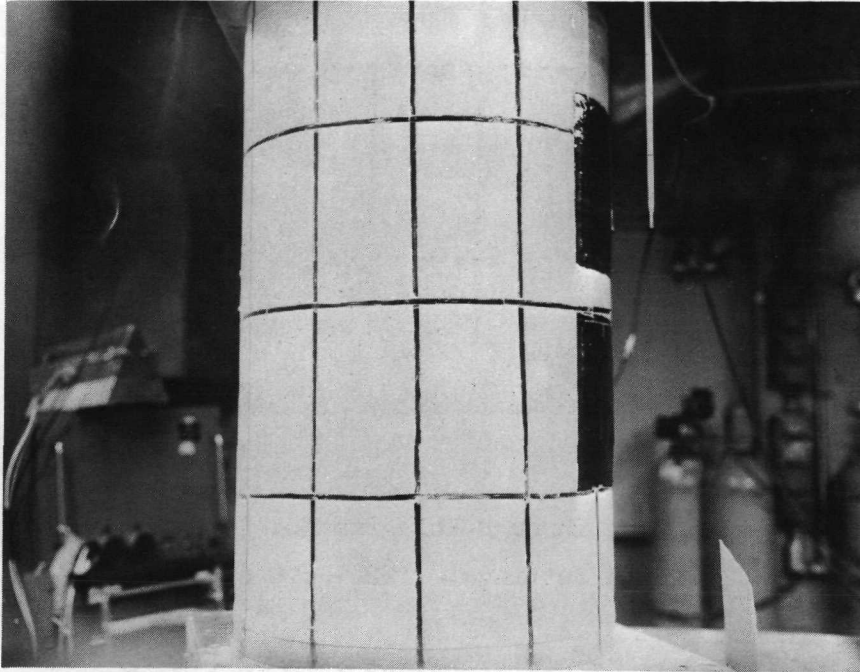
Fig. 64   Position of Motor Case After Second Rotation.
Vertical Line is at 90° Location.

A hologram, No. 157 was exposed 3 min. after heating the casing for 30 sec. The hologram density was unexpectedly high. Another hologram, No. 158 was made 2-1/2 mins. after heating the casing for 30 sec. Figure 65 resulted some 20 mins. later.

LOCKHEED MISSILES & SPACE COMPANY
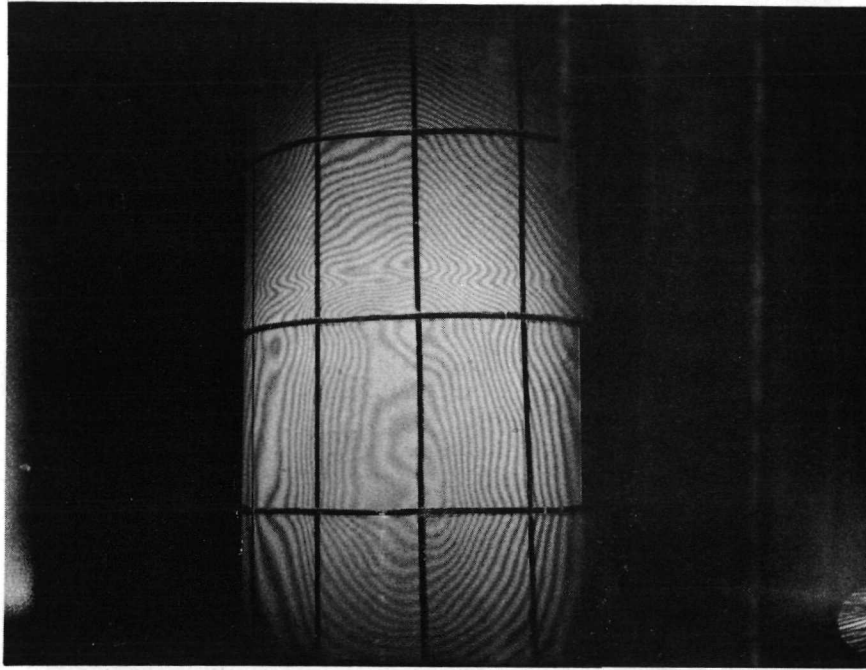
Fig. 65   Photograph Through Hologram No. 158
Camera Settings: f22 - 4.0 sec

Upon examining Figs. 63 and 65 and comparing them to Fig. 52, it seemed that the areas where concentric rings to the left of these in the center may be signalling convex displacement caused by interface disbonding. For comparison then, the technique that produced the result shown in Fig. 52 was applied to the area defined by Fig. 64.

A reverse hologram No. 160 was made identically to the method that resulted in Fig. 52. The total cylindrical surface was heated for 40 sec with the quartz lamp and 3 min later the hologram was made. The fringe field that occurred about 25 min. later is shown in Fig. 66.

LOCKHEED MISSILES & SPACE COMPANY
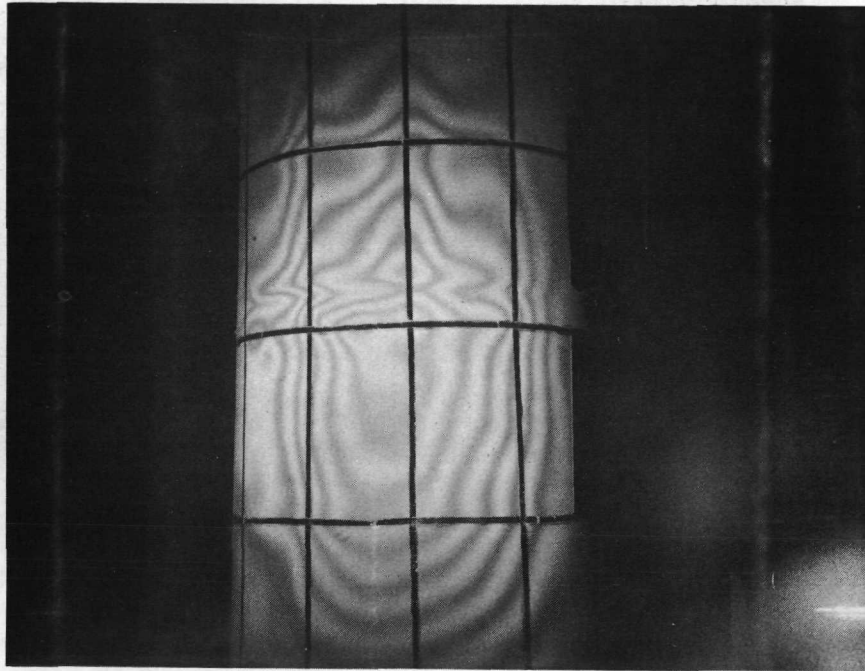
Fig. 66   Interference Pattern Effected by Reverse Hologram
          No. 160 Exposed 3 min. After Heating the Total
          Casing for 40 sec

                    Camera Settings: f19 - 4.4 sec

To raise the line density of Fig. 66, another hologram, No. 161, was made 1.5 min.
from heating the entire casing for 40 sec. The fringe field produced is shown in
Fig. 67.
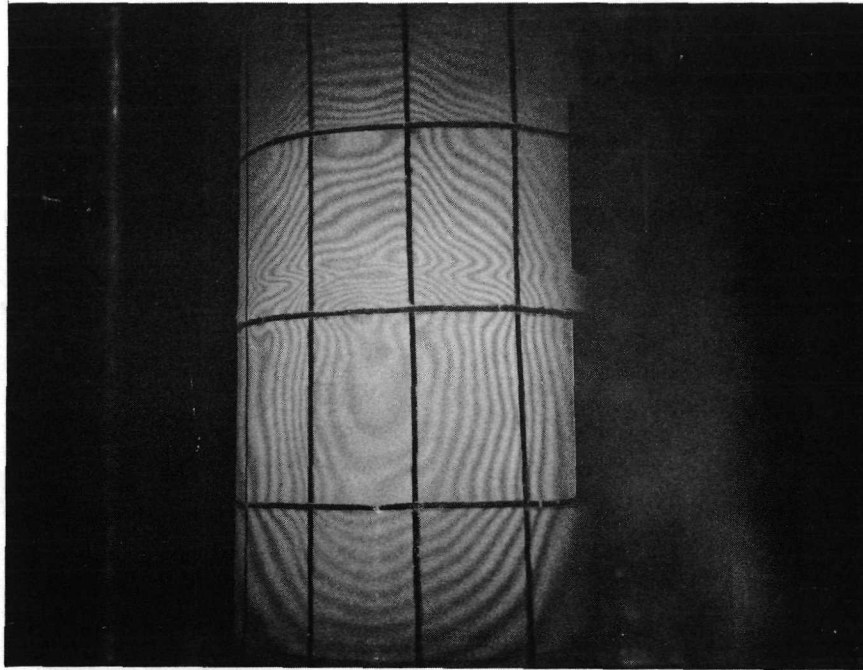
Fig. 67   Line Density Increased from Previous Figure by Making
Hologram No. 161, 1.5 min. After Heating the Entire
Casing for 40 sec.

Camera Settings: f16 - 4.5 sec

3.2.4   Static Loading

Since the results of a static load placed on the periphery of the upper cylindrical
casing was easily implemented, the tests were performed. In addition, the oppor-
tunity also offered a chance to compare the effects of a static load on a known
separated area to those on a bonded area.

To accomplish static loading, real-time hologram No. 123 was utilized. The view
through this hologram prior to applying a static load is shown in Fig. 68.
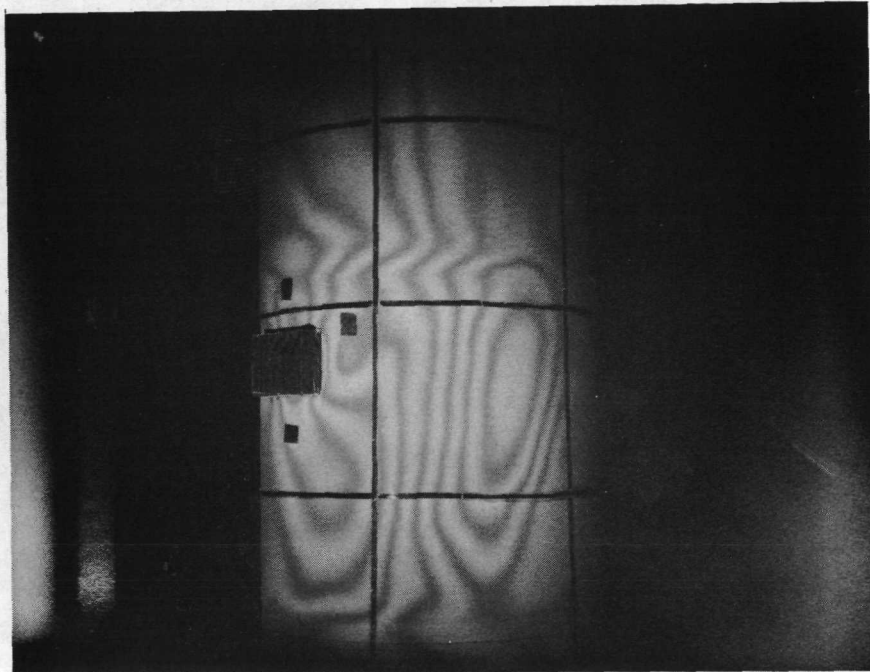
Fig. 68   View Through Real-Time Hologram No. 123 Prior to
Application of Static Load

Camera Settings: f22 -- 6 sec

A static load was continuously increased on the mounting plate attached to the
threaded holes on the upper edge of the cylindrical casing. When the line density
had maximized a photograph was taken which is Fig. 69.
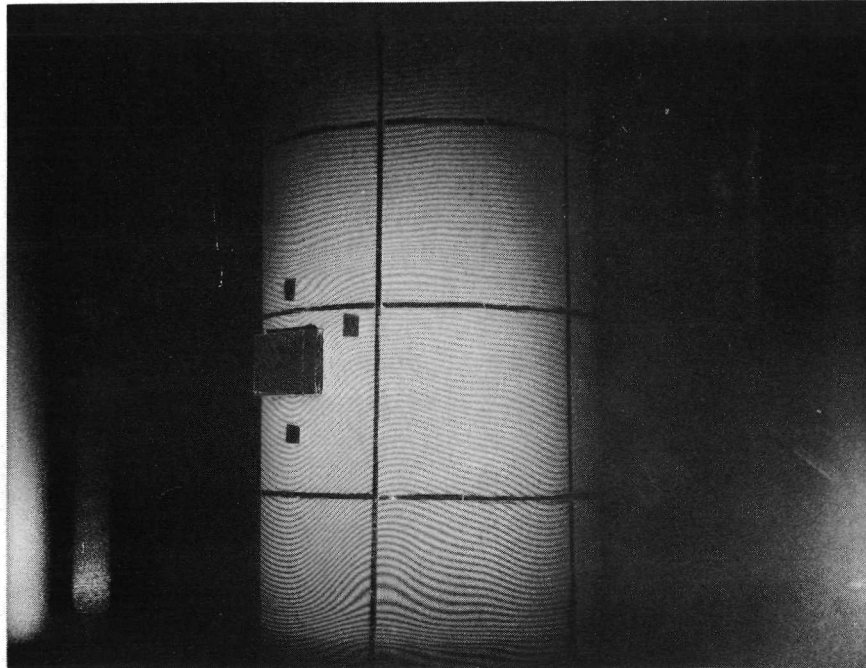
Fig. 69   Fringe Lines Produced by 40 lbs. of Mass Placed
Around the Upper Edge of Hemi-Cylinder. Center
Line was 270° Position.

Camera Settings: f22 - 6 sed

The area in the lower two quadrants to the left of the 270° line was known from radiographic tests to be separated.

A similar load generated the fringe field shown in Fig. 70. Here the center line is the 90° location.
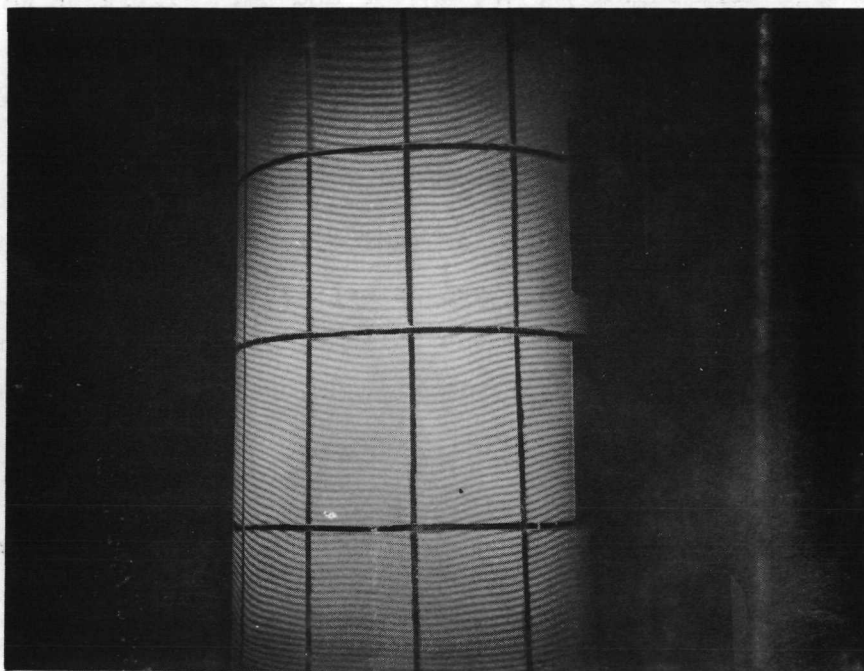
Fig. 70   Fringe Lines Produced by 35 lbs. of Mass Placed
Around the Upper Edge of Hemi-Cylinder. Center
Line was 90° Position, Lines are 30° Apart.

Camera Settings: f16 - 5.5 sec

There were no reported separation in the area pictured in Fig. 70.

LOCKHEED MISSILES & SPACE COMPANY

3.3 CORRELATION OF HOLOGRAPHIC RESULTS WITH RADIOGRAPHIC ANALYSES

Based on the expected interference pattern discussed in the previous section, and Figs. 29, 63 and 65 which tend to confirm expectations, holographic results were analyzed for pattern deviation in the area of known separation. The photographs which seemed to provide a reasonably close correlation with radiographic inspection documentation were Figs. 34, 42, 43, 52 and 54. Figure 52 was finally selected as a basis for destructive testing. The series of ellipses on the viewing centerline were considered as typical for cylindrical displacement and therefore not taken seriously.

Using Fig. 52 and a map from results of radiographic inspection, the lines on Fig. 71 were plotted. The area defined as separated by the radiographic record on motor case S/N 424 was traced by the solid black line. The fringe lines that best suggested the separated area, from Fig. 52, were traced on the casing surface as dashed lines.

Circles 1 in. in diameter were marked on the casing for penetration cuts. Penetration cuts up to 9/16 in. deep were made with a circular saw. A total of 21 circles were specified for cutting. The location of these are pictured in the following three photographs, Figs. 72, 73, and 74.
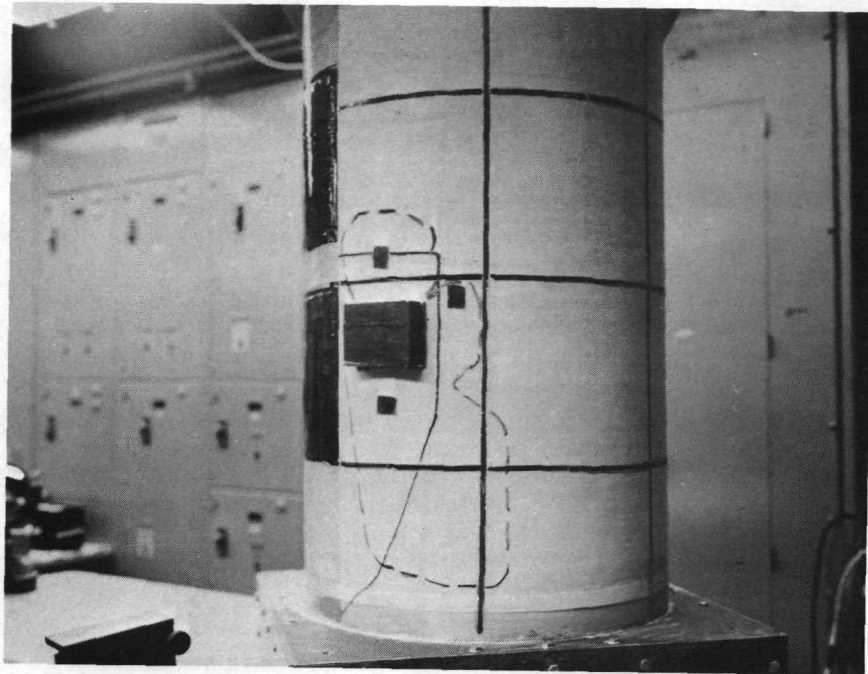
Fig. 71   Solid Dark Line Indicates Area Separated in the
           Radiograph Record of Motor Case S/N 424. Dashed
           Line was Closest Approximation as Suggested by
           Holography
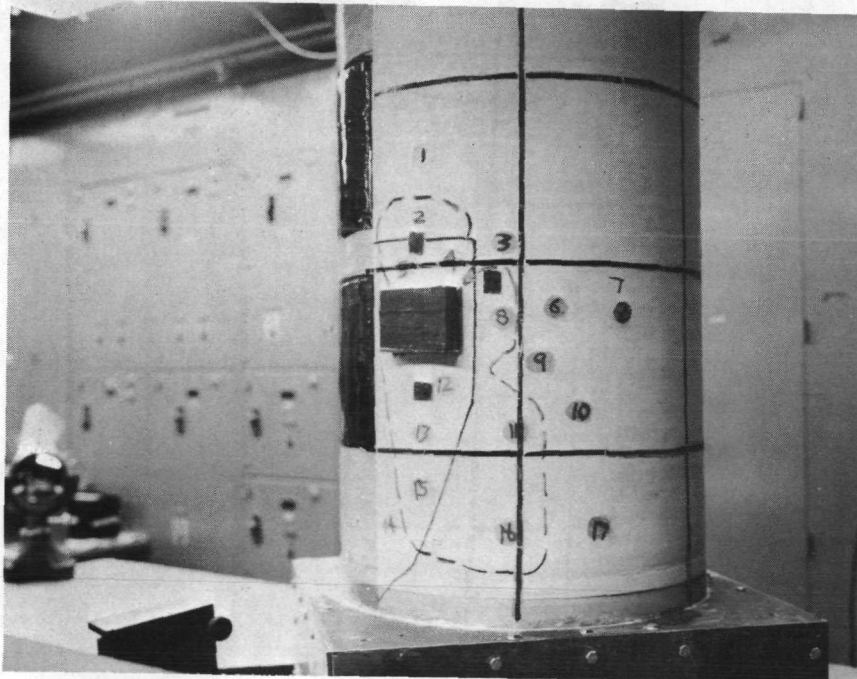
Fig. 72   Circular Areas Marked for Destructive Tests.
           (17) 1 in. Diameter Circles are Shown. Vertical
           Line is the 270° Position
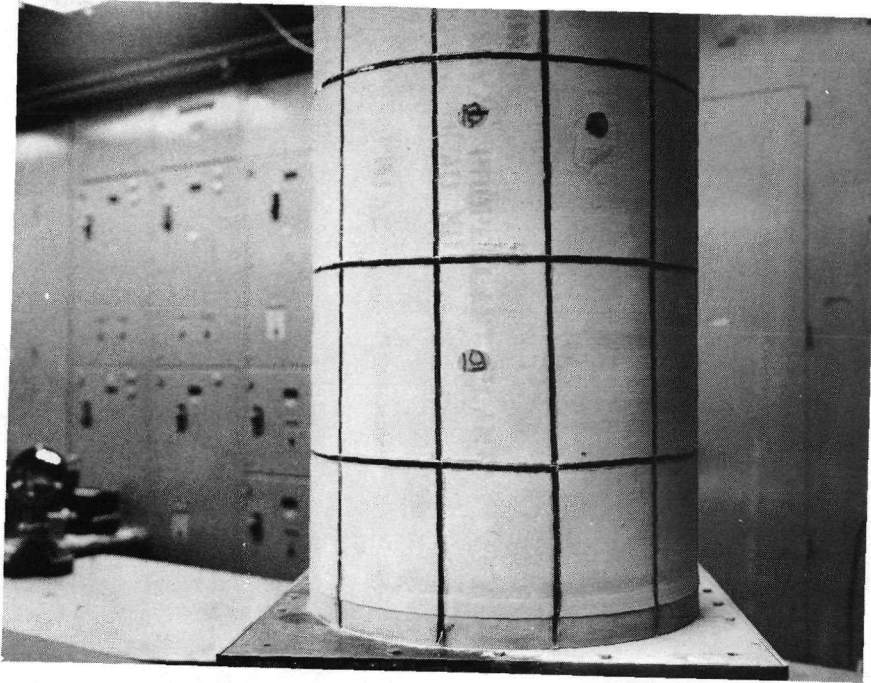
Fig. 73 (2) Circles Marked in Bonded Areas Between
180° and 150° for Destructive Tests
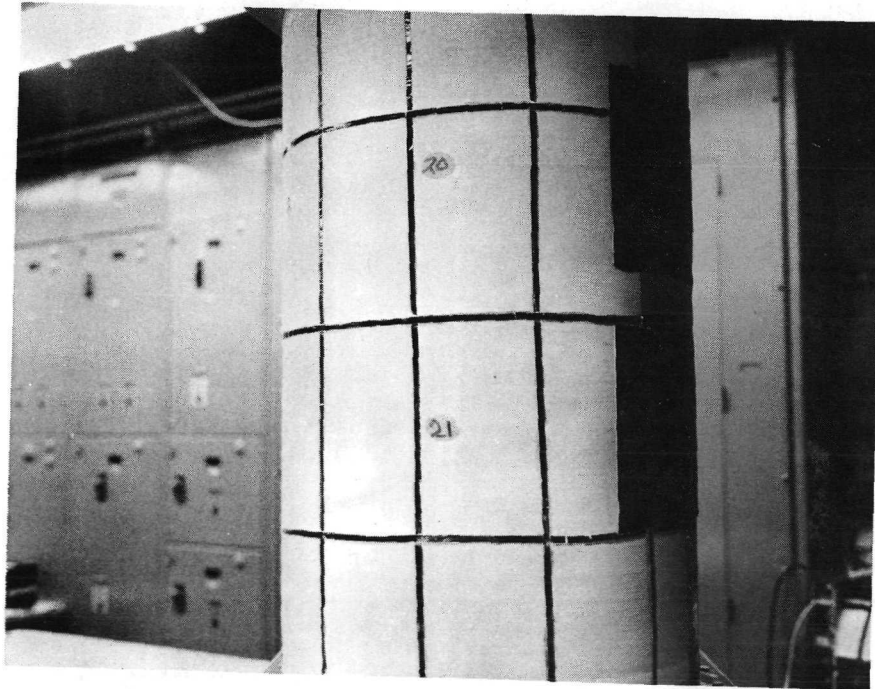
Fig. 74 (2) Circles Placed Near 90° Position for
Destructive Tests. Both Areas Were
Considered Bonded

Section 4

DESTRUCTIVE TESTING OF MOTOR CASE NPP-424

4.1 EQUIPMENT AND PROCEDURE

Destructive examination was performed on motor case S/N 424 at the Lockheed Santa Cruz Test Base. The work was done remotely to satisfy contractual safety requirements. A carbide circular saw in conjunction with a drill press was employed. A photograph of the drilling arrangement, along with the remote television camera can be seen in Fig. 75. Also visible is the gravity-fed water tank used for cooling the cutting area when drilling. The weighted drill press lever can also be seen.

The cutting operation involved a fairly simple procedure. First, the motor was positioned to the desired area. Second, the weight was fastened to the drill press lever and the coolant flow turned on. In the remote cell block the drill press was switched on while viewing the remote television monitor. A stop-switch located on the drill was adjusted beforehand for the depth of cut and it automatically interrupted the operation.

The drill press had a spindle-to-support column distance of 12 in. and an adjust-able spindle velocity. A spindle velocity of 150 rpm was used for all penetration cuts.

4.2 RESULTS OF DESTRUCTIVE TESTING

The initial penetration cuts were on 1 in. circles numbers 18, 19, 20 and 21. Since these areas were thought to be bonded, they were selected to verify perfor-mance of the cutting operation. Penetration cuts of 1 in. circles to a depth of .562 in. were accomplished successfully without shearing either the casing/liner
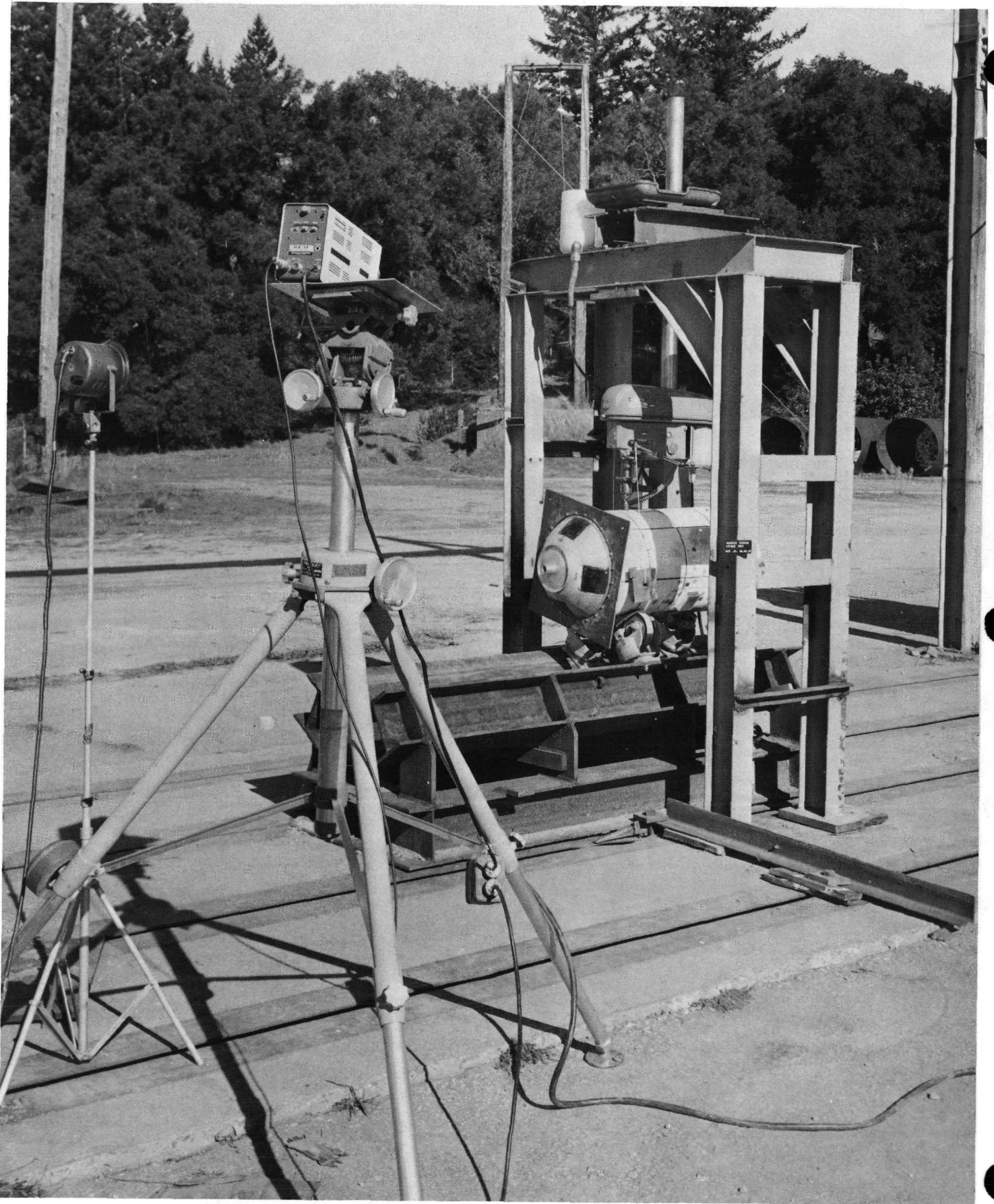
Fig. 75 Destructive Test Arrangement for Cutting 1-in. Diameter Discs
from Motor Case S/N 424

bonds or liner/propellant bonds. In addition, by inserting a pointed scriber in each circular cut, none of the four discs could be pried loose.

The motor was rotated to the **area specified for study in Fig. 72. The** remaining (17) penetration cuts were made. The sawing sequence, as well as the results, are tabulated below:

SEQUENCE AND RESULTS OF DESTRUCTIVE CUTTING 1-INCH DIAMETER DISCS IN MOTOR CASE NPP-424

Cut No.	Condition	Comment
18	Bonded	
20	Bonded	Tests to verify performance of cutting operation
19	Bonded	
21	Bonded	
1	Bonded	
2	Partially bonded	30 to 50 Unbonded-Liner/Propellant
3	Separated	No Liner/Propellant Bond - 1/8-in. gap
4	Separated	No Propellant Bond - 1/8-in. gap
5	Separated	No Propellant Bond - 1/8-in. gap
8	Separated	No Propellant Bond - 3/16-in. gap
6	Separated	No Propellant Bond - 1/8-in. gap
7	Separated	No Propellant Bond - 3/16-in. gap
9	Separated	No Propellant Bond - 3/16-in. gap
12	Separated	No Propellant Bond - 3/16-in. gap
13	Separated	No Propellant Bond - 3/16-in. gap
11	Separated	No Propellant Bond - 3/16-in. gap
10	Separated	No Propellant Bond - 3/16-in. gap
15	Separated	No Propellant Bond - 3/16-in. gap
14	Separated	No Propellant Bond - 3/16-in. gap
16	Separated	No Propellant Bond - 3/16-in. gap
17	Bonded	Liner/Propellant - Casing to Liner separated

4-3

A photograph of the motor after drilling the final (17) cuts is included as
Fig. 76. As the preceding tabulation indicated, only discs numbers 1 and 17
showed liner/propellant bonding and the latter had partial casing/linder
disbonding.

Since the majority of the designated penetration cuts actually revealed physical
separation between liner and casing, as great as 3/16 of an inch, it was found
possible to insert a flexible feeler gage, .010 in. thick, into each of the
holes and plot on the casing surface the extremity of separation. This was
done and the border was traced. This can be seen in Figs. 76 and 77 as a broken
line drawn on, and adjacent to, pieces of 3/4 in. wide paper tape.

To substantiate the line of separation, detected with a feeler gage, corresponded
to the actual separation, additional penetration cuts were performed. Four of
these are pointed out in Fig. 78.
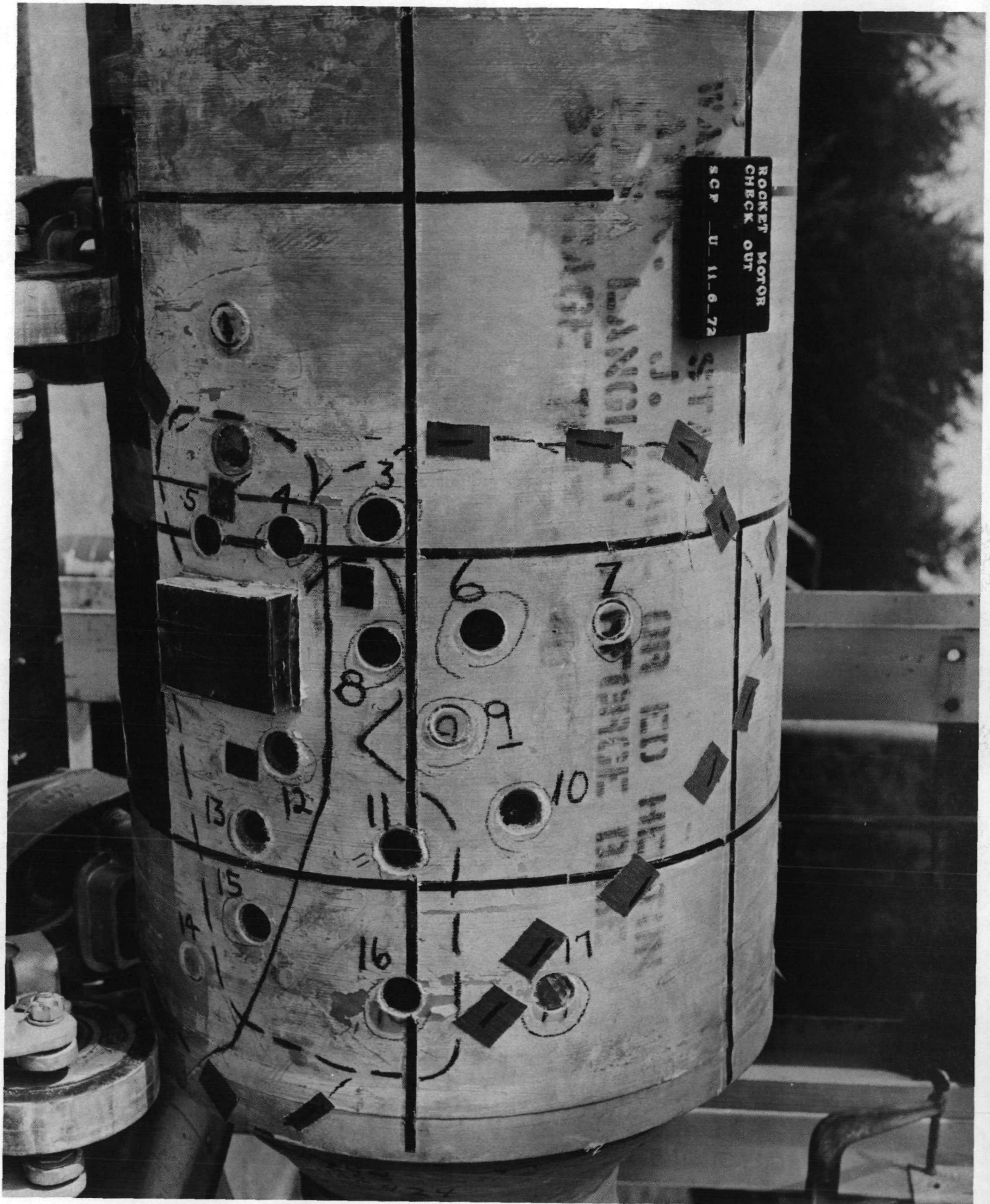
Fig. 76   Photograph of Motor Case S/N 424 After Making Initial 1-in.
Diameter Penetration Cuts into Casing to Test for Separation
Between Casing/Liner and Liner/Propellant

Fig. 77   Trace of Separated Area Between Liner and Propellant Detected
by Feeler Gage During Destructive Tests on Motor S/N 424
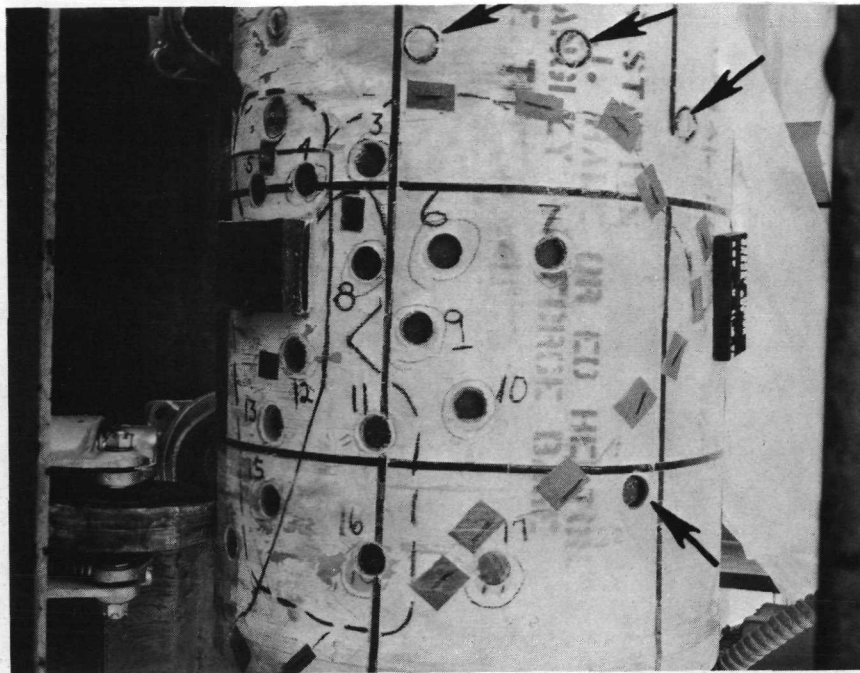
Fig. 78   Locations of Additional Penetration Cuts (Arrows)
           Made to Check Size of Separated Area Found by
           Inserting Feeler Gage into Holes Previously Cut.
           Top (3) were Bonded but Bottom Cut Revealed Void
           Between Liner and Propellant

Figure 78 shows, correlation at the top of the separated area was corroborated.
However, the lower penetration cut did reveal separation between liner and
propellant but it had not the typical gap. To pinpoint the boundary of the
separation in the lower area, (2) additional cuts were sawed and their positions
are indicated in Fig. 79.
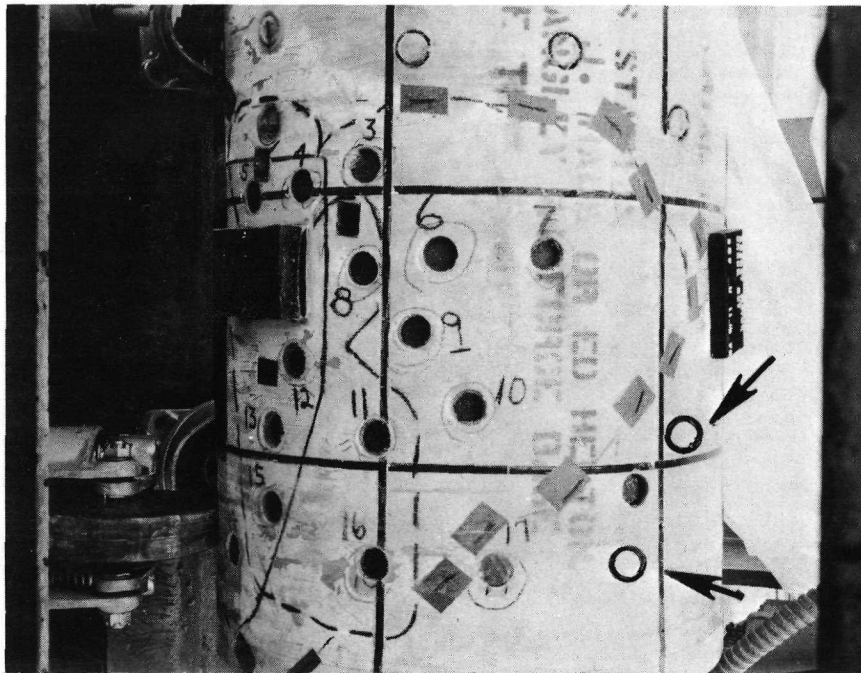
Fig. 79   Final (2) Penetration Cuts Made in Motor Casing to
Check Extent of Liner/Propellant Separation

Both of the cuts shown in Fig. 79 were bonded. It was also discovered that the
boundary of the separated zone could be estimated by tapping the casing with a
metal object. This was done. A mapping of total separation which had been
studied by holography is shown in Fig. 80.
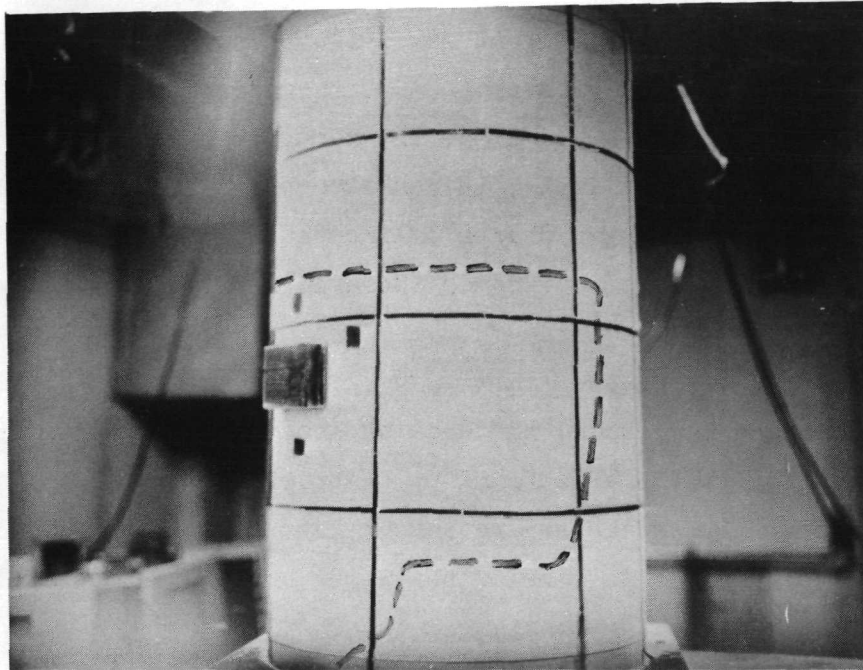
Fig. 80   Extent of Separated Line - Propellant Interface as
           Determined by Feeler Gage, Penetration Cuts and
           Surface Tapping of Motor Case S/N 424 in Area
           Studied by Holography

The removed cores were examined and some observations were made. In general,
all removable cores revealed a .010-.015 in. layer of propellant bonded to the
liner. The propellant surface was crystallized suggesting cohesiveness never
existed with the main bulk of propellant. In core Number 2 evidence of lamina-
tion in the coating of propellant was seen. In Number 17 brown lines and fibers
were seen embedded in the propellant.

The actual disbonding condition cannot accurately be defined as a liner/propellant
separation but should be considered a propellant void at the liner interface.

4.3 CORRELATION OF HOLOGRAPHIC RESULTS WITH DESTRUCTIVE TESTING

By examining Fig. 80 and Fig. 71, it is obvious that the area of liner/propellant separ ation was found to be greater than the area reported in the radiographic analysis on motor case NPP-424. Since the x-ray record did not accurately define the boundary of liner/propellant void, an attempt was undertaken to correlate holographic pictures to the void area delineated by destructive tests as depicted in Fig. 80. This, of course, presumes the area in Fig. 80 was present during holography.

One of the holograms suggesting the area of separation is shown in Fig. 81. The dashed line represents the area found by destructive testing and the solid line indicates the boundary of the separation implied by the interference pattern. The acutely bent fringe lines just below the upper horizontal dashed line locate the termination of the liner.

In analyzing real-time holograms for fringe anomalies produced by radiative or thermal stressing, non-uniform heating complicates interpretation. An example of this can be appreciated from Figs. 28 and 29. The line distortions resulted in Fig. 28 from the non-uniform heating of the quartz lamp. But, Fig. 29, a reverse hologram, shows no similar anomalies. A real-time hologram reveals the instantaneous temperature reached at a given time after heating. A reverse holo-gram is generally made some minutes after heating providing time to reach tempera-ture equilibrium of the casing. In addition, as previously discussed, the view through a reverse hologram presents an interference field effected by the summa-tion of movement caused by a cooling of about 1°F. Consequently, real-time holography observed or photographed shortly after thermal stressing may show fringe anomalies resulting from subsurface defects as well as variations in tempera-ture. However, this problem is not evident in Fig. 81 where the convex displace-ments do approximate the void area determined in destructive testing.

Although the instantaneous strain pattern approximates the separated area found in destructive testing, an analysis of the cooling behavior in real-time viewing
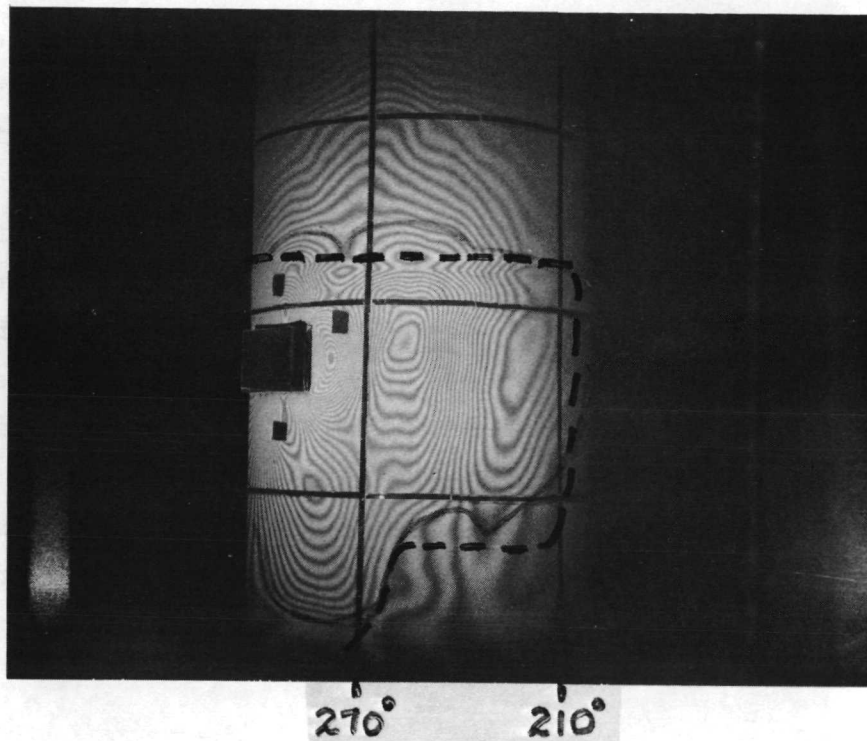
270°   210°

Fig. 81 Separated Area in Motor Casing Drawn in Dashed Line
as Detected by Destructive Testing. Solid Line is
Area Suggested As Separated by Fringe Pattern.
Interference Field Resulted 2 min. After Radiating
the Casing With A Quartz Lamp for 20 sec.

does not reaffirm the conclusion explicit in Fig. 81. True, the circular and elliptical lines support the conclusion that differential displacements, generally of curvex forms, did occur. But, after examining the series of Fig. 42 to 51, the area which contracted in cooling is smaller than that depicted in Fig. 81. Upon cooling, it would be expected that areas elongating as a result of thermal stressing would also relax after returning to ambient temperature. If the line density change below the igniter is plotted with cooling time and contrasted with a position near the 210° line, the curves in Fig. 82 result. The curve near the 270° position is a perfect cooling trace. The little or no change in line density at the 210° position implies no contraction occurred in cooling. When the dynamic behavior is analyzed in detail, the area which collapsed during cooling is accurately defined in the composite of reverse holograms of Fig. 83. Therefore, the real-time holograms agree with the area consistently defined by the reverse holograms seen throughout the text. Based on this conclusion, it must then be presumed that the disbonding between propellant and liner grew from the time of holography to time of destructive testing. This assumes that handling, tapping of the casing with a metal object, and the vibrational and compressive forces of circular sawing, as well as feeler gage insertion, loosened partially bonded areas, increasing the extent of the liner/propellant separation. The possibility seems reasonable in light of the fact that the separation apparently did grow from the time of performing radiography to the time of applying holography.
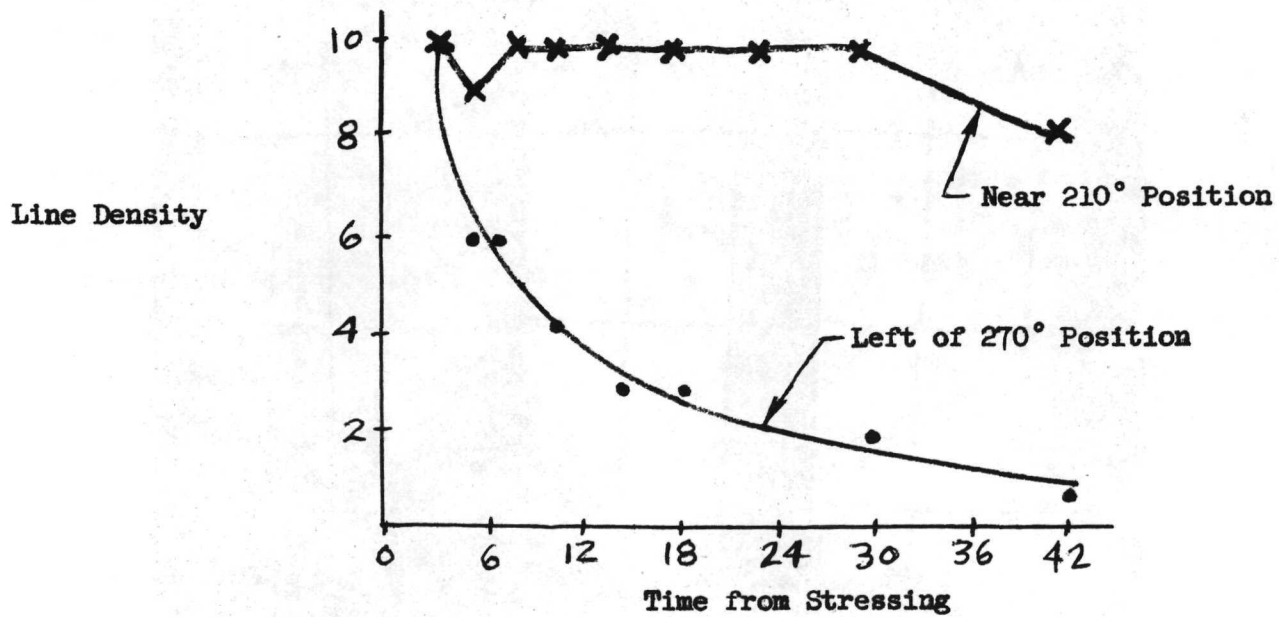
Fig. 82   Fringe Line Behavior With Cooling Time At Two
Positions Found To Be Separated At the Liner/
Propellant Interface In Destructive Testing
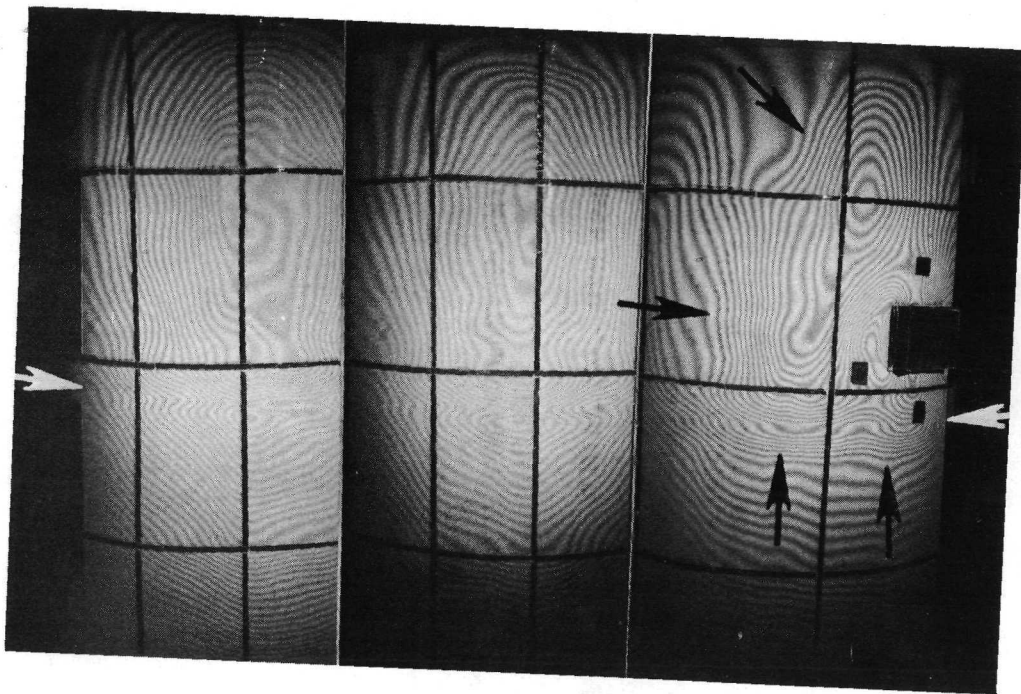
Fig. 83 Composite of Photographs Made Through Reverse Holograms.
Area Defined by Black Arrows Suggest SubSurface Separation
Centered At the 270° Position of Motor Case S/N 424.
White Arrows Show Plane of Liner Termination

Section 5

5.1   INTERFEROMETRY OF THE CYLINDRICAL CASING

A hologram records intensity and phase of a wavefront for regeneration at a later time.

A real-time or reverse hologram superimposes a virtual image over the actual object understudy. Construction and destruction of light reflected from points on the object creates light and dark lines on the superimposition seen through the hologram. The points on the surface displaces to alter the path of light by 1/2 wavelength for the first destruction and one wavelength for succeeding light lines. The general relationship that defines this is:

$$\text{where,} \qquad dp = \frac{(2N-1)}{2}\lambda$$

$$dp = \text{object displacement}$$
$$N = \text{number of dark lines}$$
$$\lambda = \text{wavelength of light}$$

By spraying the casing surface with penetrant developer, a skin of white spherical hydrocarbons are deposited. The particles are about 40 microns in diameter.

Considering the spherical geometry of the particles and the cylindrical shape of the casing, relative estimates can be made as to the expected behavior of interference lines when viewing the hologram.

Fig. 84 of the casing surface having a distended reflecting sphere.

5-1
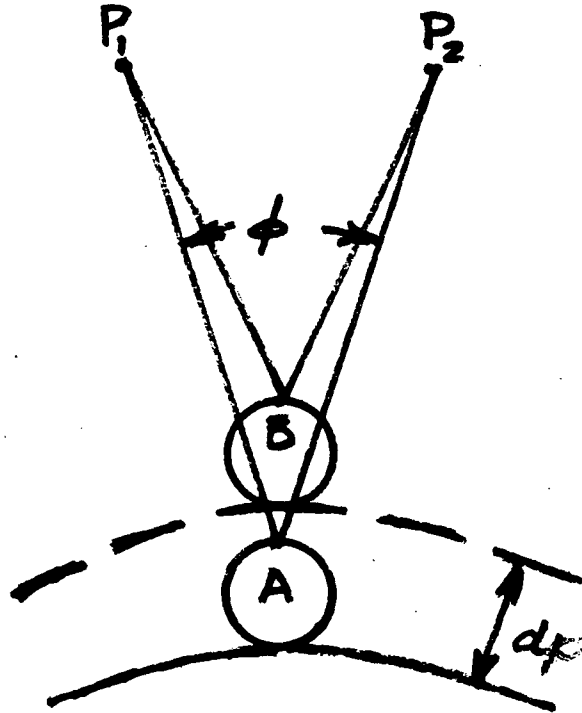
Fig. 84

The point P_1, can be considered the spatial filter while P_2 is the viewing point through the hologram. Also assumed in Fig. 84 is that the points P_1, P_2 and the sphere are in a horizontal plane.

It can be shown that the change in path length between P_1 A P_2 and P_1 B P_2 is represented by the following:

$$dl = 2\, dp \cos 1/2\, \phi$$

For off axis symmetry, in the horizontal viewing plane of Fig. 85 and a motor circumferential angle of 60°, dl is approximately equal to dp.

5-2

In a vertical viewing angle, such as shown in Fig. 85, the change in path length is:

$$dl = 2 \, dp \, \sin h$$
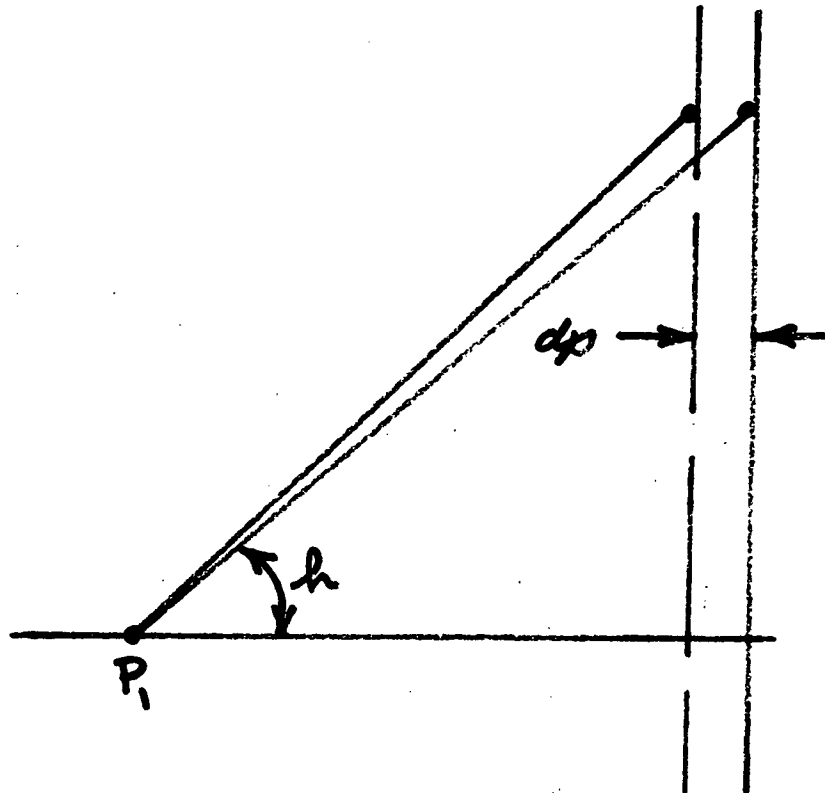
Fig. 85

By computing the angles from the actual viewing lengths, as seen through the hologram, estimates of boundary path lengths were determined and they are defined below:

$$dl_1 \approx 2 \, dp \quad \text{(on- axis viewing)}$$

$$dl_2 = dp \quad \text{(off- axis viewing)}$$

$$dl_3 = .75 \, dp \quad \text{(vertical axis viewing)}$$

Using the above relationships, it can be shown that a series of ellipses should be seen through a hologram spreading outward from the center of viewing. The mirror axis would be in horizontal plane and the major axis on the vertical plane.

5-3

This behavior can be observed in Figs. 63 and 65.

5.2 RADIANT ENERGY DELIVERED TO THE CASING

The power output of the quartz lamp was 3000 watts or 3000 joules/second. This converts to 715 calories/second. And for a 30 second period, the energy propagated amounts to 21,450 calories. Assuming this total energy raises the casing temperature by the following relationship:

$$\Delta T = \frac{q}{C\,V\,\rho}$$

where V - volume and ρ = density and C = specific heat which for fiberglass is 0.199 cal/gm $°C$. A temperature rise of 133.2$°F$ is predicted. However, when the taking into account the fact that no more than 20% of the radiant energy reaches the casing due to R^2 losses and scanning efficiency, a temperature rise of 26°F can be expected. In addition, if the surface emissivity is estimated at 0.4 and heat losses by convection and conduction are in the order of 20%, a final temperature rise of about 8°F is arrived at. Then the actual measured temperature rise for 30 seconds of approximately 6°F, seems reasonable.

5.3 AXIALLY EXPANSION AND CONTRAINT

The axially or longitudinal expansion of the motor case resulting from heating cannot be easily determined. One reason being the lack of physical data on the insulator and propellant. Another is the asymetrical geometry of the motor from an idealized cylinder. However, by using simplistic models, relative thermal displacements can be appreciated.

The maximum axially thermal movement can be estimated from the following:
$$\Delta L = L_o \propto \Delta T$$
where

L_o = length of cylindrical section
$\propto$ = coefficent of expansion
ΔT = temperature rise

For the fibergalss cylinder, unrestrained, a change in length, with a temperature rise of 10°F, would be 1500μin. However, the propellant constrains casing elongation creating a lateral compression force. An estimate of the force can be made by using,

$$\frac{F}{A} = E \propto \Delta T$$

where E = compression modules for fiberglass and $\propto$ = coefficient of expansion. Eploying the figures, E = 30 x 10^{-5} psi and $\propto$ = 4.8 x 10 in/in/°F a .055-in. wall, the total lateral applied force is 411 pounds.

5.4 RADIAL EXPANSION OF THE MOTOR CASE

For a temperature rise of 10°F, the radial free expansion of the fiberglass casing can be estimated from the following relationship:

$$\Delta r = r_0 \left(\sqrt{1 + 2\propto\Delta T} - 1 \right)$$

where r_o is the initial radius.

The change in radius calculates to be 432μ in.

If the casing is constrained in the radial direction by the bondlines, the change in the radial direction as a result of thermal tension can be estimated from:

$$\Delta t = t_o \propto \Delta T$$

where t_o is the casing thickness of .055 in. The thickness increase would be 2.64 μ in. A figure much too low to be observed by real-time holography.

5.5 CIRCUMFERENTIAL EXPANSION OF THE MOTOR CASE

By employing the subsequent formula, it can be shown that the expected circumferential free expansion of the casing would be only 136 μ in.

$$\Delta C = 2\pi r \left(\sqrt{1 + 2\propto\Delta T} - 1 \right)$$

5-5

The variables and, α , coefficient of expansion have been previously identified.

Over an angle of 120°, which is the maximum observable in real-time holography, the circumferential displacement would be about 45 μ in.

5.6 CASING COOLING BEHAVIOR

The typical cooling behavior of the casing, as anticipated, was exponential. A typical cooling curve for a 30 sec quartz lamp exposure over half the cylinder is shown in Fig. 86
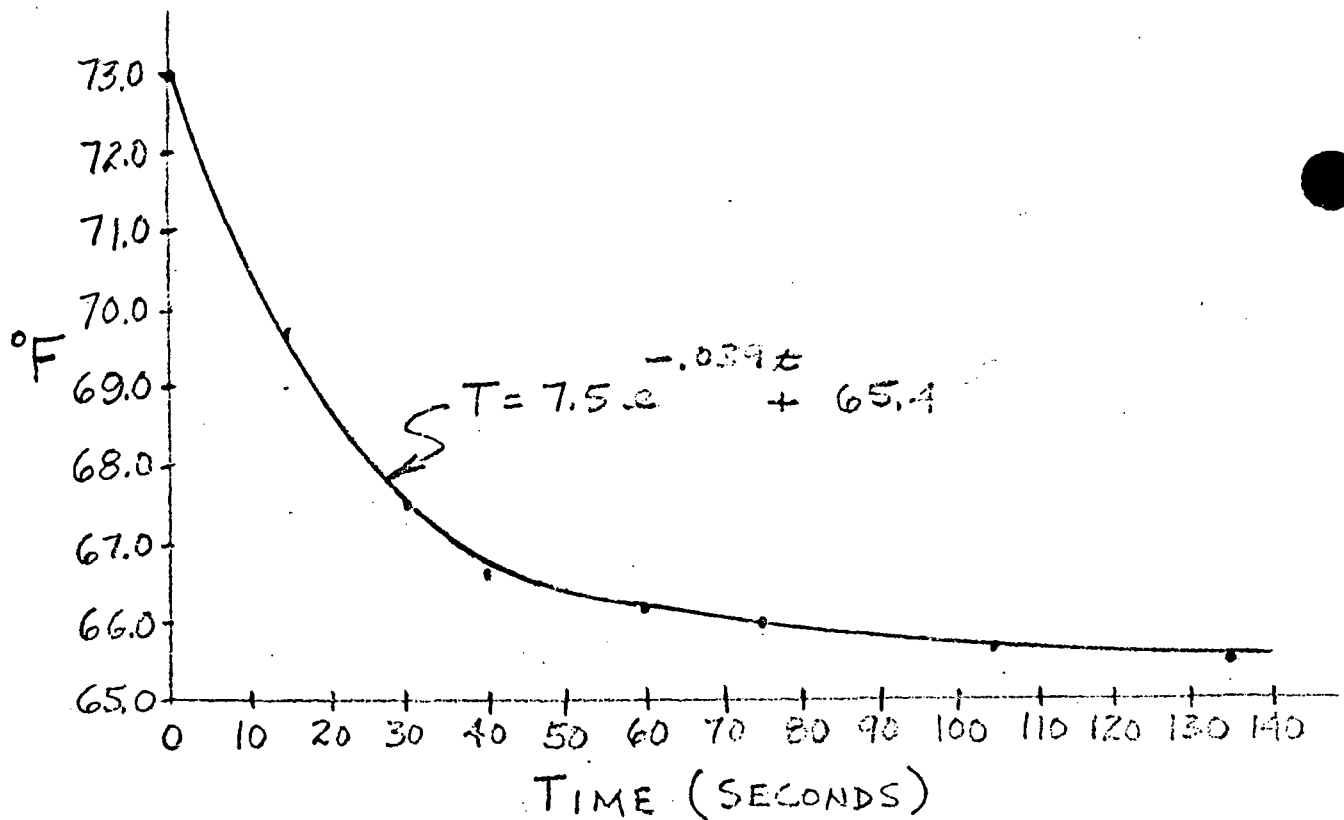
TYPICAL MOTOR CASE COOLING CURVE

$$T = 7.5\, e^{-.039t} + 65.4$$

Fig. 86

LOCKHEED MISSILES & SPACE COMPANY

The curve obeys the general exponential equation:

$$T = T_M e^{-Kt} + T_A$$

where T_M = maximum temperature change and T_A = ambient temperature and K is the decay factor.

The temperature behavior through a thin walled cylinder is represented by the following equation:

$$\theta = \left(\frac{\theta_M - \theta_o}{e^b - e^a}\right) e^{-ht+r} + \theta_M - \left(\frac{\theta_M - \theta_o}{1 - e^{a-b}}\right)$$

where
θ_M = peak surface temperature
θ_o = ambient temperature
b = outer diameter
a = inner diameter
t = time
r = radius between a and b
h = diffusivity

The derivation of this equation is included in the appendix.

The essential similarity between the two equations is evident.

5.7   REAL-TIME AND REVERSE HOLOGRAMS

The majority of the holograms made during the investigation on motor case NPP-424 were real-time and reverse.

LOCKHEED MISSILES & SPACE COMPANY

Real-time holograms were exposed prior to stressing with the quartz lamp. After developing real-time holograms the motor was radiatively stressed and then the resulting interference patterns were observed through holograms. The interference fields observed were a function of the casing temperature at that instant. Since the casing temperatures generated surface displacement, the view or photograph through a real-time hologram is an instantaneous picture of displacement.

Reverse holograms were created minutes after the motor case was radiatively stressed and subsequently observed and photographed. Some reverse holograms were produced at elevated ambient temperatures and studied many hours later when the ambient temperature had decreased. Then a reverse hologram reveals the total or sum of casing displacement occurring in cooling to ambient temperature. The graphic difference between the two types of holograms is shown in Fig. 87.

The quality of the temperature, θ, versus time, t, through the fiberglass, liner and propellant is also illustrated in Fig. 87. The peak temperatures at the three outer surfaces are θ_c, θ_l and θ_p respectively.

5.8 DIFFERENTIAL THERMAL DISPLACEMENT OF SEPARATED AREAS IN A BONDED STRUCTURE

A theoretical model to explain motor case deflection of unbonded areas produced by thermal excitation would aid in understanding and interpreting anomalies of holographic interference fields. A dependable model would also enhance the possiblity of estimating success in related applications.

A promising model to explain deflection is thermal elongation. In this approach, unbonded zones are free to expand, linearly, but bonded surfaces are restrained. An analogy is the heating of a thin disc which is subsequently forced into an area of its original diameter.

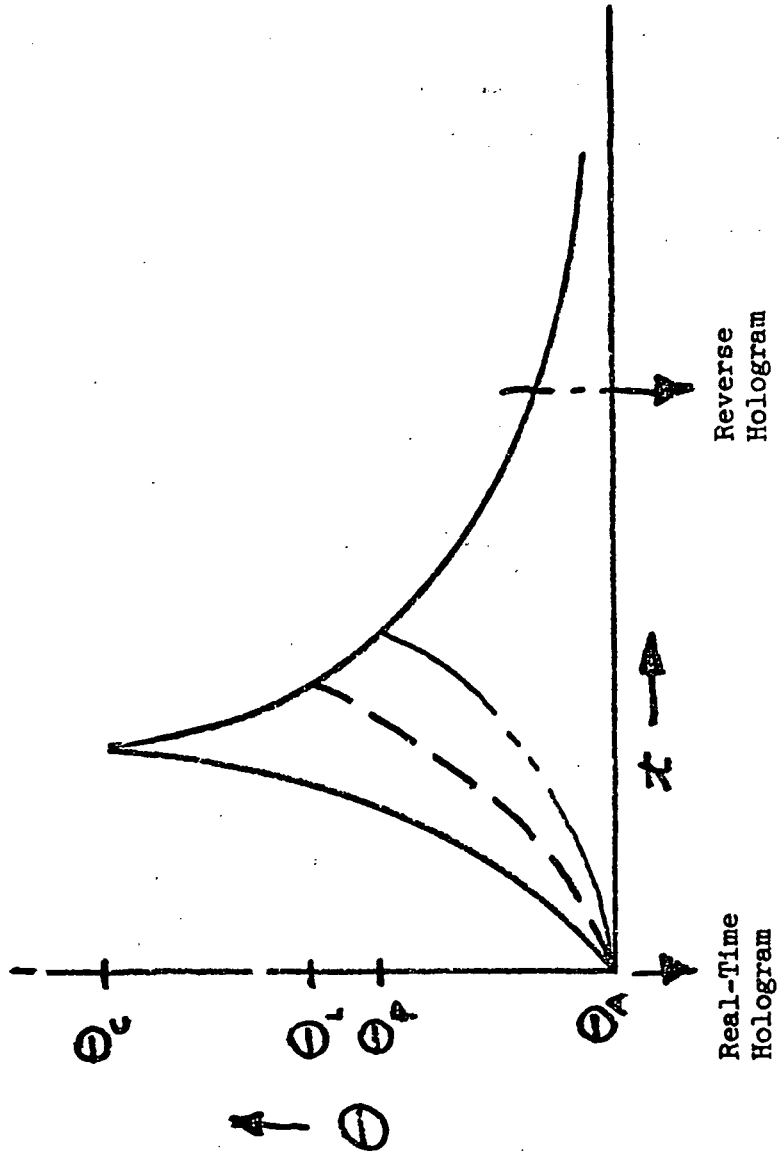LOCKHEED MISSILES & SPACE COMPANY

Fig. 87 Approximate Behavior of Temperature Vs Time in Motor Case and Estimate of Times When Real and Reverse Holograms are Made

The deflection equation for this behavior is:

$$d = R\sqrt{2\alpha\Delta T} - C\left(\sqrt{1 + 2\alpha\Delta T} - 1\right)$$

where the second term is the normal expansion expected for the fiberglass cylinder of radius C, experiencing a temperature change of ΔT.

In solving the above for temperature changes of 7°F, displacements of 10^3 microinches result. This, for diameters in inches exceeds fringe resolution in real-time holograms which ranges from about 20 to 300 microinches.

A more realistic model of thermal elongation would be an expanded area having a fixed edge.

A second model involves the deflection of a disc caused by a pressure differential produced from a temperature rise.
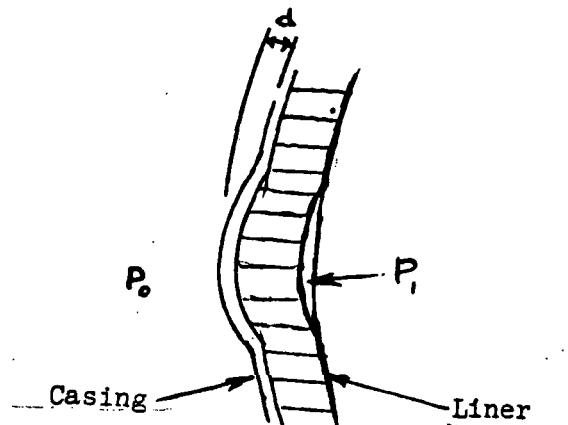
In this model $P_1 > P_o$ results from the temperature rise in the entrapped air in the disbonded volume. The derived equation for deflection of a disc of radius R is:

LOCKHEED MISSILES & SPACE COMPANY

$$d = R\left[\sqrt{\left(1-\cos\frac{\theta}{2}\right)^2 + \frac{150\cdot10^6 R\left(\frac{T_2}{T_1}-1\right)}{\theta^2 Y t}} - 1 + \cos\frac{\theta}{2}\right]$$

where

Y = Youngs modulus

θ = angle subtended by 2R

T_2 = elevated temperature

T_1 = ambient temperature

t = casing thickness

Solving the above equation for temperature differentials, T_2-T_1, of only 1-2°F produces deflections even greather than the elongation model. However, the actual temperature differentials should be computed, for it is probable that only negligible temperature increases are generated at the liner propellant interface for casing temperature changes of 7 to 8°F. If this were true, then this potential model could be rejected.

Section 6

CONCLUSIONS

6.1   ACOUSTICAL STRESSING

Applying up to 20-W of sonic stress, from 100 c.p.s. to 18,000 c.p.s. did not provide sufficient displacement to produce meaningful time-average holograms.

At stressing feequencies around 1750 cps surface movement of the fiberglass casing was suggested in time-average holograms. However, the time-average displacements had to be something less than the wavelength of the He-Ne laser, 25 microinches, for only dark spots were observed which suggests interference of less than wavelength.

Operating at the 20-W of output produced high decibel noise levels causing extreme ear irritation even with the use of ear plugs. Certainly this would make this method difficult to apply as a practical inspection process.

6.2   THERMAL STRESSING

The use of hot air guns for thermal stressing failed to raise casing temperatures for real-time holography. From thermocouple readings, temperature changes of 1 to 2°F resulted on the casing surface after 3 min. of heating. This temperature rise did not create adequate fringe line densities for meaningful surface displacement information.

6.3   RADIATIVE STRESSING

Through the application of a 3 kilowatt quartz lamp for stressing the motor casing, adequate surface displacement was experienced to accomplish real-time holography.

LOCKHEED MISSILES & SPACE COMPANY

In conjunction with radiative stressing, a fine coating of chlorinated hydro-carbons, aided in generating brilliant real-time holograms showing fringe lines of a density sufficient for displacement analysis.

Employing real-time and reverse holograms, it was possible to correlate axially and circumferential strains with a large propellant void area of about 180 in.^{2} Perfect correlation was not realized. An uncertainty exist concerning the actual void area when holography was performed. It is possible that the void area propagated in the time from performing holography to destructive testing.

Double exposure holograms were not successful because of the rapid surface displacement caused by radiative stressing during the time of hologram exposure.

6.4   STATIC LOADING

Variations in axially displacement tended to suggest the large void area in the propellant of motor case S/N 424.

Section 7

RECOMMENDATIONS

A second major casing S/N 426 has known separation, probably between propellant and liner, as defined in Fig. 89. It is recommended that the real-time holographic techniques developed in this study be applied to S/N 426. To increase illumination levels, an argon laser having 2 - 3 watts of power output should be employed. This will improve the possibility of using a fringe control lens system for interpreting line anomalies. The radiographic inspection record for this motor is shown in the appendix.

Before applying holography, pulse-echo contact ultrasonics should be attempted to define actual void area.

One of the important disadvantages of continuous wave holographic nondestructive testing is the requirement of vibration isolation from the ground sources. An air-suspended table must be employed to maintain light path distances between laser, workpiece and hologram. This requirement can be circumvented by utilizing oversized holographic plates mounted to the workpiece in conjunction with through transmission holography. The arrangement is shown below:
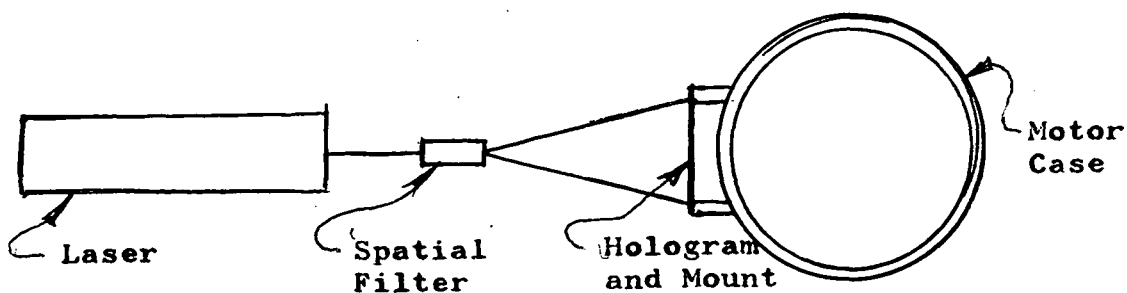
Through transmission holography has already been successfully performed. The only important path length of light that must be held constant is the distance

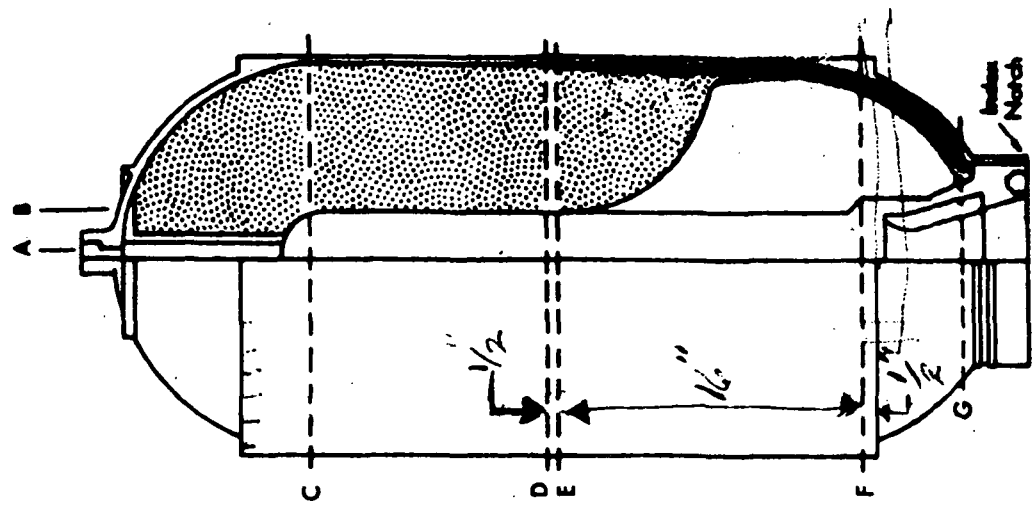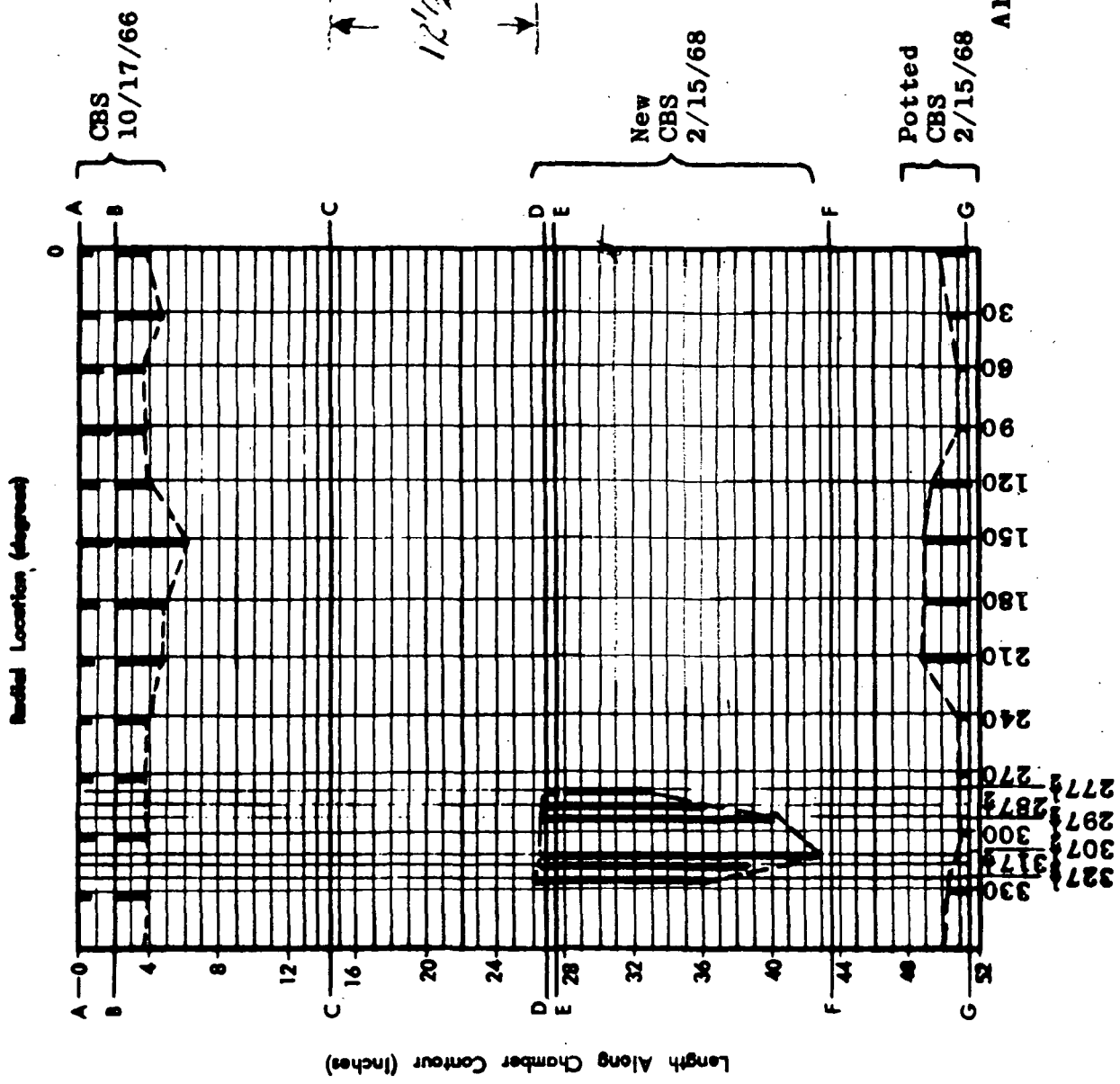**LOCKHEED MISSILES & SPACE COMPANY**

between motor case and hologram.

The obvious advantage to this method, besides eliminating the air-suspended table, is its application to field inspection of motor cases.

LOCKHEED MISSILES & SPACE COMPANY

APPENDIX

X248 RADIOGRAPHIC INSPECTION

Motor No. NPP-424

Date Inspected As noted

Radial Location (degrees)

{ CBS 10/17/66

{ New CBS 2/15/68

{ Potted CBS 2/15/68

All measurements as seen on film.

CBS Widths

Degree	Size (Hairline to)
277°	0.020"
287°	0.040"
297°	0.060"
307°	0.080"
317°	0.040"
327°	0.040"

Degrees Clockwise from Forward End

30 60 90 120 150 180 210 240 270 277 287 297 300 307 317 327 330

Length Along Chamber Contour (Inches)

0 4 8 12 16 20 24 28 32 36 40 44 48 52

A B C D E F G

Fig. 88 Radiographic Inspection Record of Motor Case
NPP-424 Showing Areas of Liner/Propellant Separations

X248 RADIOGRAPHIC INSPECTION

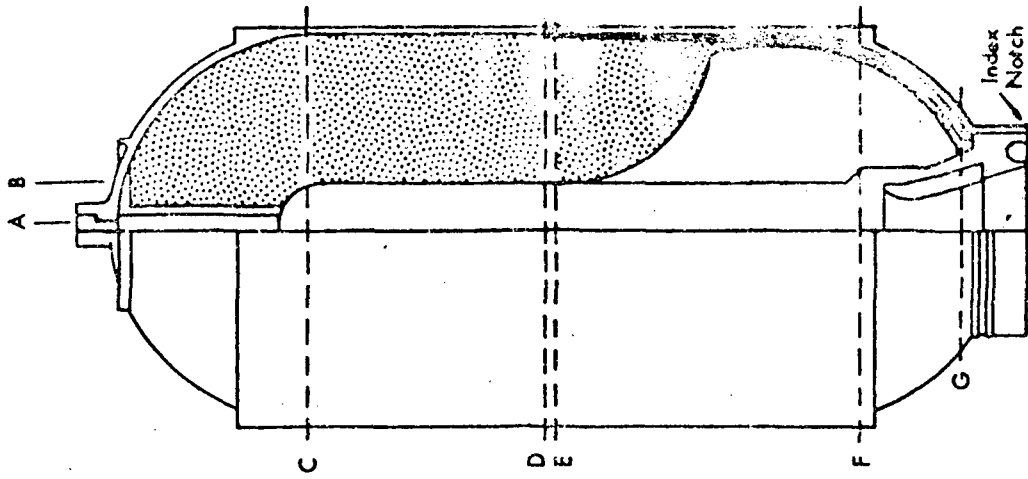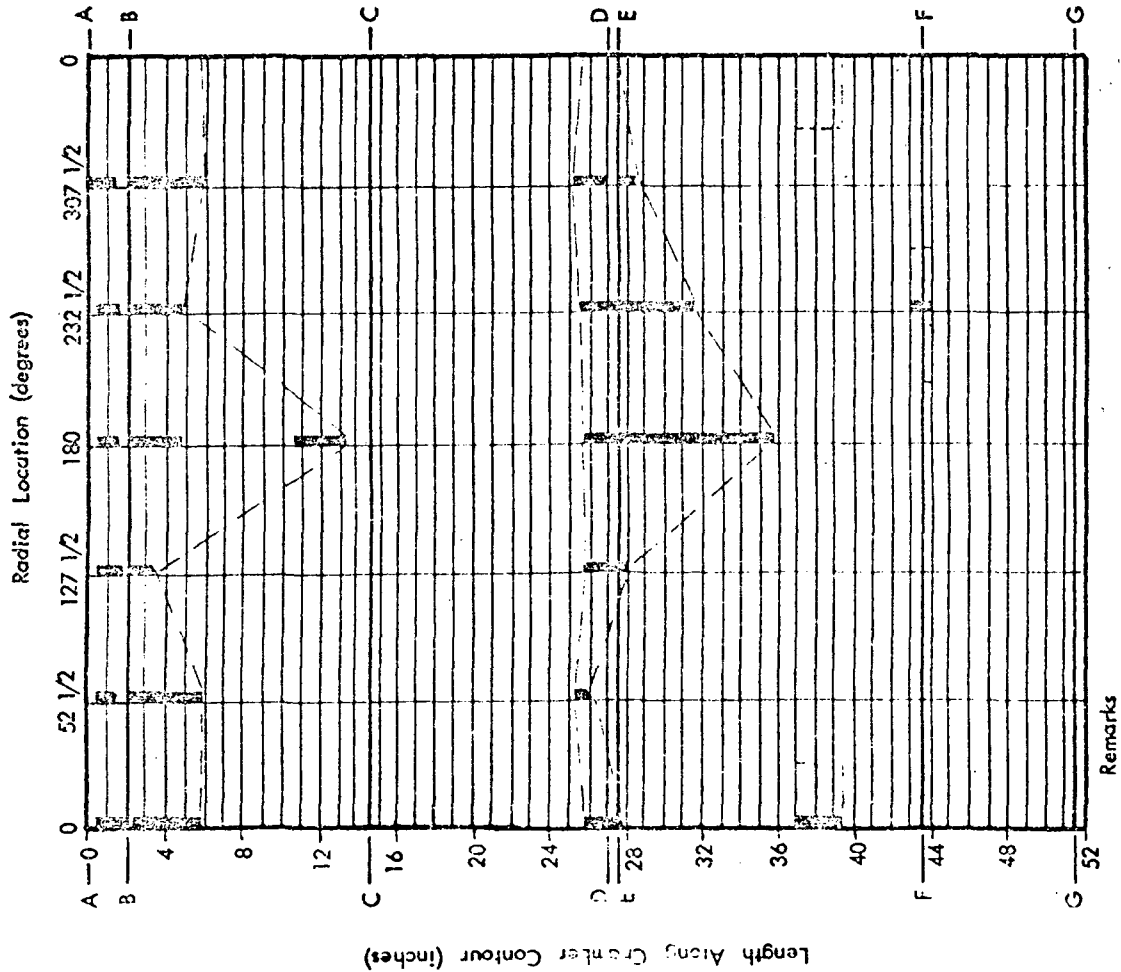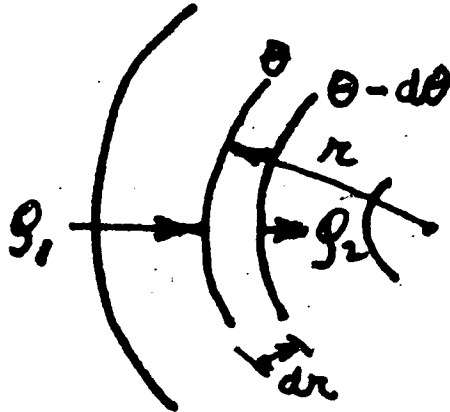| Motor No. | NPP-426 |
| Date Inspected | 12-1-67 |

Fig. 89 Radiographic Inspection Record of Motor Case NPP-426
Showing Areas of Liner/Propellant Separations

A.1 DERIVATION OF TEMPERATURE EQUATION FOR A CYLINDRICAL SHELL

The derivation of the temperature behavior through a thin walled cylinder is developed from the following picture:

The heat energy into the section dr is

$$(1) \quad Q_1 = KA_1 \frac{d\theta}{dr} \,,$$

where axial summetry is assumed. The flow out is

$$(2) \quad Q_2 = KA_2 \frac{d}{dr} \left(\theta - \frac{d\theta}{dr} dr \right)$$

Here, $\left(\theta - \frac{d\theta}{dr} dr \right)$ is the temperature at r-dr and θ in the temperature at r.

The total energy entering dr,

$$(3) \quad Q_3 = Q_1 - Q_2 \,,$$

can be arrived at from (1) and (2) such that

$$(4) \quad Q_3 = - KA_1 \frac{d\theta}{dr} + KA_2 \frac{d\theta}{dr} - KA_2 \frac{d^2\theta}{dr^2} dr$$

Now the total energy required to raise the temperature of the section can be determined from:

$$(5) \qquad Q = P \cdot \frac{A_1 + A_2}{2} \cdot C \cdot dr \cdot \frac{d\theta}{dt}$$

P - density and C = specific heat

The cooling behavior can be resolved by equating (4) to (5) and solving the resultant differential equation. But a solution would take the form $\theta = f(r, t, dr)$ which would be cumbersome, and much more difficult to reach. The problem can be simplified by assuming $A_2 \approx A_1$ which indeed is the case for large cylindrical diameters. Making the assumption, and letting (5) = (4), the subsequent relation follows:

$$(6) \qquad -h \frac{d^2\theta}{dr^2} = \frac{d\theta}{dt}$$

Of course, $h = \frac{k}{cp}$, is the diffusivity, or the rapidity of temperature changes in a material.
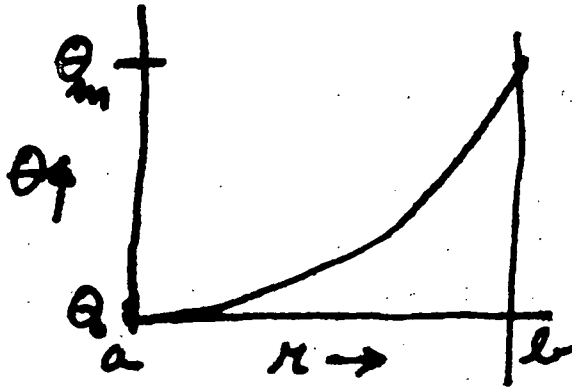
By examining the boundary conditions of cooling and knowing the decay is exponential as Fig. 86 reveals, a solution to (6) can be found.

The relation of θ with t obeys the curve below:

When t = 0, θ must be θ_m and if t = OO, then $\theta = \theta_o$.
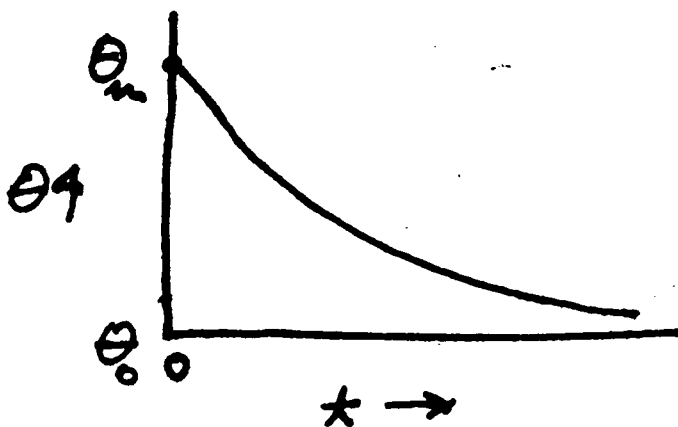
The expected $\theta = f(r)$ also is exponential, where a and b are the inner and outer cylindrical radii, respectively.

The general equation for the above curve is:

(7) $\qquad \dot{\theta} = Ae^r + B$

The constants, A and B, can be determined by applying the boundary conditions and solving simultaneous equations. For $\theta = \theta_m$ and $R = b$.

(8) $\qquad \theta = Ae^a + B$

and when $\theta = \theta_o$, $r = a$ so

(8) $\qquad \theta_o = Ae^a + B$

which leads to the following solutions for A and B.

(9) $\qquad A = \dfrac{\theta_m - \theta_o}{e^b - e^a}$

(10) $\qquad B = \theta_m - \dfrac{(\theta_m - \theta_o)}{\left(1 - e^{a-b}\right)}$

Now by combining (7), (9) and (10) with $\theta = f(t)$ in the following manner:

$$(11) \qquad \theta = \frac{(\theta_m - \theta_o)}{(e^b - e^a)} e^{-ht+r} + \theta_m - \frac{(\theta_m - \theta_o)}{\left(1 - e^{a-b}\right)}$$

A solution for (6) is reached satisfying boundary conditions.

The preceding equation does not take into account radiation loss. This can be included by modifying (7) with additional term $-g \, A \frac{dO}{dt}$, where g is the convection coefficient. But actual calculations show radiation losses to be proportionately small, about 10% of conduction losses when the case surface differential is 7-8°F.

The diffusivities for fiberglass, inuslation and propellant are 20, 13 and 9 cm/sec.°C. Then the heat flow occurs relatively **fast** in fiberglass as compared to the insulation and the propellant.